CHALMERS
UNIVERSITY OF TECHNOLOGY

Advanced Assessment of Welded Bridges for Fatigue and Brittle Fracture

Final Report - Trafikverket project number 2014-007

FARSHID ZAMIRI
MOHAMMAD AL-EMRANI
ROBERT KLIGER

Department of Architecture and Civil Engineering
Division of Structural Engineering
Steel and Timber Structures
CHALMERS UNIVERSITY OF TECHNOLOGY
Gothenburg, Sweden 2018

Advanced Assessment of Welded Bridges for Fatigue and Brittle Fracture

Final Report - Trafikverket project number 2014-007

FARSHID ZAMIRI

MOHAMMAD AL-EMRANI

ROBERT KLIGER

Department of Architecture and Civil Engineering
Division of Structural Engineering
Steel and Timber Structures
CHALMERS UNIVERSITY OF TECHNOLOGY
Göteborg, Sweden 2018

Advanced Assessment of Welded Bridges for Fatigue and Brittle Fracture

Final Report - Trafikverket project number 2014-007

FARSHID ZAMIRI

MOHAMMAD AL-EMRANI

ROBERT KLIGER

Institutionen för arkitektur och samhällsbyggnadsteknik,
Chalmers tekniska högskola 2018

Department of Architecture and Civil Engineering

Division of Structural Engineering

Steel and Timber Structures

Chalmers University of Technology

SE-412 96 Göteborg

Sweden

Telephone: + 46 (0)31-772 1000

Department of Architecture and Civil Engineering. Göteborg, Sweden, 2018

Advanced Assessment of Welded Bridges for Fatigue and Brittle Fracture
Final Report - Trafikverket project number 2014-007

FARSHID ZAMIRI
MOHAMMAD AL-EMRANI
ROBERT KLIGER
Department of Architecture and Civil Engineering
Division of Structural Engineering
Steel and Timber Structures
Chalmers University of Technology

ABSTRACT

Around 50% of steel and steel—concrete composite bridges owned by Trafikverket have been built before 1970, when there was limited knowledge about fatigue and brittle fracture of structural steel products. This was the case in particular for the usage of these products in construction of welded bridges. At the same time, fatigue deterioration in these structures is undergoing due to the escalation of freight volume as well as the increased axle loads of modern trains and lorries. Realistic assessment of residual service life of these structures is crucial in more efficient planning of repairs and avoiding unnecessary replacement costs. Therefore, more accurate condition assessment methods are important from both economic and sustainability aspects.

While the improved assessment methods for existing structures have been subject of extensive research since 1990's, their use in regular engineering practice is still limited. This study is an attempt to review the recent advances in structural assessment of welded steel bridges and to present them in a structured manner for the use of practicing engineer. In this report, a multi-step assessment methodology for fatigue and brittle fracture of welded bridges is presented, mainly based on the past research in Europe. The assessment steps are comprised of preliminary assessment (phase I), detailed investigation (phase II), and expert investigation (part III). Detailed information is given in the report for the corresponding input data (resistance-side and action-side) and modelling options for each of these assessment steps. As expected, the more advanced method is used, the more extensive set of input data and analytical effort is required. When applicable, the assessment method has been adapted to the relevant technical requirements stipulated by Trafikverket.

Finally, the application of the presented multi-step assessment is examined on a case study bridge (Göta river bridge). Phase II assessment of the bridge based on historical loading data shows insufficient fatigue life for a critical detail that has been replicated in many locations over the bridge. The results of phase III assessment suggest that intensified inspections of vulnerable details in regular time intervals are sufficient for ensuring the safe service of the structure until the end of its planned service life.

Key words: steel bridges, steel—concrete composite bridges, fatigue assessment, brittle fracture, master curve method.

Avancerad tillståndsbedömning av stål- och samverkansbro mot utmattning och sprött brott. *Final Report - Trafikverket project number 2014-007*

FARSHID ZAMIRI
MOHAMMAD AL-EMRANI
ROBERT KLIGER
Institutionen för arkitektur och samhällsbyggnadsteknik
Avdelningen för konstruktionsteknik, Stål- och träbyggnad
Chalmers tekniska högskola

SAMMANFATTNING

Ungefär 50 % av stål- och samverkansbroar som ägs av Trafikverket har byggts före 1970, då kunskapen om utmattning och sprödbrott av stålprodukter i konstruktioner var begränsad. Detta var speciellt fallet för användningen av dessa produkter vid konstruktion av svetsade broar. Det pågår samtidigt en kontinuerlig försämring i dessa strukturer orsakad av utmattning på grund av eskalering av fraktvolymen samt ökad axellasten från moderna tåg och lastbilar. En realistisk bedömning av den resterande livslängden hos dessa konstruktioner är avgörande för effektivare planering av reparationer och för att undvika onödiga ersättningskostnader. Därför är mer exakt tillståndsbedömning viktiga både från ekonomisk- och hållbarhetsperspektiv.

Även om de förbättrade tillståndsbedömnings metoderna för befintliga konstruktioner har varit föremål för omfattande forskning sedan 1990-talet, är deras användning i regelbunden teknisk praxis fortfarande begränsad. Denna studie är ett försök att se över de senaste framstegen inom tillståndsbedömning av svetsade stålbroar och att presentera dem på ett strukturerat sätt för användning av den praktiserande ingenjören. I denna rapport presenteras en flerstegsbedömningsmetod för utmattning och spröda brott av svetsade broar, huvudsakligen baserat på tidigare forskning i Europa. Bedömningsstegen består av preliminär bedömning (steg I), detaljerad utredning (steg II) och expertutredning (steg III). Detaljerad information ges i rapporten för motsvarande ingående data (bärförmågan och lastspåverkan) och modelleringsalternativ för vart och ett av dessa bedömningssteg. Som förväntat, desto mer avancerad modell som används, desto mer omfattande uppsättning av data och analytisk insats krävs. Vid tillämpning har flerstegsbedömningsmetoden anpassats till relevanta tekniska krav som fastställs av Trafikverket.

Slutligen granskas tillämpningen av den presenterade flerstegsbedömningen på en fallstudie av en bro (Götaälvbron i Göteborg). Steg II-bedömning av bron baserat på historiska belastningsdata visar otillräckligt utmattningshållfasthet för en kritisk detalj som har förekommit på många ställen över bron. Slutligen granskas tillämpningen av den presenterade flerstegsbedömningen på en fallstudie av en bro (Götaälvbron i Göteborg). Steg II-bedömning av bron baserat på historiska belastningsdata visar otillräckligt utmattningshållfasthet för en kritisk detalj som har förekommit på många ställen över bron. Resultaten av steg III-bedömningen tyder på att intensifierade inspektioner av sårbara detaljer under normala tidsintervaller är tillräckliga för att säkerställa en säker service av konstruktionen fram till slutet av den planerade livslängden.

Nyckelord: stålbroar, samverkansbroar, utmattningsbedömning, sprödbrott, masterkurva metod.

Contents

Preface

This report is a result of the work conducted within the BBT Project 2014-007 "*Advanced assessment of welded bridges for fatigue and brittle fracture"*. The project was funded by the Swedish Transport Administration (Trafikverket) and Traffic Office (Trafikkontoret) - City of Gothenburg. It was conducted in collaboration between Chalmers University of Technology, ÅF Infrastructure AB, Trafikkontoret - City of Gothenburg and COWI AB. Contact person at Trafikverket was Hans Pétursson. We would like to express our warmest thanks to all those involved in this project.

Gothenburg, February 2018

Farshid Zamiri, Mohammad Al-Emrani, Robert Kliger

Notations

Roman upper case letters

Roman lower case letters

μ_{fat}	
σ	
f_y	
$\Delta\sigma_{E,2}$	
γ_{Ff}	
γ_{Mf}	
m	slope of fatigue S-N curve ($m = 3$ or $m = 5$)
T_{Ed}	design value of service temperature
T_{Rd}	resistance-side temperature
$T_{min,d}$	lowest ambient temperature with a certain return period
ΔT_r	temperature shift by radiation loss
ΔT_σ	temperature shift due to influence of stress, flaw, and detail geometry
ΔT_R	temperature shift to provide safety margin (additive safety element)
$\Delta T_{\dot{\epsilon}}$	temperature shift due to strain rate
$\Delta T_{\epsilon pl}$	temperature shift due to cold working
t	plate thickness
t_0	reference plate thickness ($t_0 = 1\ mm$)
ϵ	strain
$\dot{\epsilon}$	strain rate
D	damage accumulation factor
n_i	number of cycles at i^{th} load block in the spectrum
N_i	number of cycles to failure for i^{th} load block in the spectrum
N_C	number of cycles corresponding to fatigue strength ($N_C = 2 \times 10^6$)
$\Delta\sigma_i$	stress range at i^{th} load block in the loading spectrum
$\Delta\sigma_C$	fatigue strength (detail category)
K_{Ed}^*	
K_{Rd}	
K_{mat}	
G_k	
T_k	

$Q_{k,i}$	characteristic value of variable load i
ψ_i	
λ_i	damage equivalent factors
F	normal force
k_m	misalignment correlation factor
k_s	thickness correlation factor
M	bending moment
m	slope of fatigue strength curve
N	number of stress cycles
R	stress ratio
t	plate thickness
γ_{Ff}	partial factor for equivalent constant amplitude stress ranges
γ_{Mf}	partial factor for fatigue strength
Φ_2	dynamic factor
ΔM	bending moment range
$\Delta\sigma$	direct stress range
$\Delta\sigma_C$, $\Delta\tau_C$	reference stress value of the fatigue strength at 2 million cycles
$\Delta\sigma_D$	reference stress value of the fatigue strength at 5 million cycles
$\Delta\sigma_E$, $\Delta\tau_E$	equivalent constant amplitude stress range related to cycles
$\Delta\sigma_{E,2}$, $\Delta\tau_{E,2}$	equivalent constant stress range at 2 million stress cycles
$\Delta\sigma_{FLM}$	stress range calculated from fatigue load model
$\Delta\sigma_L$, $\Delta\tau_D$	reference stress value of the fatigue strength at cut-off limit
$\Delta\sigma_{LM}$	stress range calculated from load model
$\Delta\sigma_m$	mean stress range
$\sigma_\perp$	stress perpendicular to the weld toe
σ_1	first principal stress
σ_2	second principal stress
σ_b	bending stress
σ_{ens}	effective notch stress
σ_{hss}	structural hot spot stress
σ_m	membrane stress
σ_{max}	maximum applied stress
σ_{min}	minimum applied stress

σ_{nlp}	non-linear peak stress
σ_{nom}	nominal stress
σ_{str}	structural stress
σ_{str}	structural/geometric stress
τ_{xy}	shear stress in x-y direction

NEW SYMBOL TABLE

T_{27J}	Temperature for which a minimum energy A_v will be larger, or equal to 27J in a Charpy V-notch impact test
$A_v(T)$	Impact energy in Joules [J] in a test temperature T for the Charpy V-notch test
K_v-value	Minimum required Charpy impact energy, Av(T), at a given test temperature, set by steel production standards.

List of abbreviations

AADT	Annual Average Daily Traffic
ALS	Accidental Limit State
CAFL	Constant Amplitude Fatigue Limit
CEN	the European Committee for Standardization
CVN	Charpy V-notch
ECCS	European Convention for Constructional Steelwork
ENS	Effective Notch Stress
FLM	Fatigue Load Model
FLS	Fatigue Limit State
HFMI	High-Frequency Mechanical Impact Treatment
IIW	International Institute of Welding
JRC	Joint Research Centre (European Commission)
LEFM	Linear Elastic Fracture Mechanics
LDF	Load Distribution Factor
LM	Load Model
NDT	Non-destructive testing
SHSS	Structural Hot Spot Stress
SLS	Serviceability Limit State
UDL	Uniformly Distributed Load
ULS	Ultimate Limit State
VAFL	Variable Amplitude Fatigue Loading

POD	Probability of detection
WRS	Welding Residual Stresses

1 Introduction

As a result of economic growth and increased demands in developed countries, a rapid growth of traffic has occurred during the past decades. Both highway and railway traffic have increased considerably during the past few decades. The traffic has grown both in terms of number of axles and axle loads. A qualitative measure of how the highway traffic volume has developed over the past half-century is given in Figure 1.1. Also, for the case of railway bridges, higher speeds of modern trains translate into higher cyclic load ranges for the structures.

Consequently, a considerable part of the bridge stock in developed countries, including Sweden, are aging under these ever-increasing traffic loads. A large proportion of these bridges were built in the first half of last century. As can be seen in the diagram in Figure 1.2, as of the year 2016 nearly one-third of in-service steel and composite bridges managed by Trafikverket have been built before 1950. These bridges were built according to the governing standards at the time of their construction, which do not correspond to stricter construction norms that are in place now. The average age of all steel bridges reported in the Figure is 51 years.

Structural degradation in steel bridges occurs mainly due to two phenomena: corrosion and fatigue. For some older steel material, a third factor, increased embrittlement in steel (aging), might contribute to degradation too.

Considering the economic and environmental costs of replacing the aging infrastructure, keeping the existing infrastructure in service is obviously preferred. Spending the limited resources for replacing the existing bridge stock should be kept to an absolute minimum. Of course, this should be done while having the structural performance of existing bridges within the desired safety margins. Frequently, this leads to requirements for more in-depth condition appraisal of existing bridges. The simpler assessment methods, that are similar to the design procedures for new connections, could show that the service life of the details is consumed, while physical examination of existing details does not show signs of degradation.

Also, a contradictory problem can occur: sometimes fatigue cracking is observed in the details before they reach their theoretical fatigue life. Several cases of immature cracking of steel bridge connections are reported by (Al-Emrani and Kliger 2009; Lukić et al. 2011).

The current project is aimed at addressing these two issues by providing more advanced tools and procedures for more accurate condition assessment of existing welded bridges. There is a consensus in the research community for the use of multi-step assessment procedures (Wenzel 2009). That is when a simple structural check of a detail or a structure shows unsatisfactory performance, a second more in-depth structural safety assessment takes place. The sequence of steps with increasing complexity in methods and techniques continues until an informed decision on the bridge can be made based on a cost-benefit analysis. The assessment methodology presented here is a multi-step one.

A more advanced structural assessment procedure calls for more extensive input data, accordingly. This input data concerns both resistance-side information (e.g. material properties, defects) and load-side data (traffic-loads, environmental loads). Clarifications and guidelines are given in subsequent chapters on how to collect and process this information.

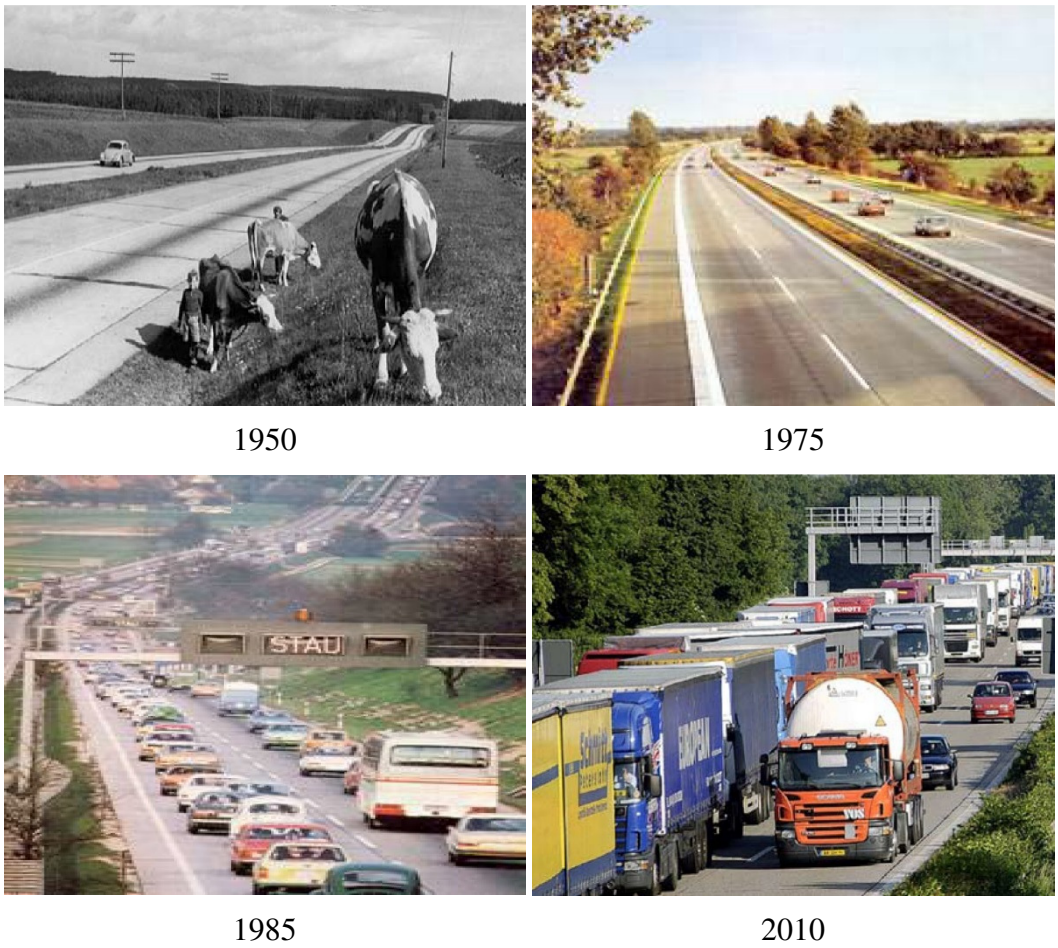

Figure 1.1 The increase of road traffic during the past decades (Naumann 2011).

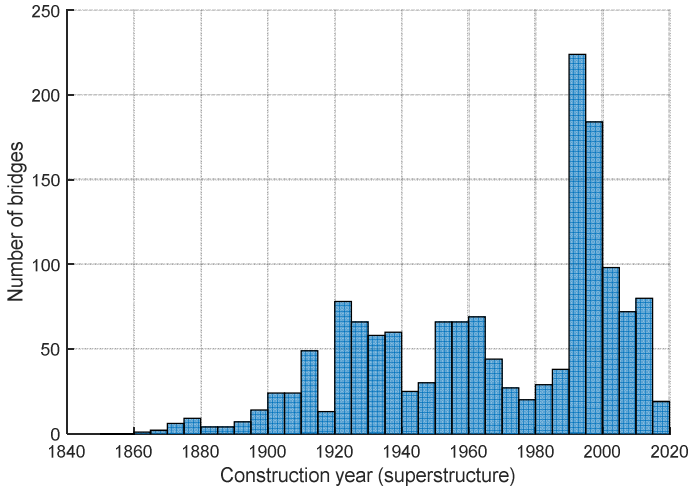

Figure 1.2 Histogram of existing steel road and railway bridges managed by Trafikverket (2017); construction year refers to the year that the superstructure was built or renewed. The bridges managed by Swedish municipalities are not included in these statistics.

1.1 Scope

This report provides the methodology for assessment of remaining service life of existing bridges regarding fatigue and brittle fracture. Structural degradation due to corrosion is not addressed here, nor does the possible interactions between corrosion and fatigue cracking. An appropriate corrosion protection is assumed to be in place. The application of these recommendations is limited to structures exposed to normal environmental conditions and temperature ranges between -40 and 150°C. (Kühn 2013). Repairs and upgrading measures to extend the service life of the structure are outside the scope of this report. The minimum plate thickness for structural components is assumed as 8 mm.

In case the results of assessment for an existing bridge show unsatisfactory performance of the structure, interventions and remedial measures will become necessary. Various interventions can be made regarding a structurally deficient bridge. These include:

- Temporary or permanent load restrictions
- Intensified monitoring and inspection
- Structural repair and upgrading
- Replacement

These interventions are not dealt with in this report.

Usually, fatigue and fracture assessment come after that the evaluation of the static load-bearing capacity of the bridge is carried out. This essential first part is not covered here and is assumed to be done according to the existing rules (Trafikverket 2015b, 2015a).

1.2 Workflow

The multi-step assessment procedure for fatigue and brittle fracture assessment of welded bridges presented here is mainly based on three-step ECCS-JRC recommendations (Kühn et al. 2008) and JCSS model code (JCSS 2001). A brief, general presentation of the three phases of assessment is given in the following; they are presented in more detail in Chapter 2. If the result of the assessment by an earlier phase shows a satisfactory remaining fatigue life, the evaluation in a subsequent phase(s) will not be necessary.

- Phase I – Preliminary Evaluation: In this step, simple calculation methods and models are used for verifying the safety of the structure. Material data, actions, and analysis methods can be taken according to the regulations for the design of new structures (EN 1993-part 1-9). For missing information, conservative assumptions can be made. Although this phase starts with the study of the original design documents, the focus should be on the actual state of the structure. Thus, it is important to gather information on how the bridge was built and maintained. The output from this step should include a list of fatigue and fracture critical members.
- Phase II – Detailed investigation: If the checks from the previous phase show low safety for some details, detailed investigation should take place. The input data regarding resistance side and action side are updated in this phase. The engineer may need the help of specialized laboratories and experts for

assistance. Information on the structure (resistance) and loads are updated using limited tests and measurements. More refined calculation models of the structural system will be used in this step.

- Phase III – Expert investigation: For the cases when a decision involves large consequences in terms of social or economic risk, an expert investigation is required. A team of experts should review and check the outcomes of the previous phase II. The task will continue with more advanced assessments tools and models (Non-destructive tests, probabilistic methods, fracture mechanics calculations). Detailed global and local finite element models may become necessary. Measurements (displacements, strains, accelerations, etc.) in this stage will help to obtain more accurate information on existing actions on the details. They can also assist in calibrating and validating calculation models. Advanced NDT may be used for characterization of defects and cracks.

Figure 1.3 A measure of required input data for different assessment phases is shown in Figure 1-3. As procedures suggest, the extent and accuracy of the input data and analysis methods will increase in accordance with the complexity of the assessment procedure. The idea is to progressively reduce the unknowns and ambiguities concerning the studied structure by taking the above assessment steps. This, of course, is done at the expense of increased complexity and associated costs of evaluation. The assessment steps are explained in more detail in the following sections.

Phase I, and to an extent part II, basically present the conventional practice for bridge assessment in Sweden, only in a more organized manner. While the methods and concepts of Phases I and II should be easy to follow for a practicing engineer, some expert knowledge on fracture mechanics and probabilistic methods will be helpful for effective utilization of Phase III methods.

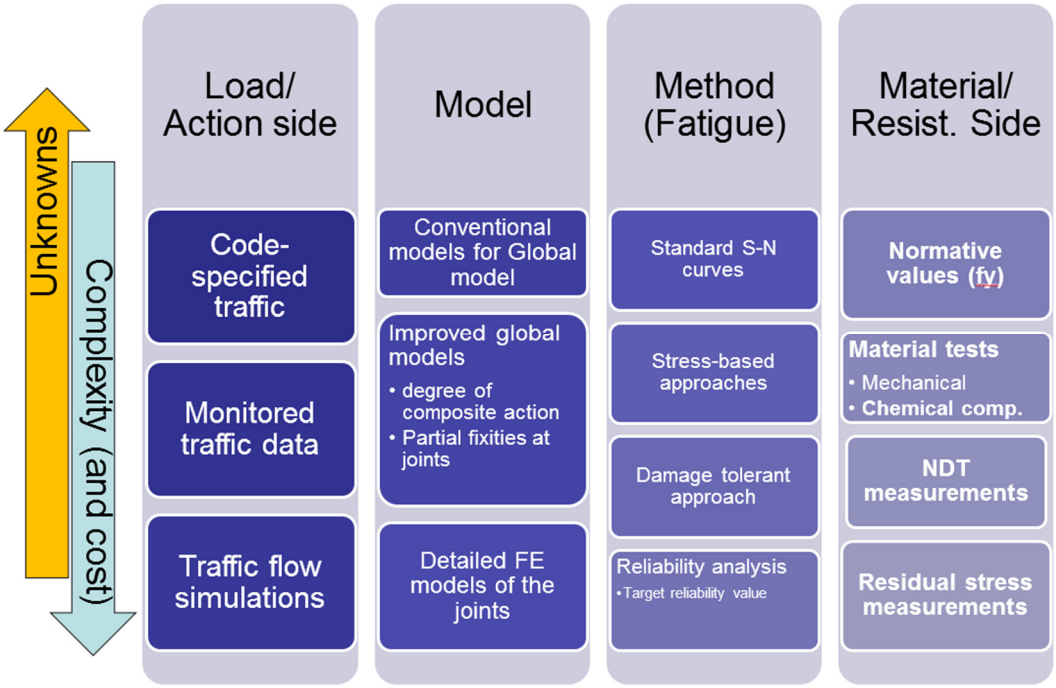

Figure 1.3 Bridge assessment procedures: Increased complexity vs reduced uncertainty.

1.3 Structure of the report

The organization of the report is presented in *Figure 1.4*. Following this chapter (Introduction), basis of evaluation (design equations) for the three phases will be presented in Chapter 2. Chapters 3, 4, and 5 lay out the details of methodology, discussing resistance-side parameters, action-side factors, and modelling options for various assessment phases. Chapter 6 demonstrates the application of the developed methodology for Götaälvbron (the Göta River Bridge) as a case study. Chapter 7 contains the summary and future work.

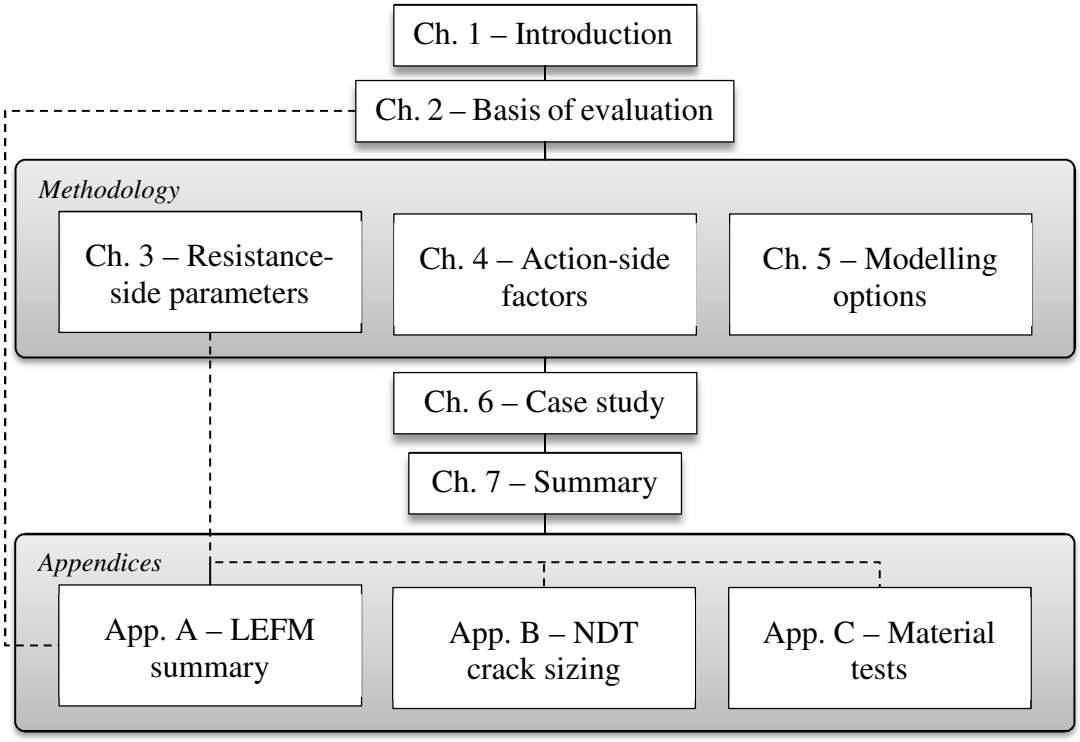

Figure 1.4 Organization of the chapters in this document.

2 Basis of evaluation

This chapter outlines the structural verification procedure for each of the three phases of the proposed multi-step assessment methodology. The resistance-side and action-side data to be used in each step are expressed in brief (they are further explained in their own dedicated chapters). The chapter also presents the design inequalities for each of the assessment phases.

2.1 Phase I – Preliminary assessment

As it was noted in the previous section, phase I includes simple methods to eliminate uncertainties regarding the safety of a studied bridge and to identify critical details in the structure. At this stage of the assessment, the input data consists of collecting readily available data. The safety checks are carried out as is done for a new structure, using current codes and making conservative assumptions when a lack of information exists. This phase involves the following tasks:

1. Resistance-side data:
    a. The data required for this step are fairly basic; namely structure's geometry and configuration, dimensions of members and connections, steel grade, and existing information on material toughness (Charpy test data, etc.).
    b. In-depth study of the original bridge drawings and documents, especially fatigue calculations. The latter might not exist for older bridges, for which limited knowledge on fatigue performance of welded structures existed at the time of construction.
    c. Review of construction documents and any subsequent modifications of the original design. Obviously, it is the actual state of the bridge that is important, not the as-designed or as-built bridge. In this regard, previous inspection and maintenance reports are a valuable source of information. BaTMaN (or similar bridge management system) should be consulted for this data. Check the conformity of the construction to the design documents. Highlight if any deviations from original design documents have been made subsequently.
    d. Visiting the bridge site, observing general condition of the bridge, qualitative inspections, and noticing signs of structural degradation (cracking, corrosion, excessive vibration, damages joints and supports). Basic measurements (e.g. plate thickness measurement) may be necessary. Regardless of whether extensive or little documentation exists, still a site visit is recommended.
2. Action-side data: Conservative values for permanent loads, code-specified load models and partial safety factors from Eurocode will be used.
3. Modelling: Hand calculations or simple beam element models can be used. These calculations are quick and are aimed to give a good estimation of the structural safety level. They will show which members or details are critical and need further assessment.

4. Fatigue assessment: is carried out according to Eurocode's nominal stress S-N curves (see Section 2.1.2). The details that show unsatisfactory fatigue life ($\mu_{fat} < 1$ according to Equation (3-2)) need to be evaluated more thoroughly for the next step (Phase II). It is recommended to collect a list of those details for further investigations, arranged by priority.
5. Brittle fracture assessment: At this stage, Charpy test results can be used to evaluate the sufficiency of material resistance to brittle fracture (see Section 2.1.1).
6. Outcome: In the case that structural safety is not satisfied for all the analyses mentioned above, a list of critical details (fatigue and fracture critical members) is reported together for justifications for more in-depth assessments. Some older bridges had been built before the modern concepts of design against fatigue and brittle fracture was introduced. If this is the case for the studied bridge, poorly designed or erected details (regarding fatigue and brittle fracture) should be pointed out in the report. These include for example following cases:
    a. load-carrying fillet welds,
    b. corner welds that give rise to three-dimensional state of tensile residual stresses (e.g. transverse stiffener welded to both web and flange),
    c. beams with cover plates,
    d. low weld quality, (especially large undercuts, porosity, and lack of fusion).

2.1.1 Brittle fracture assessment in phase I

Toughness is the ability of the material to resist brittle fracture. Charpy V-notch (CVN) impact energy test has been used extensively as an indicator of fracture toughness during approximately last six decades. Other test methods have been used sporadically (Izod, Charpy U-notch, etc.), but CVN absorbed energy has remained the single most frequent material parameter mentioned in virtually all structural steel product standards for the provision of a minimum fracture resistance (Ogle, Burdekin, and Hadley 2013). This is despite considerable shortcomings of the Charpy test in predicting the brittle fracture for many types of steel structure, including bridges (See below). The factors contributing to the widespread use of Charpy test are the simplicity of the test method, relatively easy specimen preparation, and requirement of only small amount of sample material. That is why Charpy test data are almost always available in the original bridge documentation. Based on Charpy absorbed energy results, Table 3-7 is given in Section 3.5.1 as the maximum allowable plate thickness for modern steels to prevent brittle fracture as a function of service temperature and stress level in the detail. Results shown in the table are the result of extensive fracture mechanics calculations with conservative assumptions for the numerous uncertainties in the resistance-side and action-side of the design equation.

Note that the risk of brittle fracture for a structural detail cannot be accurately evaluated solely based on the CVN impact energy at a specific test temperature. There are several factors that determine the risk of brittle fracture in a component. Rarely those factors are similar for a Charpy specimen and a real structural component. These factors are (Nussbaumer, Borges, and Davaine 2012):

- Service temperature

- Loading speed

- Size, shape, and type of cracks (or crack-like flaws, e.g. weld undercut)

- Dimensions of the structural member (also named thickness or constraint effect)

- Residual stresses

- Ratio of total stress experienced by component to material's yield strength, σ/f_y.

All these factors are considered in preparation of table of permissible thicknesses in Eurocode 3 part 1-10 (2005a) for prevention of risk of brittle fracture. To account for effect of each of the above factors on brittle fracture, proper assumptions (generally conservative) have been made pertaining to new structures which are executed according to EN 1090-2 (2008). That is why the requirements given in Section 3.5.1 are very conservative and probably will not be met by most older steel material. In those cases, assessment should proceed to phases II and III.

In case Charpy test data are not at hand for the studied bridge, no assessment can be made regarding the risk of brittle fracture until material tests are carried out. In such a situation, it would be better to consider proceeding to Phase III assessment and carrying out fracture toughness tests (see Section 3.5.3), which is a more accurate indicator of material toughness, compared to Charpy tests.

2.1.2 Fatigue assessment in phase I

Following the check-as-new-design approach of this assessment phase, damage equivalent method is used for evaluation of existing bridges. The principles of the method are shown in Figure 2.1. Basically, the factored stress range $\gamma_{Ff}\ \gamma_{Mf}\ \Delta\sigma_{E,2}$ is compared to fatigue strength (S-N curve) on the corresponding number of cycles to assess the fatigue safety, which is shown by parameter μ_{fat} (cf Equation (3-2)). The choice of fatigue resistance S-N curve is made via detail category tables (cf Section 3.4.1). To account for the variable amplitude nature of traffic loading, damage equivalent method according to EN 1993 part 2 (2006) shall be used.

If $\mu_{\mathrm{fat}} < 1$, the studied detail does not fulfil the safety requirements (with conservative assumptions). This means that more refined assessment of the element is needed (phases II and III). Based on μ_{fat} values, a list of candidate details for subsequent analyses (phases II and III) can be collected. This list of details with lowest μ_{fat} values, can determine the remaining fatigue life of the whole structure (for the case that no intervention is to be done). However, this estimation will be a conservative one.

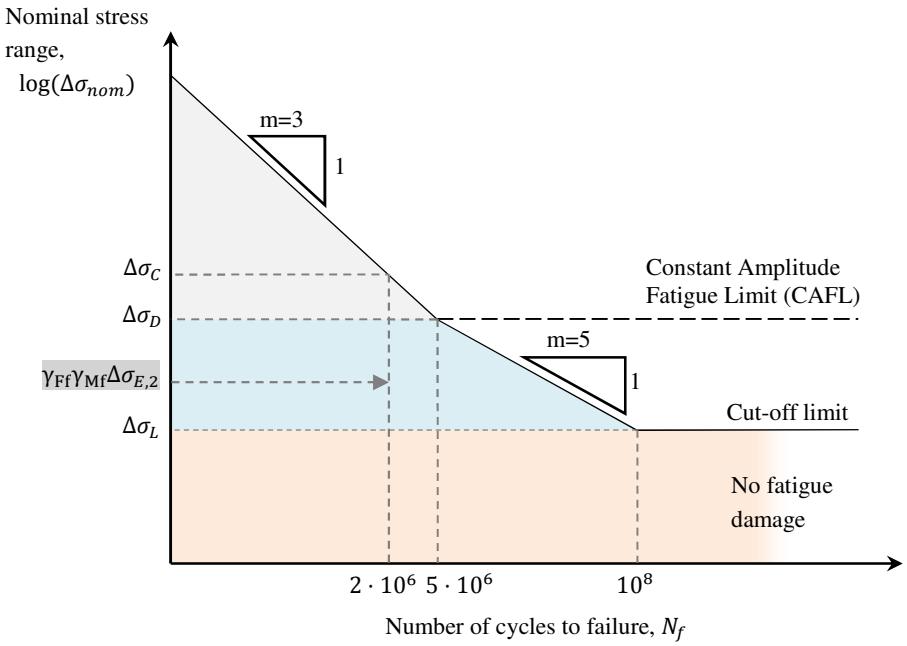

Figure 2.1 Evaluation of fatigue safety of the bridge details using S-N curves according to (EN 1993 2005a).

2.2 Phase II - Detailed investigation

In this phase, the conventional tools are used in a more comprehensive manner to re-evaluate only those members and details that showed unsatisfactory performance in the previous phase.

1. Resistance-side data: the tendency in this step should be to use pre-existing material data (from the previous phase) in a more refined analysis, and not to collect more material data. However, if a need for more test data has deemed necessary in the previous step (e.g. lack of past tensile test or CVN results), a limited test campaign might be considered.
2. Action-side data: the actual loading might be higher or lower than the design values. Realistic values for the permanent loads should be taken in this phase. As for the traffic loads, historical traffic load data (if available) should be used. Whenever uncertainty in the determination of loads exists, conservative assumptions based on conventional load models available in the standard should be used.
3. Modelling: simple global FE models, made of truss, beam, and shell elements are suitable at this level of assessment. Ideal support conditions and steel—concrete composite action (i.e. no deformation at the interface) can be assumed for boundary conditions.
4. Fatigue assessment: using the historical traffic data (and projected future traffic), a fatigue assessment based on cumulative damage approach (Palmgren-Miner's damage index) will be performed in this phase. As an alternative to nominal stress method, structural hot-spot or notch stress methods can be used, as presented by (Al-Emrani and Aygül 2013).

5. Brittle fracture assessment: the critical members are evaluated based on their stress level and material toughness according to Eurocode 3 part 1-10 (2005b). This is done using the table of permissible thicknesses given in the standard.
6. Outcome: at the end of this phase, those structural details that have shown inadequate performance even with a refined assessment are listed. Based on a cost-benefit analysis, recommendations can be made as to start the repair and upgrade work or continue with more detailed phase III evaluations. Usually, in case there is a weak detail or member that is replicated many times across the structure, it will be worth to accept the costs of advanced assessment and instead save on costs due to interruption of service of the bridge.

2.2.1 Brittle fracture assessment in phase II

The concept for control of brittle fracture in Eurocode 3 is based on the temperature-dependence of fracture toughness (cf Section C.3.1.1). Given the temperature-dependency of toughness properties and using master curve approach (K. Wallin 2002), see Section C.3.1.1, the fracture mechanics design criteria (K-method) can be rewritten as a minimum service temperature criteria (T-method). Table 3-7 in the previous section is also prepared based on the same assumption. Design criteria is transformed into the form of temperatures comparison (T-method):

$$T_{Ed} \geq T_{Rd} \tag{2-1}$$

The resistance-side temperature T_{Rd} in the above relation is calculated according to Section 3.5.2. Reference temperature, T_{Ed} at the detail susceptible to fracture is calculated from:

$$T_{Ed} = T_{min,d} + \Delta T_r + \Delta T_\sigma + \Delta T_R + \Delta T_{\dot{\epsilon}} + \Delta T_{\epsilon pl} \tag{2-2}$$

where:

$T_{min,d}$: lowest ambient temperature with a certain return period,

ΔT_r : temperature shift by radiation loss, $\Delta T_r = -5℃$ according to EN 1991-1-5 (2009),

ΔT_σ : temperature shift due to influence of stress, flaw, and detail geometry[1],

ΔT_R : temperature shift to provide safety margin (additive safety element, see below),

$\Delta T_{\dot{\epsilon}}$: influence of strain rate (loading speed),

$\Delta T_{\epsilon pl}$: influence of cold working

It is observed that unlike other familiar cases in Eurocode that use partial factors (multiplicative safety elements), safety concept is introduced into design by means of a temperature shift ΔT_R (additive safety elements). The details of transformation of fracture mechanical design equation to minimum service temperature design criteria is given in (G. Sedlacek, Feldmann, et al. 2008; Nussbaumer, Borges, and Davaine 2012).

For the purpose of Phase II, again Table 3-7 (maximum permissible thicknesses) can be used with the following considerations:

[1] The term ΔT_σ sums up the underlying fracture mechanics calculations and temperature-dependency of fracture toughness (master curve approach).

- Three stress levels, namely $\frac{0.25\sigma}{f_y(t)}$, $\frac{0.50\sigma}{f_y(t)}$, and $\frac{0.75\sigma}{f_y(t)}$, are given in the table. For intermediate values, linear interpolation should be used. thickness-dependent yield stress is calculated from following relation:

  $$f_y(t) = f_y - 0.25 \cdot t/t_0 \quad (2\text{-}3)$$

  where t is the plate thickness in mm and $t_0 = 1$ mm.

- The temperature effect of stress, flaw, and geometry (fracture mechanical term) are already considered in preparation of the table and are not required to be calculated; i.e. $\Delta T_\sigma = 0℃$
- Temperature shift as the safety element is equal to $\Delta T_R = 0℃$; i.e. it is already included in the values shown in the table
- The values in the table are calculated with the assumed strain rate of $\dot{\epsilon_0} = \frac{d\epsilon}{dt} = 1 \times 10^{-3} s^{-1}$; This value covers dynamic effects of majority of transient loads, including traffic loads and normally is not required to be included in the calculation. In case a higher load rate (e.g. impact) is available, the effect of strain rate $\dot{\epsilon}$ should be taken into account by corresponding temperature shift expression (EN 1993 2005c):

  $$\Delta T_{\dot{\epsilon}} = -\frac{1440 - f_y(t)}{550} \times \left(\ln \frac{\dot{\epsilon}}{\dot{\epsilon_0}}\right)^{1.5} \quad (2\text{-}4)$$

  where $\dot{\epsilon}$ is the strain rate in s^{-1}.

- Typically, cold worked rolled elements are not used for the bridge members; therefore, it is assumed that $\Delta T_{\epsilon pl} = 0$.

2.2.2 Fatigue assessment in phase II

As was stated before, Palmgren-Miner damage accumulation rule is used in this phase to consider variable-amplitude nature of traffic loading:

$$D = \Sigma \left(\frac{n_i}{N_i}\right) \leq 1 \quad (2\text{-}5)$$

Where n_i is the number of cycles occurring at stress range magnitude $\Delta\sigma_i$ of the loading spectrum; and N_i is is the number of cycles corresponding to the fatigue strength at stress range value of $\Delta\sigma_i$. The Palmgren-Miner method assumes that the fatigue failure has occurred when the damage index D reaches a certain value. This value in Eurocode is chosen as $D = 1$, as indicated in the above Equation.

N_i is calculated as:

$$N_i = N_C \cdot \left(\frac{\Delta\sigma_C}{\gamma_{Mf} \cdot \gamma_{Ff} \cdot \Delta\sigma_i}\right)^m \quad (2\text{-}6)$$

Instead of nominal stress method, alternative stress-based fatigue evaluation methods, namely structural hot spot stress (SHSS) method, and effective notch stress (ENS) methods can be used. Al-Emrani and Aygül (2013) have presented a comprehensive explanation of these methods together with examples and use cases. The reader is referred to this comprehensive document for details of the application of these methods.

2.3 Phase III - Expert investigation

For special cases where large risks exist in the case of a failure, and when the results from the two previous steps have shown an unsatisfactory performance of structural members, an expert investigation can be used for more accurate assessment of the structure. The main tool to use in this stage is the fracture mechanics approach for both fatigue damage prognosis and brittle fracture of structural details.

The fracture control in Phase III deals with structural strength in presence of cracks, and the time required for cracks to grow to an unsafe size. Thus, in the so-called damage tolerance analysis two factors should be determined:

1. the effect of cracks on strength (brittle fracture or ductile tearing)
2. the crack growth as a time-dependent phenomenon (fatigue)

Linear Elastic Fracture Mechanics (LEFM) is used for determining the above factors.

From fracture mechanics viewpoint, the failure occurs when the applied force that tends to extend the crack (the crack driving force) surpasses the material's resistance to the extension of that crack. The material's resistance is called the material's fracture toughness.

For the successful application of LEFM, more extensive input data are required. An advantage of the method is that it does not require the past (historical) load data; only current and future loading data are required. Instead, it requires more information on material properties (fracture toughness, crack growth rate, etc.), plus information about the existing flaws (cracks or crack-like defects) in the structure.

Although the Eurocode EN 1993-1-9 (2005) allows the use of the damage-tolerant method for fatigue assessment, it does not give relevant guidelines for doing so. It is also worth noting that under current Swedish National Annex TRVFS 2011:12 (Trafikverket 2012) only the safe-life method is allowed for the design of new structures.

2.3.1 Brittle fracture assessment in phase III

EN 1993-1-10 allows for the use of fracture mechanics for advanced assessment. This Eurocode includes commentary document (G. Sedlacek, Feldmann, et al. 2008) which provides extensive details and guidance on the application of the method for several cases, including the evaluation of existing bridges. The commentary document gives three different alternatives for assessment against brittle fracture. Nonetheless, in maintaining the same safety margin, all of them remain consistent with the temperature comparison concept (T-method) presented in Equation (2-1). Here, one method designated as *case 2b* is presented which is a K-method, i.e. comparing fracture toughness of the material against applied stress intensity factors:

$$K_{Ed}^{*} \leq K_{Rd} \tag{2-7}$$

Where K_{Ed}^{*} is the design value of applied stress intensity factor K_{Ed}, combined with secondary effects from local plasticity and residual stresses. K_{Rd} is the temperature-dependent material's fracture toughness. We can rewrite Equation (2-7) as:

$$K_{Ed}^{*} \leq K_{mat}(T_{Ed}) \tag{2-8}$$

This means the fracture toughness value should be measured for the lowest design temperature T_{Ed}, according to Equation (2-2). Note that for this case, the safety element is taken as $\Delta T_R = -40℃$.

For clarification, the design situation for brittle fracture is of an accidental nature. Several conditions should co-exist for brittle fracture to take place: occurrence of frequent design load at an already propagated crack, while the temperature is the lowest design temperature, the low temperature being the accidental action (leading action). Thus:

$$E_d = E\{G_k; T_k; \psi_1 \cdot Q_{k,1};\ \psi_{2,i} \cdot Q_{k,i}) \tag{2-9}$$

where

G_k	: characteristic value of permanent action effect,
T_k	: lowest service temperature
$Q_{k,1}$	: characteristic value of the traffic load (or dominant variable load),
$\mathrm{Q_{k,i}}$	: characteristic value of accompanying variable loads,
ψ_1 and $\psi_{2,i}$	: representative load combination factors per EN 1990.

Design value of stresses: To consider the effect of residual stresses on the fracture, their characteristic value is added to the combination. The conclusion from the commentary document was that a value of $\sigma_{res} = 100MPa$ added to the design stresses. Therefore, the combination of actions to consider for calculation of σ_{Ed} becomes:

$$\sigma_{Ed} = \sigma_G + \psi_1 \cdot \sigma_Q + \sigma_{res} \tag{2-10}$$

Design value of crack size: The design approach for phase III is damage tolerant. It means that a safe service period is considered for the structure which is defined as the period between major inspections or the period until the bridge will be decommissioned. Therefore, for calculation of crack size, its growth from its current/initial size (a_0) to its size at the end of safe service period (Δa_{FCG}) should also be considered:

$$a_d = a_0 + \Delta a_{FCG} \tag{2-11}$$

Where a_d is the final crack size at the end of safe service period. a_0 is either postulated (see 3.4.3.3) or preferably measured by non-destructive testing (see Appendix B). Crack growth from fatigue crack growth, Δa_{FCG}, can be estimated by the method given in Appendix A, Equation (A-8).

Design value of plasticity-corrected stress intensity factor, K^*_{Ed}: following relation is used for calculation:

$$K^*_{Ed} = \frac{K_{Ed}}{k_{R6} - \rho} \quad \text{in } \left[MPa\sqrt{m}\right] \tag{2-12}$$

where

- K_{Ed} is elastic stress intensity factor calculated according to Appendix A, for a crack size of a_d and an applied stress of σ_{Ed}:

- k_{R6} is the plastic correction factor for the R6 Failure Assessment Diagram (FAD). See Table 2-5 in commentary document for calculation method. k_{R6} value is in the range [0.816,1] and can be conservatively taken as 0.816.
- ρ is the correction factor for local residual stresses and again, can be calculated from directions given in the commentary document of EN 1993-1-10 (G. Sedlacek, Feldmann, et al. 2008).

The assessment steps for phase III described above are summarized in Figure 2.2.

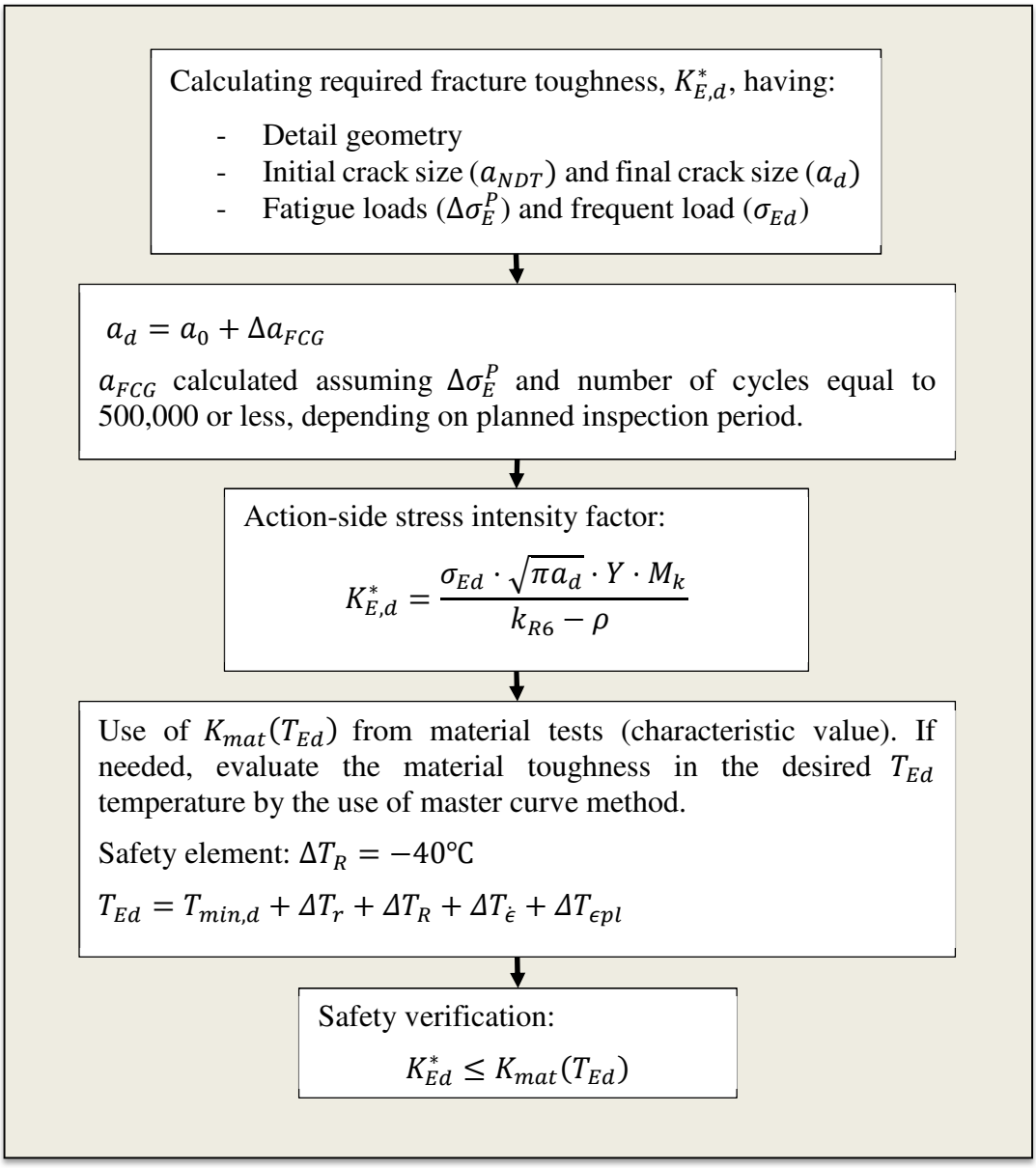

Figure 2.2 Summary of brittle fracture assessment for Phase III (K-method) according to (G. Sedlacek, Feldmann, et al. 2008).

2.3.1.1 Alternative method: assessment of safe service period

The safety concept for the phase III assessment described above (the temperature shift concept) is consistent with assessments of phases I and II. All the methods presented

so far assess the structural safety at a level equivalent to that of new structures. Improvements in assessments only come from accurate determination of resistance-side and action-side parameters. The alternative method presented in this section does not follow those safety considerations. It is based on the so-called "safe service period" approach originally given in the commentary document (G. Sedlacek, Feldmann, et al. 2008) for existing riveted bridges. In the "safe service period" approach, the objective is to evaluate the interval between inspections, T_{insp}, such that it is smaller (by a margin) than the calculated safe service life of the critical detail(s) in the bridge, $T_{service}$:

$$T_{insp} = \frac{2}{3} * T_{service} \tag{2-13}$$

where $T_{service}$ is the time (i.e. number of cycles) required for a postulated crack to grow to its critical size. The safe service period is schematically presented in Figure 2.3; inspection intervals are a fraction (two-thirds) of the safe service period. At the end of each inspection interval, main inspection of critical details should take place. If fatigue cracking in critical locations is observed, they will be repaired. After the main inspection, the postulated initial crack size in the detail is reset to a_0 and another safe service period starts. Equation (2-13) can be used if "damage tolerance" is applicable, which means the two following conditions should be observed:

1. The variable loads on the structure should be monitored
2. At the end of each inspection interval, a main inspection for detecting cracks and flaws in the critical details should be conducted using proper NDT methods.

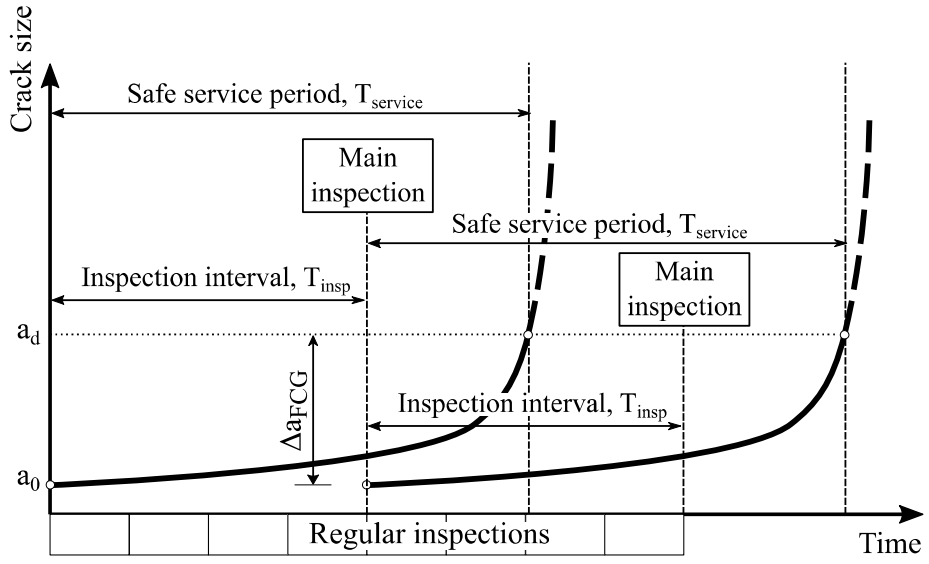

Figure 2.3 Determining inspection intervals in the "safe service period" approach. Inspection intervals are a fraction of safe service period; safe service period is determined as the time required for a postulated crack to grow from its initial value a_0 to the design value a_d. After each main inspection, if no defect is found (or the defects are repaired), a new safe service period can be started.

For the alternative assessment method, the dominant action is the variable traffic load. Moreover, the load and resistance partial factors are taken as $\gamma_F = \gamma_M = 1$ (G. Sedlacek, Feldmann, et al. 2008). The design equation in this method is similar to Equation (2-8), but the check is done for the service temperature $T_{min,d}$ instead of design temperature T_{Ed}:

$$K^*_{Ed}(a_d) \leq K_{mat}(T_{min,d}) \tag{2-14}$$

In order to evaluate the inspection intervals:

- Calculate critical crack size a_d by solving the inequality (2-14) as an equation,
- Calculate the number of cycles in safe service period, $N_{service}$, from Equation (A-9); subsequently evaluate $T_{service}$,
- Evaluate inspection interval time from (2-13).

2.3.2 Fatigue assessment in phase III

The assessment in this phase is done by crack growth calculation from linear elastic fracture mechanics (LEFM) approach, as presented in Appendix A (see Section A.3). One advantage of the method compared to the so-called stress-based fatigue classification methods (nominal stress method, structural hot spot stress method, notch stress method) is that, the LEFM approach can provide valuable information on prognosis of crack growth, i.e. crack size and crack growth rates at different stages of loading history. Equation (A-8) is used for calculation of crack growth under constant amplitude loading condition. For crack propagation under variable amplitude loading, see Section A.3.1 and previous BBT report (Zamiri, Leander, and Al-Emrani 2016).

The fatigue resistance of a detail is considered exhausted when the fatigue crack grows to a critical length. So, the limit state for control against fatigue can be written as (JCSS 2001):

$$a_N \geq a_d \tag{2-15}$$

where a_N is the length of the crack after N loading cycles and a_d is the critical crack length. a_d can be calculated as explained in Section 2.3.1.1 or can be approximately taken as half of the thickness of the cracked plate. The number of cycles required for crack size a_0 to reach the size a_d will determine the fatigue life of the detail. If necessary, this number of cycles, N_P, can then be used for determination of the time interval between inspections according to Equation (2-13).

This fatigue assessment method is quite similar to the safe service period approach (Section 2.3.1.1). The only difference is that for the safe service period approach, the effect of low service temperatures ($T_{min,d}$) is included in the evaluation of critical crack length a_d.

2.4 Summary

The basis of evaluation and corresponding limit states for control of fatigue and brittle fracture in each of the three assessment phases were given in this chapter. Resistance-side and action-side parameters for each step were briefly presented as well. A summary of the multi-step evaluation method discussed in this chapter is shown in Figure 2.4.

For the brittle fracture assessment, the safety format is based on the temperature shift and is the same in phases I, II, and III. The three phases differ only in evaluation accuracy of the action-side and resistance-side data. The only exception is the “safe service period” method that is presented as an alternative method for phase III assessment.

Phase I – Preliminary assessment

Using simple analysis methods to clarify uncertainties about structural safety of the bridge. The bridge is considered as if it is being designed as new.

Resistance-side data:

- Site visit(s)
- Material properties from design documents ($R_{eL,5\%}$, CVN, K_{Ic}, etc.), §3.4.1 and §3.5.1
- Chemical composition §3.2

Action-side data:

- Traffic loads §4.2.2

Modelling method: Chapter 5
Fatigue evaluation, $\mu_{fat} = \Delta\sigma_c/(\gamma_{Ff} \cdot \gamma_{Mf} \cdot \Delta\sigma_{E,2})$ §2.1.2
Brittle fracture evaluation §2.1.1

Output: List of critical details, report on preliminary safety checks, conformity of the bridge to the design documents, past inspections and present condition of the bridge.

Phase II – Detailed assessment

Implement more refined analyses on the critical members identified in the previous step. Input data is supplied form information collected from phase I.

Resistance-side data:

- Local approaches for fatigue §3.4.2
- T_{K100} for brittle fracture §3.5.2

Action-side data

- Traffic loads §4.2.3

Modelling method: Chapter 5
Fatigue evaluation, $D = \Sigma(n_i/N_i) \leq 1$ §2.2.2
Brittle fracture evaluation §2.2.1

Output: Determining remaining fatigue life of the critical details.

Phase III – Advanced assessment

Implement more refined analyses on the critical members identified in the previous step. Input data is supplied form information collected from previous step.

Resistance-side data:

- Material tests §3.5.3 and Appendix C
- NDT §3.4.3.2 and Appendix B

Action-side data

- Load monitoring and Stress measurements §4.2.4

Modelling method Chapter 5
Fatigue evaluation, LEFM §2.3.2 and Appendix A
Brittle fracture evaluation § 2.3.1

Output: Determination of remaining service life and safety of critical details with improved accuracy. Information about the progress of damage process, inspection intervals

Figure 2.4 Summary of multi-step evaluation procedure. chapter and section numbers refer to the relevant parts in the current report.

3 Resistance-side parameters

Ductile fracture occurs when the stresses acting on the member surpass its ultimate tensile strength. In contrast, brittle fracture occurs as a combination of three critical factors: a low material toughness, stresses acting on the member, and a flaw (pre-existing or developed from fatigue process). These three factors are illustrated in Figure 3.1. In this chapter, two of these factors, namely flaws and material toughness properties are discussed. These two factors are considered under collective term resistance-side parameters.

In the first section of this chapter, a brief review of historical steel types used in welded structures and chemistry of construction steel alloys are discussed, as this knowledge is necessary for an assessment project.

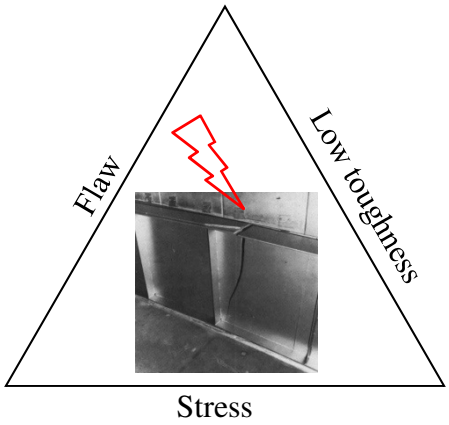

Figure 3.1 *The three factors that contribute to brittle fracture. The image in the middle: Brittle fracture of welded girder in King's bridge, Melbourne, after Boyd (1970).*

3.1 Intro to historic steel types

The steels produced in the first half of 20th-century show larger inhomogeneity in their microstructure and mechanical properties. This is due to the difficulty in eliminating impurities and controlling alloy composition by older steel manufacturing methods. Early production standards stipulated lower quality requirements, compared to the standards that are in place to date. Some phenomena, e.g. lamellar tearing, were not implemented in codes until the late 1960s after catastrophic failures took place (Boyd 1970).

In contrast, the composition and mechanical properties for different types of steel currently used for the construction of new bridges are well-defined by the modern standards, such as EN 10025 (2004). Also, strict controls are in place to ensure compliance of steel products with those standards. These factors provide the safety basis required for the design of new structures. Since these preliminary safety requirements for material production were not in place for older steel and composite bridges, the material strength (and its variation) needs special consideration in the structural assessment.

3.1.1 Steelmaking methods

For the old steels, the impurities in the final material (thus the material quality) were affected considerably by the early production methods. That is why a brief review of the prevalent methods is presented here. Figure 3.2 (in German) presents the prevalence of various methods (in terms of percentage of annual steel production worldwide) in different eras for the past two centuries.

The invention of low-cost Bessemer converter in the middle of the 19th century led to rapid increase in the use of steel in machines and structures, including steel bridges (Hobbacher 2000). In this method, excess carbon is removed from molten pig iron[2] by oxidation through blowing air into it. The decarburized liquid steel is then cast into ingots for subsequent manufacturing processes, e.g. rolling.

Further refinements of Bessemer process were introduced by Sydney Thomas in 1880, and later by Robert Durrer in 1948 (Basic oxygen method or Linz-Donawitz method). LD process is still the most popular steelmaking method; two-thirds of world's steel is produced using this method.

Open hearth furnace was invented by Siemens and further developed by Martin for use in steelmaking in 1865. The steel produced by Siemens-Martin method was less brittle compared to Bessemer steel and Thomas steel since it was exposed to much less nitrogen during the production. The good quality of steel in the open-hearth furnace was obtained at the expense of its slow operation speed. At its peak time, Siemens-Martin steelmaking method was used for around 75% of world steel productions; but most open-hearth furnaces were shut down by the early 1990s, mainly due to the time-inefficient production. Currently, this method is used for manufacturing of less than 10% of the steel produced worldwide.

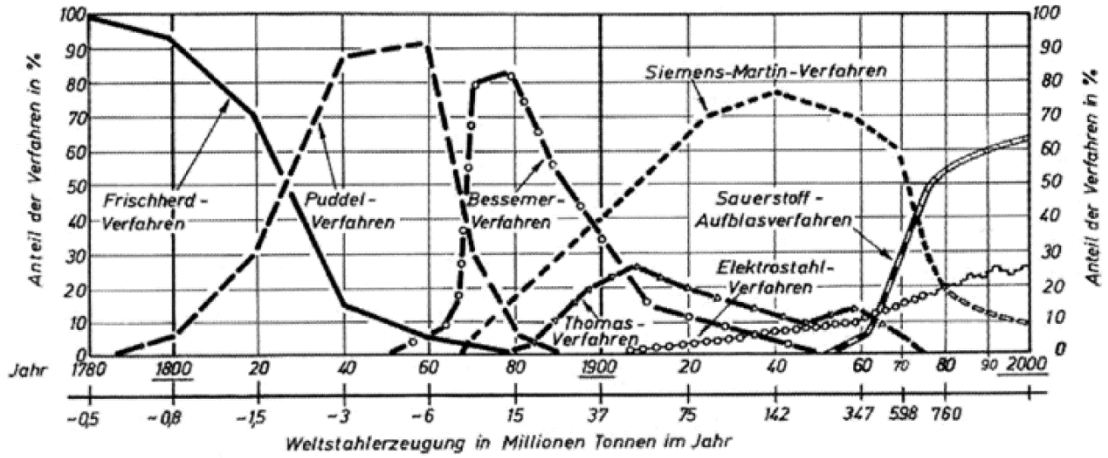

Figure 3.2 Comparison of annual worldwide production of different steels 1780—2000 (vertical axis: percentage of different production methods); according to Bosshard & Plätzer (2013), originally from Prokop (2012).

[2] Pig iron is an intermediate product in steel making, which has a high carbon content (3.5%-4.5%)

With the development of electric arc furnaces (EAFs) after WWII, scrap steel could be melted quickly, efficiently and without the use of fossil fuels. The heat required for the melting of the steel is provided by electric arcs at temperatures of up to 3000 °C. Less than one-third of the world's steel production is obtained from scrap metal; This proportion is expected to increase further in the future (Bosshard and Plätzer 2013).

In the Bessemer process, the converter has a clay lining (acidic), which makes it suitable for processing of only low-phosphorus pig iron (Eriksson 2011). In the Thomas process the lining was changed to basic (dolomite), therefore a high-phosphorous-content pig iron could also be converted. In the Siemens-Martin process, better control of alloying elements and impurities is possible; As a result, the nitrogen content of Siemens-Martin steel is lower than that of Bessemer and Thomas steels.

Another important manufacturing factor contributing to the quality and grade of final product is the heat treatment process. For a review of various heat treatment processes (hot rolling, normalized rolling (N), thermo-mechanically rolling (TM), quenching and tempering (QT)), refer to Günther (2005). A timeline of steel production for construction steels of welded structures is presented in Figure 3.3. Table 3-1 summarizes the construction steels used for welded structures in the past century.

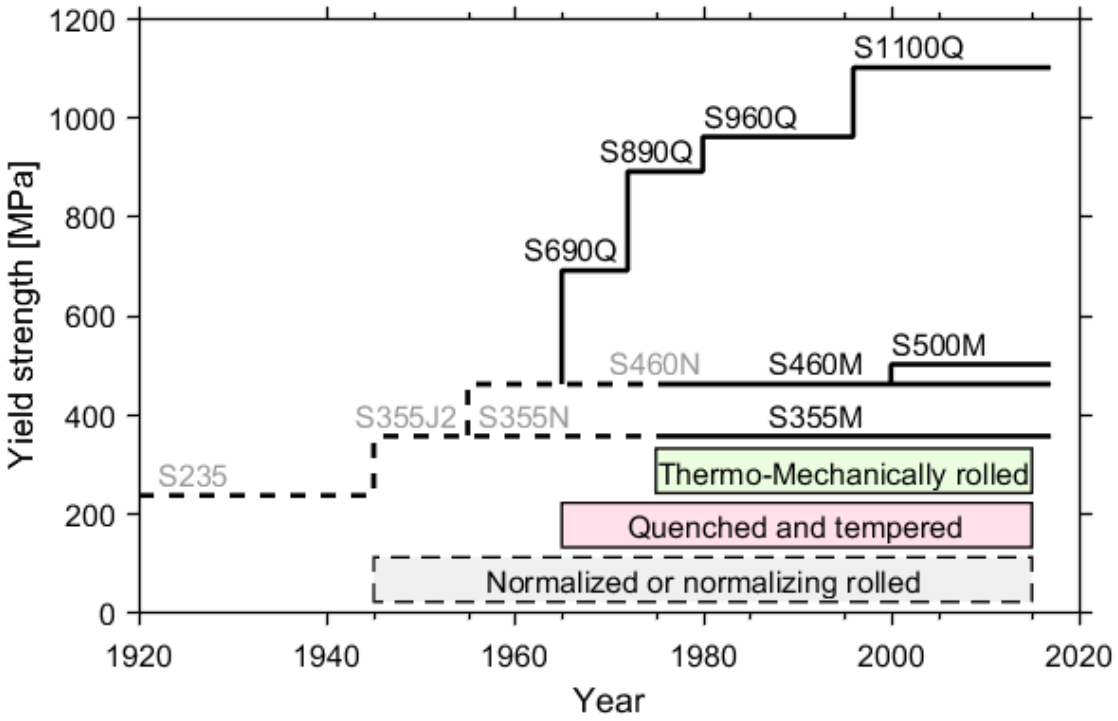

Figure 3.3 Timeline of the introduction of different steel grades into European steel market; Modified from (Günther 2005).

Table 3-1 Summary of characteristics of mild construction steels produced in the 20th century onwards; from Günther (Günther 2005; Kühn et al. 2008). For older steels consult (Rosemarie Helmerich 2005; Kühn et al. 2008; Tobias Larsson 2009).

	Mild steel (20th century)			
Steelmaking method	Blast process • 1855 – ~1900 Bessemer steel (in construction) • 1880 – ~1980 Thomas steel • 1948 – To date Linz-Donawitz steel Heart process • 1865 – ~1990 Siemens-Martin steel			
Heat treatment	Hot rolling	Normalized or normalizing rolled	Thermomechanical rolling	Quenching and tempering
Microstructure	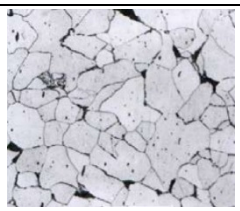 Ferrite/Pearlite	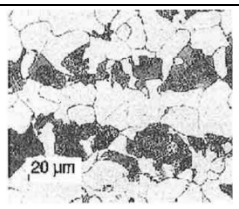 Ferrite/Pearlite, finer grains	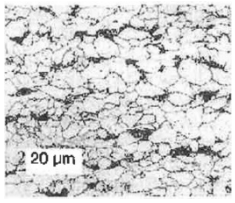 Ferrite/Pearlite + Bainite	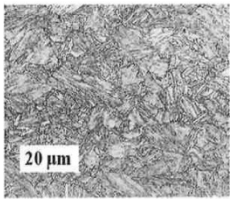 Bainite
Steel grades	S235 S275	S355J2 S355N/S355NL S460N/S460NL	S355M S460M S500M	S690Q S890Q S960Q S1100Q
Comments	The main production method until 1950. Control composition and impurities for older steels. $f_{uk} \approx$ 235-275 MPa $f_{yk} \approx$ 370-440 MPa $A_g \approx$ 15-25%	Fine grain steels. Until 1950, S355J2 (previously named St52), was known as high strength steel.	Excellent weldability due to low alloying elements in the composition.	High strength steels

It should be noted that the characteristics of steels that are used in welded structures built from 1966 onwards are fully consistent with general technical delivery conditions provided by modern Eurocodes, such as EN 10025 (2004) (Kühn et al. 2008).

3.2 Chemical composition

Chemical analysis can be used for identification of old steel material. The chemical composition of a steel alloy is a major factor that contributes to its mechanical properties, although chemical composition is not the only factor in steelmaking that contributes to the mechanical properties of the final product. There are other important factors in manufacturing that will contribute to the microstructure and mechanical properties of the steel product; namely thermal and mechanical treatment (e.g. rolling, tempering, normalizing).

The main alloying element for Bessemer and Thomas steels is carbon, whence coming the name Carbon steel. The high strength was achieved by increasing the carbon content, at the expense of reduced ductility and toughness. Carbon steels showed poor performance in terms of brittle fracture, especially after their use in early welded structures. The occurrence of disasters before and after WWII led to post-war efforts to improve the weldability of steels by limiting carbon-content and eliminating slag inclusions, Phosphorus and Sulphur content.

Further developments resulted in the introduction of "killed steel" in which Silicon was added to the alloy. Excess oxygen in the molten steel reacts with silicon to form solid silicon oxide, instead of causing porosity (bubbles) in the solidified ingot, as is the case for older "rimmed steel" products.

To retrieve part of reduced yield stress due to the reduction of carbon content, manganese was added to the steel alloy. Manganese affects the toughness in a complex manner, but its overall effect is slight increase the toughness. Nevertheless, its effect on yield strength is more noticeable. All modern structural steels are of this so-called "Carbon-Manganese" (C-Mn) steel type.

The only construction steels available in Europe until 1970's consisted of equivalents of St37 (S235), St52 (S355), and St44 (S275). The oil crises in the 70's motivated innovations in saving materials and energy. This led to the development of high strength low-alloyed (HSLA) steels (Ponge 2005). For HSLA steels, in addition to carbon (content 0.05–0.25%) and manganese (up to 2%), very small amounts of "micro-alloying" elements (titanium, vanadium, niobium, etc. are added to produce a fine-grain microstructure. Reducing the grain size is the only method for increasing both yield strength and toughness of steel at the same time. The other methods (e.g. alloying with carbon) have a detrimental effect on toughness while increasing the yield strength (Ponge 2005).

Table 3-2 presents typical element contents of traditional steelmaking methods, along with the effect of various elements on mechanical properties of steel (yield strength, ultimate tensile strength, Charpy V-notch energy) and its weldability (see also Section 3.2.2). As the table shows, Sulphur, Phosphorus, and Nitrogen have a detrimental effect on ductility, toughness, and weldability. Therefore, they are considered as impurities, not alloying elements.

Table 3-2 Typical element contents in the steel alloy for older steelmaking methods, together with the effect of alloying elements on properties of low carbon steel (+ denotes increasing effect, − denotes decreasing effect); Adapted from (Tobias Larsson 2009). Maximum allowable element contents for modern steel S355J2 are given for comparison.

Element	Element content [weight%]				Effect on properties				
	Bessemer steel	Thomas steel	Siemens-Martin steel	*S355J2*[*]	R_m	R_{eh}	A_g	CVN	Weldability
C	0.02-0.1	0.1-0.2	0.1-0.2	*0.2*	+	+	−	−	−
Si	≥ 0.08	< 0.08		*0.55*	+	+	−	−	−
Mn	0.3-0.5	0.4-0.5	0.4-0.5	*1.6*	+	+	−	+	+
P	0.04-0.07	0.04-0.12		*0.025*	+	+	−	−	−
S	< 0.1	≈ 0.01	≈ 0.01	*0.025*	−			−	−
N	> 0.01	> 0.01	< 0.01	*≈ 0.0*	+		−	−	−
Cr					+	+	+	−	−
Ni					+	+	−	+	
Mo					+	+	−	−	+
Cu				0.55	+	+	−	−	
Al					+		−		−

[*] Maximum allowable values according to EN 10025-2 (2004)

3.2.1 Through-thickness property variation

Eriksson (2011) has provided a detailed explanation of the phenomena occurring during casting and rolling of old steels. In brief, the metal ingot cools down and solidifies from its outer envelope towards the inner core. Lower solubility of impurities, gases, and alloying elements in the solid state leads to higher concentration of these components in the parts that will solidify the latest (i.e. at the inner core). Accordingly, the outermost parts of the ingot are the "cleanest" and of higher mechanical properties, compared to its inner core. Traditional hot rolling would not change this non-homogeneity in through-thickness composition. This means the rolled plate that has produced from a non-uniform ingot still contains the same impurities in its midplane, while the parts close to the surface are of higher quality. The through-thickness non-homogeneity should be considered when material samples are to be tested for older steels, especially thick-plate members. One method to take into account this inhomogeneity effect is given by Sedlacek et al. (2008) based on the work of Kühn (2005) as a shift of transition temperature.

3.2.2 Weldability

According to American Welding Society (AWS), weldability is defined as "The capacity of a metal to be welded under the fabrication conditions imposed into a specific suitably designed structure and to perform satisfactorily in service". The weldability issue should be addressed in the assessment phase; because it will be needed for subsequent repairs and interventions of the structure.

For modern steels produced after 1966, weldability can be determined using carbon equivalent (CEV) formula from International Institute of Welding (IIW):

$$CEV = C + \frac{Mn}{6} + \frac{Cr + Mo + V}{5} + \frac{Ni + Cu}{15} \quad (3\text{-}1)$$

Where the element symbols represent weight percent of the corresponding elements in the steel alloy of the parent metal. A carbon equivalent (CEV) of 0.4 or lower indicates a very good weldability, meaning that there is little potential for cracking in the heat-affected zone (HAZ) of the welded joint.

However, for older steels use of common carbon equivalent Equation (3-1) is not recommended (Kühn et al. 2008), because it was originally developed to address the weldability of modern steels. Instead, Kühn et al. (2008) suggest the diagram in Figure 3.4 for the first proof of weldability of old steels. As can be seen, the high content of nitrogen, sulphur and phosphorous in older steels have an undesirable impact on the weldability. The effect of nitrogen on brittleness of steel is explained in more detail in the following section. In case the results of chemical tests are not available, Kühn et al. (2008) have provided some simple on-site tests for preliminary tests for weldability.

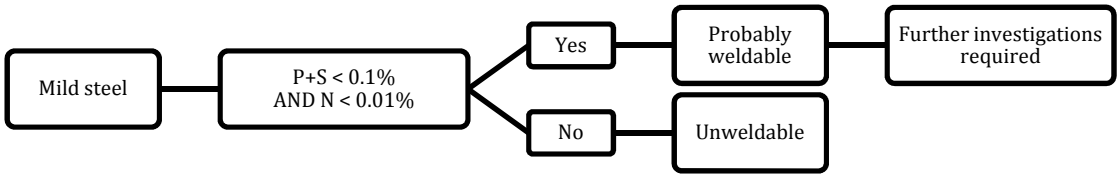

Figure 3.4 Preliminary proof of weldability for old steels; Adapted from Kühn et al. (2008).

3.2.3 Ageing

Nitrogen is an impurity in the steel alloy that has a detrimental effect on its toughness. The nitrogen atoms tend to diffuse in the ferritic lattice structure and concentrate at dislocations, therefore blocking the movement in the dislocations, which in the macroscopic level means lower ductility and higher brittleness. This phenomenon is called aging. In fact, both interstitial elements, nitrogen and carbon, can contribute to the aging phenomena, but the role of nitrogen is dominant (C. Klinger et al. 2011).

The diffusion process of nitrogen atoms is unnoticeable in ambient temperatures, but it is accelerated at elevated temperatures (especially above 200°C, thermal aging), such as during the slow cooling after a heat treatment or in the HAZ region after welding. Ageing also occurs when plastic deformations take place (strain aging). In modern steels, aluminium is added as a deoxidizing agent to diminish the effect of aging (Shafie and Sabardin 1997). Aluminium combines with oxygen and nitrogen to form aluminium oxide and aluminium nitride.

Table 3-3 shows typical nitrogen content for various steelmaking processes. One steelmaking process notorious for high nitrogen content in the final product is the Thomas process. Thus, Thomas steels generally show low toughness and the effect

could be worse at the weld HAZ or in the areas that have undergone plastic deformation (e.g. cut edges or stamped holes in the plates).

To show an example of failures in Thomas steel, the failure of a riveted power transmission tower in Germany can be mentioned. Klinger and colleagues (2011; 2013) investigated the case in detail. The conclusion was that combined effect of increased loads, low temperature and brittle material at the location of stamped holes led to brittle fracture in the tower. Figure 3.5 shows the microstructure of the studied Thomas steel. Nitride plates that block the deformation within the grain are visible in the image.

In their study of the effect of aging on steels produced in three different eras, (Shafie and Sabardin 1997) observed that aging manifests the following changes in characteristics of carbon steels:

- Increase in the yield point and the tensile stress
- Decrease in ductility (they observed ~20% reduction in the ductility of their studied steels)

They pointed out that the mechanical properties and chemical analysis are equally important for the assessment of aging in the steel material. The decrease in ductility (from aging), combined with the presence of high sulphur and phosphorous content leads to a steel material highly susceptible to brittle fracture.

Due to complex nature of aging effect and its high dependence on cold working and temperature history, a quantification of aging in relation to the nitrogen content cannot be easily made.

Table 3-3 Typical nitrogen content (in weight percentage of steel alloy) for various steelmaking process; adapted from Bofors handbook (Thelning 1984).

Steelmaking process	N [%wt]
Bessemer	0.014
Thomas	0.012
Siemens-Martin	0.007-0.010
Linz-Donawitz (LD)	0.004

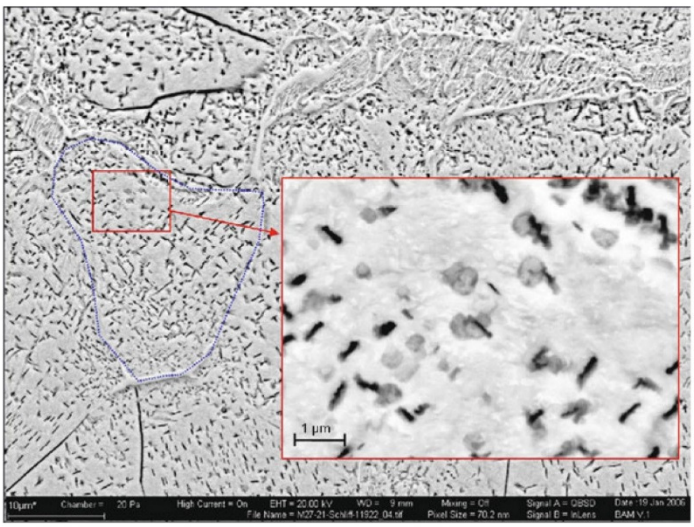

Figure 3.5 Microsection of Thomas steel sample from the collapsed power transmission tower. The dotted line indicates a ferrite grain. The accumulation of nitride plates (seen as black lines) within the grain is observable in the close-up image. (C. Klinger et al. 2011).

3.3 Strength and ductility

One of the key features for identification and assessment of old steel bridges is the tensile strength of their material. If the steel grade is known, the values given by the document "TDOK 2017:0267 – Bärighetsberäkning av broar" (Trafikverket 2017) can be used. The data for this document is derived from the extensive study conducted in the framework of sustainable bridges (Tobias Larsson 2009; Sustainable Bridges 2007). If the material properties for the studied steel are not known, TDOK 2017:0267 recommends using those of the steel SS 1311(f_{yk} = 220 MPa, f_{uk} = 360 MPa). The modulus of elasticity is the same for all steel grades, i.e. E=210 GPa.

3.4 Fatigue strength

3.4.1 Phase I: detail categories

Fatigue assessment based on detail categories (also named classification method, nominal stress method, or fatigue C-classes) is the basic and most widely used fatigue design method. It is the method of choice for most of the newly designed structures but is also an analysis option fit for the purpose of Phase I assessment, which is to identify the critical details rapidly and with acceptable accuracy. Based on large datasets of fatigue test results for different welded details with various configurations, a number of design S-N curves are presented in the part 1-9 of Eurocode 3 (2005a). The Eurocode provides a set of 14 equally-spaced fatigue resistance S-N curves, see Figure 3.6.

The fatigue strength S-N curves pertaining to the nominal stress method for welded structures include the influence of material, geometry and weld quality; therefore, when using this method for the welded structures built earlier than 1970, where weld quality standards were not consistent with modern era, the suggested detail category by the Eurocode 3 should be reduced by one or two fatigue classes to account for lower weld quality (i.e. potentially larger weld defects).

For the fatigue limit state, the safety level μ_{fat} is calculated as:

$$\mu_{fat} = \frac{\Delta\sigma_c}{\gamma_{Ff} \cdot \gamma_{Mf} \cdot \Delta\sigma_{E,2}} \tag{3-2}$$

Where:

$\Delta\sigma_c$: fatigue strength at 2 million cycles (or detail category),

$\Delta\sigma_{E,2}$: equivalent constant amplitude stress range corresponding to 2 million cycles,

γ_{Ff} : partial factor for equivalent constant amplitude stress range $\Delta\sigma_{E,2}$,

γ_{Mf} : partial factor for fatigue strength $\Delta\sigma_c$.

$\Delta\sigma_c$ is the resistance-side factor that is taken from corresponding detail category. $\Delta\sigma_{E,2}$ belongs to the load-side, see Equation (4-1). Figure 3.7 depicts usual detail categories available in a composite bridge deck with I-girders for easy referencing.

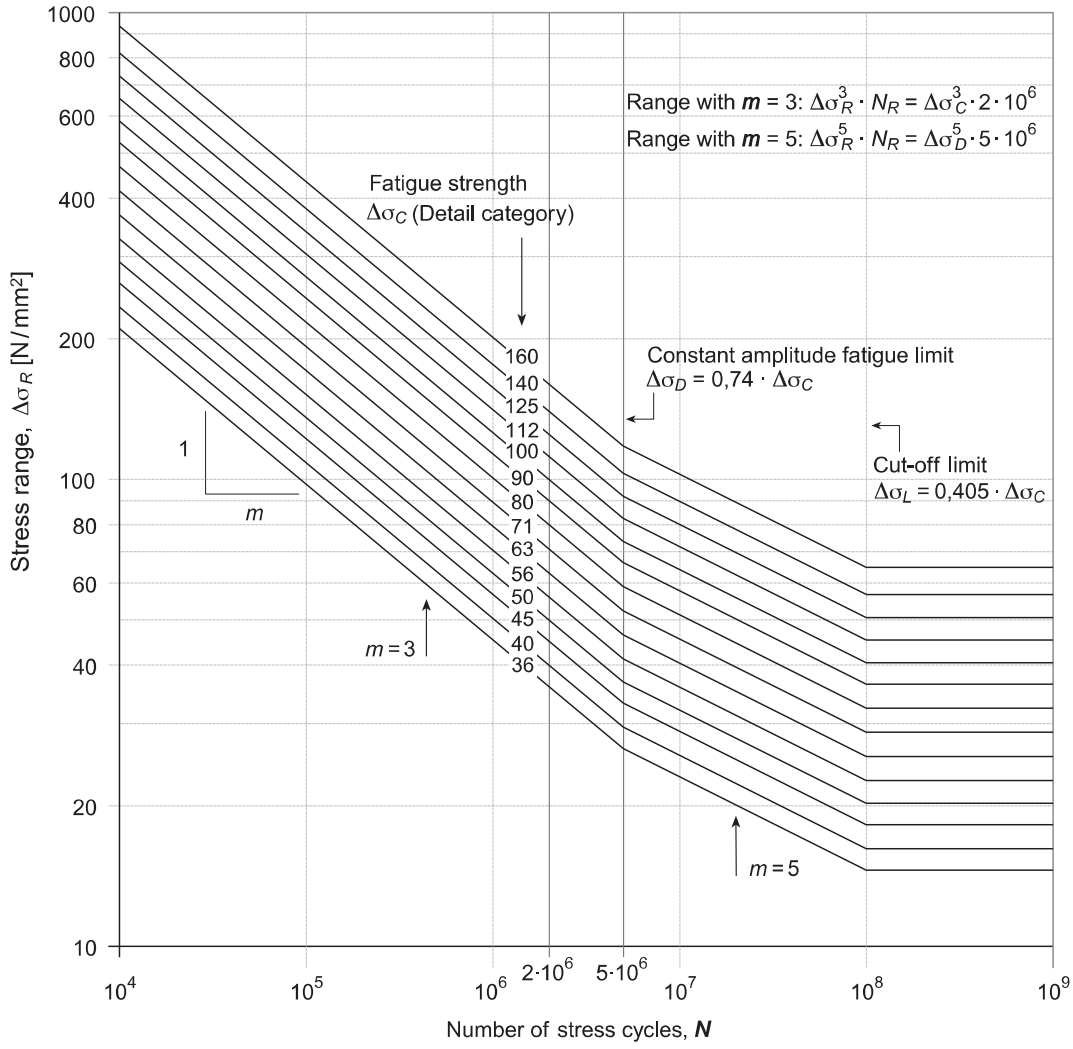

Figure 3.6 The Eurocode 3 fatigue strength classes. Diagram according to (SIA 2013).

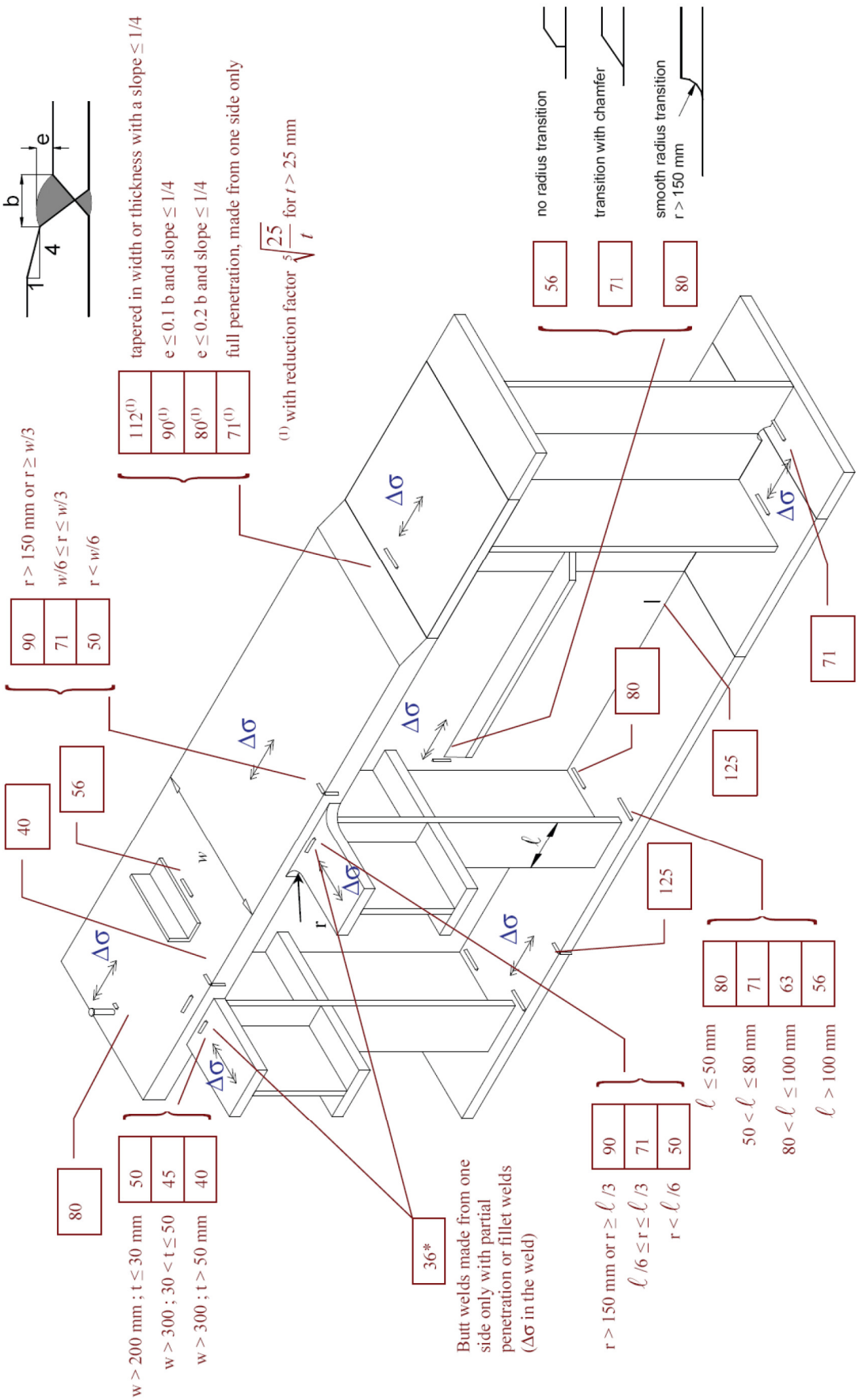

Figure 3.7 Typical detail categories in a two girder composite bridge according to Eurocode 3, reproduced from (Davaine, Imberty, and Raoul 2007).

3.4.2 Phase II: Local stress-based approaches

For the phase II, in addition to nominal stress method, two other alternatives that can yield more accurate predictions for the remaining fatigue of the details can be used. The two alternative methods are structural hot spot stress (SHSS) method and effective notch stress (ENS) method. These methods, also called local approaches, have following advantages compared to nominal stress method:

- The evaluation is based on local stress state in the vicinity of the fatigue cracking site. Therefore, these methods are not bound to a limited number of geometries and welded detail configurations, as is the case for classification method. Basically, if a studied detail cannot be attributed to one of the available detail categories in Eurocode, the classification method cannot be used.
- These methods utilize the advantages of finite element method. When a detailed FE model of the detail is at hand, both SHSS and ENS can be used with minimal post-processing, while classification method might need even more post-processing for integration of local stress state to estimate far-field nominal stresses.

The concept of local approaches can be described using Figure 3.8. The figure shows increase of surface stresses near a weld toe prone to fatigue cracking. This increase is due to two distinct factors:

1. Change in structural configuration (macro-geometry) which acts as a stress riser near the weld toe.
2. Local geometry of the weld results in a notch effect. This notch effect causes a drastic increase in the stress in the region very close to the weld toe (if the notch radius at the weld toe is assumed to be zero, the elastic stress will be singular at that point).

The stress corresponding to the first factor above is hot spot stress, while the stress corresponding to both factors is notch stress.

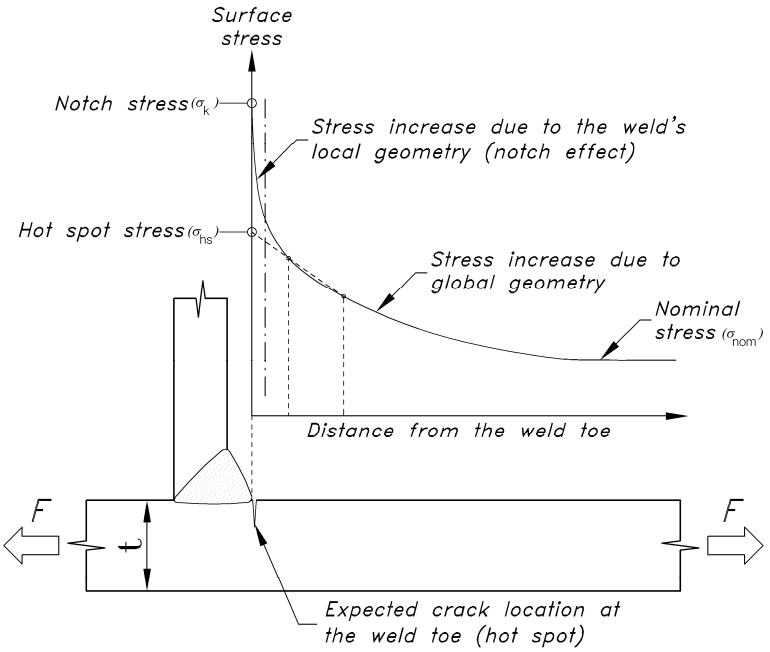

Figure 3.8 Variation of the surface stresses (perpendicular to weld toe) in the vicinity of the weld toe (Zamiri 2009).

Note that SHSS is a fictitious value; it is estimated by extrapolation of the surface stress towards weld toe from two appropriate points which are located within a reasonable distance from the weld toe. The two points are normally taken at the distances 0.4t and 1.0t from the weld toe (t being the plate thickness). When building the detailed finite element model of the connection for SHSS analysis, special care should be taken for using relevant element size and type, as is stipulated by IIW standard (Hobbacher 2008). A detailed explanation of the method with case studies can be found in a former TRV report prepared by (Al-Emrani and Aygül 2013). Note that SHSS method is not suitable for assessing the risk of root cracking.

The effective notch stress method is a step further towards accurate simulation of the stress state in the weld toe (or weld root) region. Correspondingly, the method needs more data regarding local weld geometry (e.g. weld profile, fillet weld angle, butt weld geometry) for the weld toe radius, the method fixes a certain radius (generally r=1mm) according to Neuber's rule. It is also more demanding in terms of small element sizes near the weld, as can be seen in Table 3-4 and Figure 3.9.

Table 3-4 FE mesh requirement according to IIW standard; from (Al-Emrani and Aygül 2013).

Element type		Element size		
		Relative size	r = 1mm ($t \geq 5$mm)	r = 0.05mm ($t < 5$mm)
Hexahedral	Quadratic	$\leq$ r / 4	0.25mm	0.012mm
	Linear	$\leq$ r / 6	0.15mm	0.008mm
Tetrahedral	Quadratic	$\leq$ r / 6	0.15mm	0.008mm

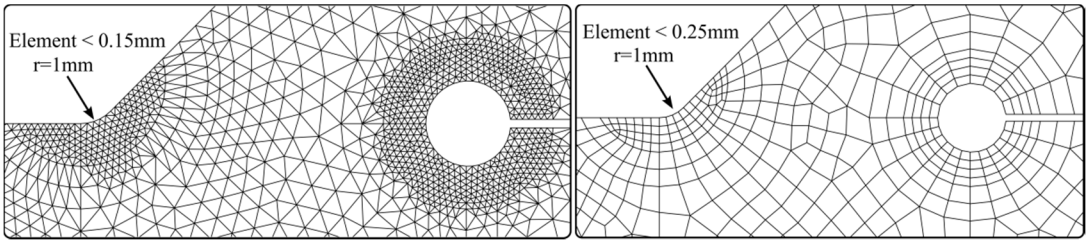

Figure 3.9 Illustration of FE mesh requirement (see Table 3-4); adopted from (Al-Emrani and Aygül 2013).

3.4.3 Phase III: LEFM-based assessment

Assessments in phase III are based on crack growth calculations using linear elastic fracture mechanics (LEFM). In this approach, the fatigue life of the detail is calculated as the time needed for a pre-existing crack to grow to a critical size. As can be seen in crack propagation Equations (A-8) and (A-9), resistance-side data in a LEFM-based assessment are comprised of two sets of data:

- Material properties: Paris-Erdogan constants (C and m) and threshold SIF ΔK_{th}
- Initial crack shape and dimensions a_0 and $\left(\frac{a}{c}\right)_0$ (for elliptical cracks)

These two sets of input data are discussed in the following subsections.

3.4.3.1 Material properties

In this subsection, characteristic values for material resistance in a fracture mechanics-based fatigue life assessment are presented. Details of calculations are given in Appendix A.

Several test results have shown that crack propagation life for C-Mn steels is independent of their mechanical properties (e.g. yield strength) (Günther 2005). The characteristic values (mean+2SD) for Paris-Erdogan parameters (C and m), and threshold stress intensity factor ΔK_{th} are shown in Table 3-5. These values should hold for the modern steel products produced after 1960s.

For older steels, or whenever in doubt, the values can be estimated experimentally for the structure under study, see Appendix C. When the crack propagation tests cannot be done, the values given in Table 3-6 proposed by Kühn et al. (2008) can be used.

Table 3-5 Characteristic values for welded steel details to be used in Equation (A-8), recommended by IIW (Hobbacher 2008)(† $R = \frac{\sigma_{max}}{\sigma_{min}} = \frac{K_{max}}{K_{min}}$).

Units	Paris law parameters	Threshold values ΔK_{th} as a function of stress ratio R †			
		$R \geq 0.5$	$0 \leq R \leq 0.5$	$R < 0$	Surface crack depth <1 mm
K $[N/mm^{3/2}]$ da/dN [mm/cycle]	$C = 5.21 \times 10^{-13}$ $m = 3.0$	63	$170 - 214R$	170	≤ 63
K $\left[MPa\sqrt{m}\right]$ da/dN [mm/cycle]	$C = 1.65 \times 10^{-11}$ $m = 3.0$	2.0	$5.4 - 6.8R$	5.4	≤ 2.0

Table 3-6 Recommended characteristic values for parameters in Paris' relation and threshold stress intensity factor range ΔK_{th} for old steels used in existing bridges, according to (Kühn et al. 2008).

Units	Paris' formula parameters	Threshold values ΔK_{th} for all R-ratios
K $[N/mm^{3/2}]$ da/dN [mm/cycle]	$\mathrm{C} = 4 \times 10^{-13}$ $m = 3.0$	63
K $\left[MPa\sqrt{m}\right]$ da/dN [mm/cycle]	$\mathrm{C} = 1.3 \times 10^{-11}$ $m = 3.0$	2.0

3.4.3.2 Flaws

Fatigue damage to structural details occurs in the form of cracks in the highly stressed regions. The cracking can occur either due to primary loading, or by secondary effects, e.g. the cracking at the connection of the diaphragm beam to two parallel main girders due to the differential displacement between the two main girders. In a study of more than 100 fatigue damage cases in steel and composite bridges, Al-Emrani & Kliger (2009) observed that the vast majority (>90%) of the reported cases had occurred due to the secondary effects, which is also called deformation induced cracking. The secondary effects in decks were frequently overlooked at the design phase of earlier steel and composite bridges. Al-Emrani & Kliger also pointed out "poor detailing, with unstiffened gaps and abrupt changes in stiffness at the connections between different members" as major contributing factor to the fatigue cracking in most cases.

Non-destructive methods can be used when a crack is detected. It is important to determine whether it is a pre-existing flaw from fabrication, or is it a fatigue crack which is growing. While the former is dormant and not impairing the use of structure, the latter (propagating cracks) opens and closes under cyclic loads and can damage the member or the whole structure.

As for the propagating cracks, they still might be acceptable (from structural point of view) if they are not located in fracture critical members. The consequence of failure for a secondary member (e.g. a cracked diaphragm beam) might deem acceptable by the engineer and the owner of the bridge. In contrast, fatigue cracks in main load-bearing elements can pose significant risk to the safety and service of the structure.

To characterize the cracks for LEFM-based assessments of phase III, following steps should be taken:

i. Identification and sizing of the cracks through proper non-destructive inspection (NDI) techniques,
ii. Determining whether the cracks are propagating or not,
iii. Upper-bound approximation of the generally irregular shape of the detected cracks to simple geometries (e.g. a 2D semi-ellipse) for use in the LEFM calculations.

The relevant NDI methods for steel and composite bridges are discussed in Appendix B. In general, every inspection should start with visual inspection. It is the most widely used method for the bridges, and still, the majority of flaws are detected by this method. Trafikverket's requirements for inspection of construction works (Trafikverket 2014b), requires an extensive visual inspection to be carried out at least each 6 years within the framework of main inspections (huvudinspektioner). In case cracks are found or some details are susceptible to cracking, Trafikverket requires documenting the location and size of the crack, as well as the use of "special inspections" which can be interpreted as ND inspections.

Regarding the task (ii) above, the engineer may review the structural system and structural analysis results to determine if the crack is propagating under cyclic (traffic) loads. Alternatively, the growth of the cracks can be studied by studying the past inspection reports and/or intensify monitoring for the cracks.

Idealization of the real cracks for use in the LEFM calculations is discussed in Section 3.4.3.2.1.

3.4.3.2.1 Categorization of defects

Non-destructive inspections detect flaws and cracks of various shapes which are generally irregular. On the other hand, analytical solutions for fracture mechanics problems are based on simple geometries, mainly elliptical and semi-elliptical cracks (see Figure 3.10). Therefore, the detected cracks should be categorized to an equivalent idealized crack. A common assumption is to consider an ellipse that circumscribes the cracked region, as is shown in Figure 3.11. The details of categorization of cracks from NDT for various geometries and crack configurations are given in IIW standard (Hobbacher 2008) as well as some other codes (BS 7910 2013; Pyttel et al. 2007; ASME 1998).

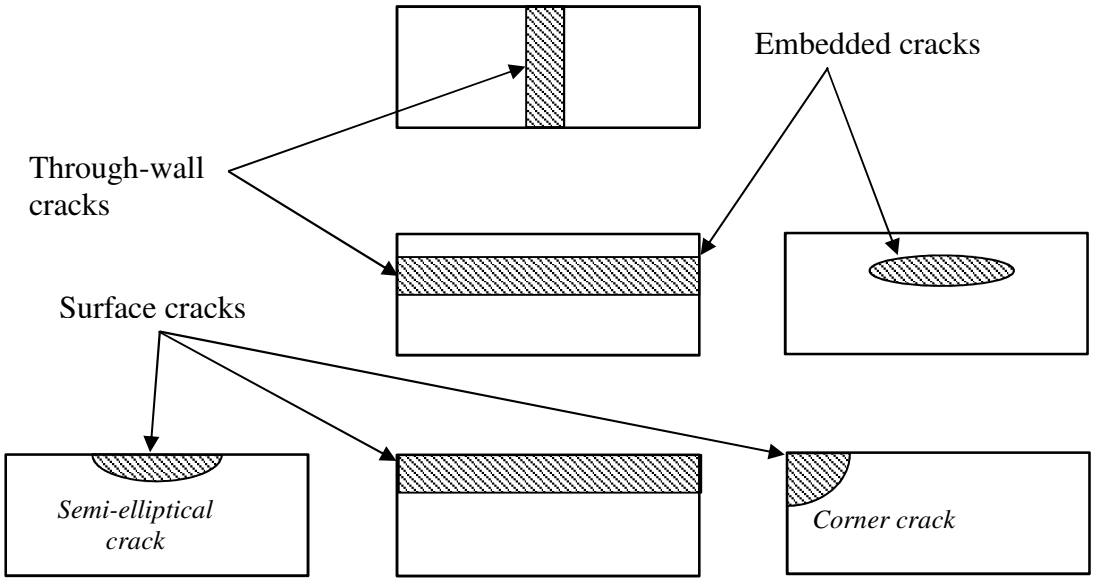

Figure 3.10 Types of idealized cracks.

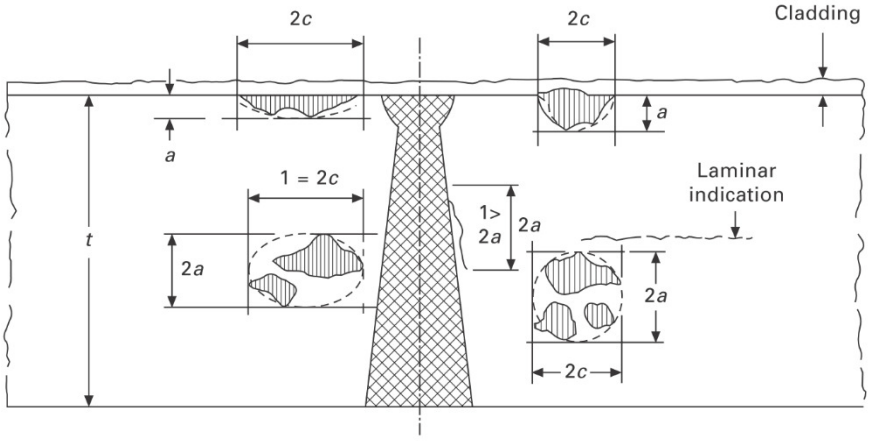

Figure 3.11 Transfer of NDT flaw measurements into elliptical cracks (ASME 1998) according to (Hobbacher 2011).

In practice, it happens frequently that multiple cracks and flaws are located close to each other. These cracks may interact as if there is a combined larger crack. To consider these possible interactions, some recommendations exist in the codes. One common such situation is shown in Figure 3.11: the circumscribing ellipse (for internal cracks) or semi-ellipse (for surface cracks) is drawn for the combined set of smaller cracks which are near each other.

3.4.3.3 Initial crack size and crack shape evolution

Choice of initial crack size a_0 has a large impact on the calculated fatigue life from Equation (A-9). Initial crack size can be estimated from non-destructive tests (See Appendix B), or, in case cracks are not detected, it should be postulated. In the latter case, the crack size can be assumed as the smallest detectable crack size of corresponding NDT method.

Alternatively, for the case a crack cannot be detected by ND inspections, background document of Eurocode 3 part 1-10 suggests a conservative value for initial crack size (G. Sedlacek, Feldmann, et al. 2008; Nussbaumer, Borges, and Davaine 2012):

$$a_0 = 0.5 \cdot \ln\left(\frac{t}{t_0}\right) \text{ for } t \geq 15mm \tag{3-3}$$

$$a_0 = 0.5 \cdot \ln\left(1 + \frac{t}{t_0}\right) \text{ for } t < 15mm \tag{3-4}$$

Where $t_0 = 1mm$ is the reference thickness. These formulas are also used in Eurocode 3 part 1-10 for its underlying fracture mechanical calculations.

Two-dimensional cracks are generally idealized to elliptical cracks (for internal flaws) or semi-elliptical cracks (for external flaws). The aspect ratio $\frac{a}{c}$ (a is crack depth, and 2c is crack width) has a significant effect on the evaluated stress intensity factors and hence on the crack life. The background document also gives an estimation for surface length of the semi-elliptical crack. Two cases are considered:

- The weld line is long, such as the case of a transverse attachment. In this case, several initial cracks form and then coalesce to form one larger crack. In this case, crack width will be:

$$2c_0 = 13.3 \cdot a_0 \quad (3\text{-}5)$$

- The weld is short, such as the case for the end weld in a longitudinal attachments or shear stud welds. For this case, the crack shape is closer to a circle and can be estimated from the following relationship:

$$2c_0 = 5 \cdot a_0 \quad (3\text{-}6)$$

Evolution of crack size and crack shape (for the latter case above) are presented in Figure 3.12.

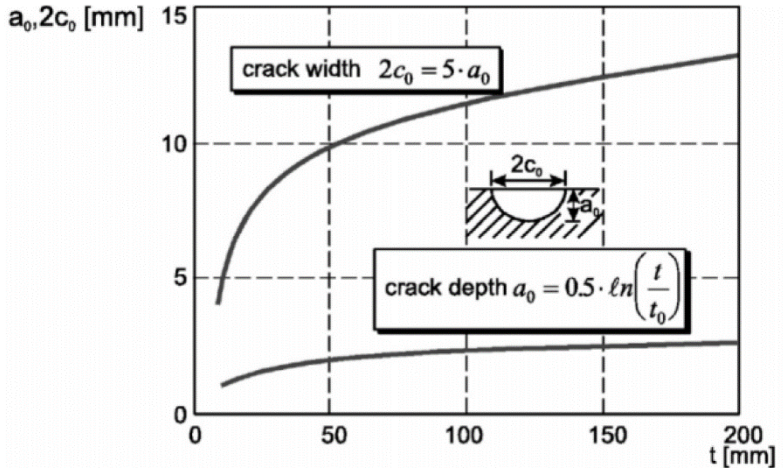

Figure 3.12 Crack size and aspect ratio change for transverse attachments according to Equations (3-3),(3-4), and (3-6) (G. Sedlacek, Feldmann, et al. 2008).

Another method for calculation of two-dimensional crack growth (i.e. crack shape), is to evaluate the crack growth individually in the directions of the two main axes of the ellipse; i.e. da/dN and dc/dN are calculated with corresponding ΔK_a and ΔK_c, respectively. a and c are the cardinal points of the ellipse that forms the analytical crack front. This method is generally considered more accurate, than the approximations given by Equations (3-5) and (3-6). Fatigue crack growth software, e.g. AFGROW (See Table A-1), use this method for their analyses.

3.5 Resistance against brittle fracture

3.5.1 Phase I

As already stated in Chapter 2, for the preliminary assessment phase, the table of maximum permissible plate thicknesses from EN 1993 part 1-10 (2005c) can be used. It gives the maximum allowable thickness for different steel grades, based on the minimum service temperature and level of applied stresses. Three levels of applied stresses are considered: high ($\sigma_{Ed} = 0.75f_y$), medium ($\sigma_{Ed} = 0.50f_y$), and low ($\sigma_{Ed} = 0.25f_y$). For the intermediate values of stresses, linear interpolation between the values given in the table should be performed.

The table is the result of extensive fracture mechanical analyses on the details with various geometries. For plate thicknesses above the values given in the table, there is a risk of brittle fracture. The details of the analyses are given in the commentary (G. Sedlacek, Feldmann, et al. 2008). If the studied steel grade is not known or is not conforming to EN10025 steel grades (i.e. for steels produced before 1970), the values corresponding to steel grade S235JR (first row in the table) can be assumed. The underlying assumptions for the table are given in Section 3.5.2. When using the table, those preconditions should be met.

Table 3-7 Maximum allowable plate thickness in [mm] for modern steel grades at different reference temperatures and working stress levels (EN 1993 2005c). Yield stress $f_y(t)$ is a function of service temperature, but its variation with temperature can be safely neglected for the range of working temperatures in Sweden.

Steel grade	Sub-grade	Charpy energy CVN		Reference temperature T_{Ed} [°C]																					
		at T [°C]	J_{min}	10	0	-10	-20	-30	-40	-50	10	0	-10	-20	-30	-40	-50	10	0	-10	-20	-30	-40	-50
				σ_{Ed} = 0,75 $f_y(t)$							σ_{Ed} = 0,50 $f_y(t)$							σ_{Ed} = 0,25 $f_y(t)$						
S235	JR	20	27	60	50	40	35	30	25	20	90	75	65	55	45	40	35	135	115	100	85	75	65	60
	J0	0	27	90	75	60	50	40	35	30	125	105	90	75	65	55	45	175	155	135	115	100	85	75
	J2	-20	27	125	105	90	75	60	50	40	170	145	125	105	90	75	65	200	200	175	155	135	115	100
S275	JR	20	27	55	45	35	30	25	20	15	80	70	55	50	40	35	30	125	110	95	80	70	60	55
	J0	0	27	75	65	55	45	35	30	25	115	95	80	70	55	50	40	165	145	125	110	95	80	70
	J2	-20	27	110	95	75	65	55	45	35	155	130	115	95	80	70	55	200	190	165	145	125	110	95
	M,N	-20	40	135	110	95	75	65	55	45	180	155	130	115	95	80	70	200	200	190	165	145	125	110
	ML,NL	-50	27	185	160	135	110	95	75	65	200	200	180	155	130	115	95	230	200	200	200	190	165	145
S355	JR	20	27	40	35	25	20	15	15	10	65	55	45	40	30	25	25	110	95	80	70	60	55	45
	J0	0	27	60	50	40	35	25	20	15	95	80	65	55	45	40	30	150	130	110	95	80	70	60
	J2	-20	27	90	75	60	50	40	35	25	135	110	95	80	65	55	45	200	175	150	130	110	95	80
	K2,M,N	-20	40	110	90	75	60	50	40	35	155	135	110	95	80	65	55	200	200	175	150	130	110	95
	ML,NL	-50	27	155	130	110	90	75	60	50	200	180	155	135	110	95	80	210	200	200	200	175	150	130
S420	M,N	-20	40	95	80	65	55	45	35	30	140	120	100	85	70	60	50	200	185	160	140	120	100	85
	ML,NL	-50	27	135	115	95	80	65	55	45	190	165	140	120	100	85	70	200	200	200	185	160	140	120
S460	Q	-20	30	70	60	50	40	30	25	20	110	95	75	65	55	45	35	175	155	130	115	95	80	70
	M,N	-20	40	90	70	60	50	40	30	25	130	110	95	75	65	55	45	200	175	155	130	115	95	80
	QL	-40	30	105	90	70	60	50	40	30	155	130	110	95	75	65	55	200	200	175	155	130	115	95
	ML,NL	-50	27	125	105	90	70	60	50	40	180	155	130	110	95	75	65	200	200	200	175	155	130	115
	QL1	-60	30	150	125	105	90	70	60	50	200	180	155	130	110	95	75	215	200	200	200	175	155	130
S690	Q	0	40	40	30	25	20	15	10	10	65	55	45	35	30	20	20	120	100	85	75	60	50	45
	Q	-20	30	50	40	30	25	20	15	10	80	65	55	45	35	30	20	140	120	100	85	75	60	50
	QL	-20	40	60	50	40	30	25	20	15	95	80	65	55	45	35	30	165	140	120	100	85	75	60
	QL	-40	30	75	60	50	40	30	25	20	115	95	80	65	55	45	35	190	165	140	120	100	85	75
	QL1	-40	40	90	75	60	50	40	30	25	135	115	95	80	65	55	45	200	190	165	140	120	100	85
	QL1	-60	30	110	90	75	60	50	40	30	160	135	115	95	80	65	55	200	200	190	165	140	120	100

3.5.2 Phase II

The resistance-side temperature T_{Rd} in Equation (2-1) is calculated from following correlation (G. Sedlacek, Feldmann, et al. 2008):

$$T_{Rd} = T_{K100} + \Delta T_t \tag{3-7}$$

where T_{K100} can be estimated either from Charpy transition temperature T_{27J} using Sanz correlation (see below), or calculated using Master curve method (see Section C.3.1.1) from Equation (C-16). The correlation between T_{27J} and T_{K100} is as follows (Nussbaumer, Borges, and Davaine 2012):

$$T_{k100} = T_{27J} - 18\ °C \tag{3-8}$$

ΔT_t in Equation (2-2) is the term to consider the reduction in transition temperature due to through-thickness inhomogeneity of fracture toughness (see Section 3.2.1). ΔT_t is calculated from following empirical formula:

$$\Delta T_t = 12.9 \cdot \tanh(2.1 \cdot \ln(t) - 7.6) + 12.8 \quad (3\text{-}9)$$

Where t is the plate thickness in [mm]. Figure 3.14 shows the ΔT_t curve as a function of plate thickness. Strictly speaking, ΔT_t should be applied only when the tip of the critical crack is located in the core region of the plate, see Figure 3.13. But as a conservative assumption for Phase II assessment, ΔT_t may be always applied, without calculation of the crack tip location.

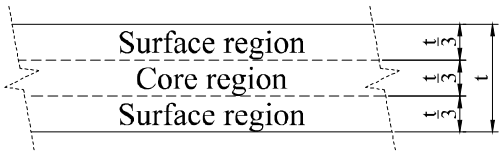

Figure 3.13 Definition of surface region and core region in the through-thickness direction of a plate with thickness t.

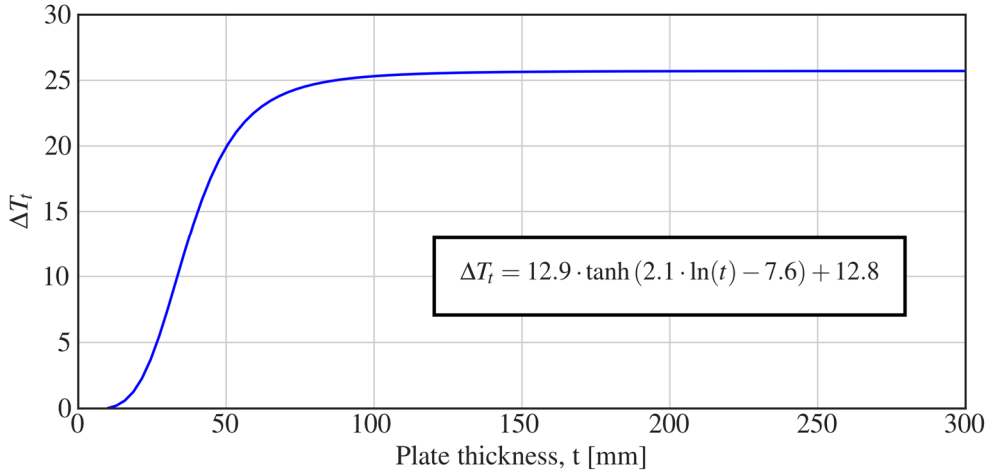

Figure 3.14 Change in transition temperature due to the influence of plate thickness.

3.5.3 Phase III

Form the discussion at Chapter 2, resistance-side factors for this phase include material fracture toughness at the design temperature $K_{mat}(T_{Ed})$, and initial crack size a_0. Similar to Section 3.4.3.2 for control against fatigue crack growth, the initial crack size can either be postulated or measured using non-destructive inspections.

For measurement of K_{mat}, guidelines are given in Appendix C (Section C.3.1). If the existing fracture toughness data are to be used, master curve method (Section C.3.1.1) can be used for transforming the results from the test temperature into the design temperature.

Based on the analysis of several tests results on old construction steels (riveted bridges), Kühn et al. (2008) suggest the characteristic value of $J_{mat}(at - 30\,℃) = 17N/mm$. According to equation (A-5) this is equal to:

$$K_{mat}(-30℃) = 54\ MPa\sqrt{m} \quad (3\text{-}10)$$

Given the considerable scatter of the fracture toughness data for old steels, the lower bond value given above might not be of much help in evaluating the risk of brittle fracture, because it is too low. It is advisable to either use existing test results, or perform new fracture toughness tests to get a more accurate value of fracture toughness. Larsson and Lagerqvist (2009) came to a similar conclusion in their study of mechanical properties of steel material collected from old bridges (constructed before 1940).

4 Action-side factors

The methods for updating the action-side information, including permanent and variable loads, for the three assessment stages are discussed in this chapter. The updated information can be gathered either by considering existing data (e.g. history of traffic loading on the bridge) or by on-site measurements (monitoring). While the engineer can start assessment in phase I with code-driven loads, more realistic load models will be required for phase III. Thus, the monitoring is treated in more detail in this chapter. In carrying out any measurement or monitoring operation, it will be the engineer's task to identify the parameters that have the largest impact on the assessment result. Subsequently, the quality of obtained data from measurements can be kept in a reasonable proportion to the costs.

Typically, the traffic loads are the dominant variable actions for fatigue assessment of bridges. Wind actions do not need to be considered in Phase I assessment. If wind loads are to be included in the subsequent assessment phases, their typical values can be obtained from Eurocode EN1991-1-4(2005).

4.1 Permanent loads

Determination of the permanent loads (dead weigh) is straightforward. The values of permanent actions are the same for all three assessment phases. It should be noted that if during site visits it appears that there is significant difference between designed cross section geometries and the sections used in the actual structure, the updated cross section geometries should be used for calculation of permanent loads.

Another issue investigated by some researchers is that whether the partial factor for permeant actions, γ_G, for the assessment of bridges should be taken as the same value for design of new bridges, or it can be reduced. The results of such a study conducted in Switzerland for SIA 160 (similar to EN 1991) revealed that for the case of composite bridges, a reduction 5% to 10% in γ_G could be achieved, while the reduction in the case of steel bridges was negligible (Kühn et al. 2008). In contrast, the Trafikverket's "Krav" document (Trafikverket 2017) suggests values between 1 to 1.2 for the partial factor for permanent loads (refer to Tabell 2-12 in the Krav document). It does not differentiate between different construction types (steel/concrete/composite). When the "Krav" document is used for assessment, load combination A should be considered for ULS checks (including brittle fracture) and load combination C will be used for fatigue limit state checks. Also, load combination E (military vehicles) might be relevant for ULS controls.

4.2 Traffic loads

To simplify complex variable loading from traffic on the bridges, standardized "Fatigue Load Models (FLMs)" are introduced in EN 1990 and EN 1991-2 for both railway and road bridges. These FLMs are equivalent load models that tend to simulate the "real" traffic loading on the bridge and simplify the calculations for a design or assessment situation, while satisfying safety requirements. It is important that the engineer has a clear understanding of application scope and evaluation basis of each of these fatigue load models. In the following section, these FLMs are introduced. For a thorough review of fatigue load models, see Al-Emrani & Aygül (2013).

4.2.1 Fatigue Load Models (FLMs) in Eurocode

4.2.1.1 FLMs in Road bridges

Five fatigue load models for road bridges are introduced in EN 1991-2, as summarized in Table 4-1. These load models are defined and calibrated according to a wide range of real traffic data from various locations in Europe. The choice of appropriate load model depends on the fatigue verification method used in the corresponding assessment phase. Figure 4.1 shows the choice of appropriate FLM in respect to fatigue assessment method.

Table 4-1 Summary of Fatigue Load Models for road bridges Eurocode in EN 1991-2 (2003). For detailed explanation of the load models, see (Al-Emrani and Aygül 2013).

FLM 1 – similar to static loading LM1

1 LORRY SILHOUETTE	2 Axle spacing (m)	3 Frequent axle loads (kN)	4 Wheel type (see Table 4.8)
	4,5	90 190	A B
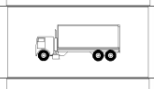	4,20 1,30	80 140 140	A B B
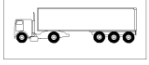	3,20 5,20 1,30 1,30	90 180 120 120 120	A B C C C
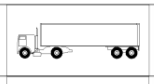	3,40 6,00 1,80	90 190 140 140	A B B B
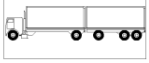	4,80 3,60 4,40 1,30	90 180 120 110 110	A B C C C

FLM 2 – set of "frequent" lorries

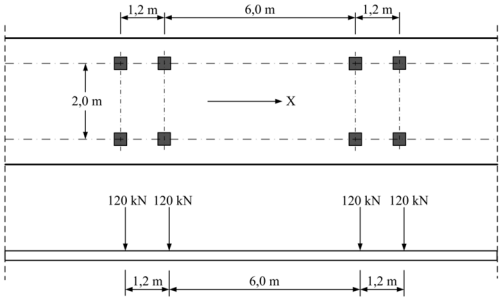

FLM 3 – single vehicle model

VEHICLE TYPE			TRAFFIC TYPE			
1	2	3	4	5	6	7
			Long distance	Medium distance	Local traffic	
LORRY	Axle spacing (m)	Equivalent axle loads (kN)	Lorry percentage	Lorry percentage	Lorry percentage	Wheel type
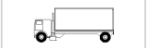	4,5	70 130	20,0	40,0	80,0	A B
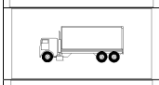	4,20 1,30	70 120 120	5,0	10,0	5,0	A B B
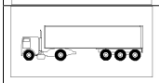	3,20 5,20 1,30 1,30	70 150 90 90 90	50,0	30,0	5,0	A B C C C
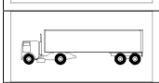	3,40 6,00 1,80	70 140 90 90	15,0	15,0	5,0	A B B B
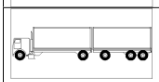	4,80 3,60 4,40 1,30	70 130 90 80 80	10,0	5,0	5,0	A B C C C

FLM 4 – set of "standard" lorries

Direct application of the traffic load measurements in the structural analysis by implementation of proper statistical methods, according to EN 1991-2 Annex B.

FLM 5 – Recorded load traffic data

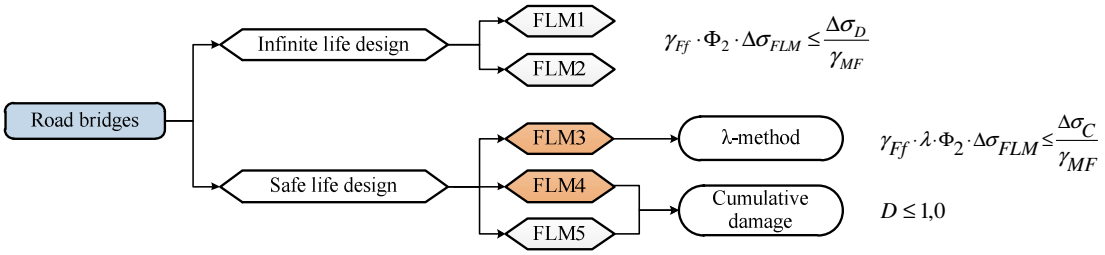

Figure 4.1 Application scope of FLMs for road bridges.

Fatigue load model 1 is defined to be used in "infinite fatigue life" design check, where all the stress ranges fall below factored fatigue limit $\frac{\Delta\sigma_D}{\gamma_{Mf}}$ (see Figure 3.6). FLM1 is a direct derivation of characteristic load model (LM 1) used in ULS design; the concentrated axel loads (Q_{ik}) are multiplied by 0.7 and uniformly distributed loads (q_{ik} and q_{rk}) are multiplied by 0.3. Fatigue verification with FLM 1 is comprised of comparison of the stress ranges calculated from this model to the constant amplitude fatigue limit (CAFL).

Fatigue load model 2 is defined as a set of five standardized frequent lorries (see Table 4-1), representing most common lorries in Europe. Axel loads, wheel types, and axel distances are given for each lorry. Like FLM1, fatigue load model 2 is intended to be used in infinite fatigue life check. Therefore, for fatigue verification, stress ranges generated from the passage of each lorry should be compared against CAFL.

Fatigue load model 3 includes a single vehicle with four axels, each axel weighing 120 kN. FLM3 is intended to be used with the damage equivalent factor method, i.e. λ −method, see Figure 4.1. The model is sufficiently accurate for road bridges with spans longer than 10 m, but it tends to give conservative results for shorter spans (G. Sedlacek, Merzenich, et al. 2008). Also, for bridge spans larger than 40 m, an additional vehicle like the original FLM3 vehicle, but with a lower axel weight (36 kN), should be considered with a minimum centre-to-centre distance of 40 m on the same lane.

Fatigue load model 4 is comprised of a set of 5 different lorries (similar to FLM2). The various lorries differ with each other in number of axels, axel spacing, and axel loads. Again, the axel weights and dimensions of the lorries are like the most common heavy vehicles on European roads. These lorries represent the effect of "real" heavy traffic loads on road bridges. "Real traffic" for different types of road traffic (long distance, medium distance and local traffic) are simulated by defining various compositions of lorries as the percentage of the heavy traffic volume. Also, the total number of lorries crossing the road bridge (N_{obs}) is defined in the norm for application of FLM4. The traffic composition and properties of lorries recommended for FLM 4 is the same as for FLM 2; Only the characteristic axle loads corresponding to the average loads are reduced. This load model is intended to be used with the damage accumulation method (Palmgren-Miner rule). This includes a time history analysis of passing traffic lorries followed by a cycle counting procedure. Compared to previously introduced load models, this load model gives more precise results for the fatigue resistance of short span bridges.

Fatigue load model 5 is basically direct application of recorded traffic data on the bridge. This load model is intended to be used to for accurate fatigue verification of important bridges, such as cable-stayed bridges, suspended bridges, or other complex bridge structures. It can also be applied to bridges with "unusual" traffic. For fatigue

assessment with FLM5 traffic measurement data need to be extrapolated during the future service life of the bridge with advanced statistical analyses. Annex B of EN 1991-2 provides additional information for these analyses.

Having the **number of load cycles** for FLM1 and FLM2 is irrelevant, because the design/assessment is intended for infinite fatigue life. On the other hand, number of cycles for FLM3 and FLM4 are required. For the newly designed bridges, EN 1991-2 and TRV Krav Brobyggande (Trafikverket 2016) give the number of cycles as a function of "traffic category". The traffic category is determined by the mean daily traffic volume in a highway, measured for one year. The unit of the traffic volume is given as annual average daily traffic, abbreviated AADT (ÅDT in Swedish).

For the case of existing bridges, the load models given in TRV Krav Bärighetsberäkning (Trafikverket 2017) should be used. To account for past loading on the bridge more precisely, the historical traffic data can be obtained from authorities. Some information might be obtained from permanent truck weighing stations or toll stations, too (Kühn et al. 2008).

4.2.1.2 FLMs in Railway bridges

Like fatigue load models for road bridges, each of the fatigue load models for the railway bridges is associated with its intended design method. Since the fatigue is the dominant limit state in the design of railway bridges, "infinite life design" is not used for their design; because it leads to an extreme an uneconomic design. Instead, the "safe life" design principle is used. Therefore, fatigue load models for railway bridges are associated with either λ −coefficient method or damage accumulation method. Figure 4.2 depicts the application scope of various fatigue load models.

The load models for railway bridges given in EN 1991-2 are only applicable to standard and wide track gauge railways. In bridges with more than two tracks, fatigue loads should be applied to a maximum of two tracks in the most unfavourable positions for the investigated detail.

Fatigue load models for λ −coefficient method: three load models, namely LM71, SW/0 and SW/2 are introduced in Eurocode, as shown in Table 4-2. LM 71 is directly driven from load model 71 for static design, neglecting any ULS adjustment factor ($\alpha = 1$). Load models SW/0 and SW/2 are to be used in addition to LM71 for the case of continuous railway bridges under standard and heavy rail traffic, respectively.

Fatigue load models for cumulative damage method: EN 1991-2 requires that the fatigue design spectra used in this method should be evaluated based on the so-called "traffic mixes". A traffic mix is a set of train load models. Each train load model is in turn composed of several wagons with specific axel loads and axel spacing. Three different traffic mixes are defined in Appendix D of EN 1991-2 which represent standard traffic, heavy traffic, and light traffic conditions. Besides, a traffic volume per year is required for the design. The standard traffic mix in EN 1991-2 is based on a traffic volume of 25 million tonnes per year.

Train models in Swedish TRV "Bärighet" document: To better represent the rail traffic for each individual country, EN 1991-2 allows for specification of train load models by national authorities. For assessment of existing bridges in Sweden, these load models are determined by Trafikverket (2017). They are presented in Table 4-3 to be used in conjunction with damage accumulation method.

Figure 4.2 Application scope of FLMs for railway bridges according to EN 1991-2.

Table 4-2 Summary of Fatigue Load Models for railway bridges associated with λ-coefficient method, according to EN 1991-2 (2003).

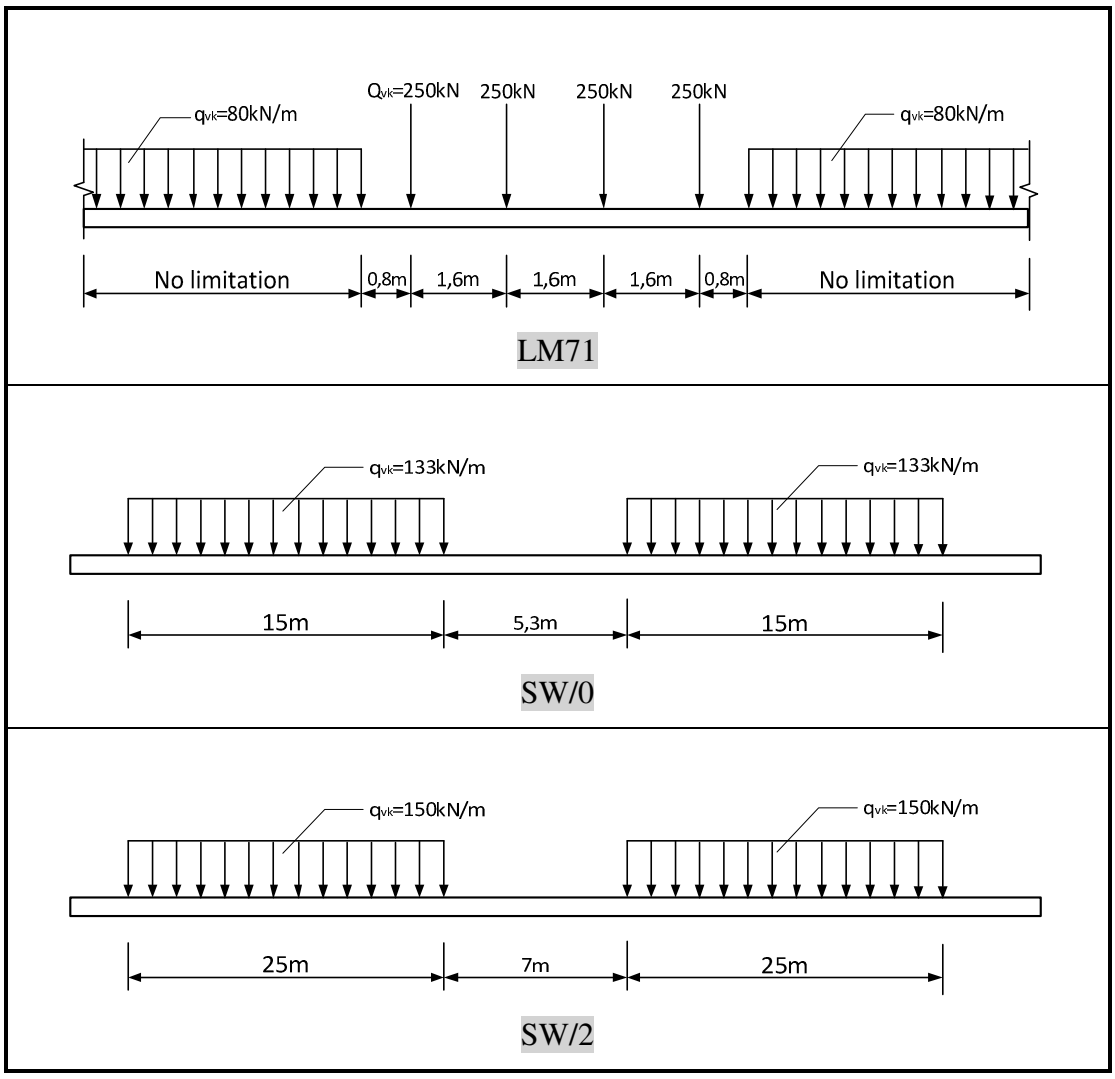

Note that Trafikverket regulations require that in the case of double tracks, train traffic load to be applied on one track only. For the damage accumulation method, the partial load factor is taken as $\gamma_F = 1$.

To simplify fatigue assessment based on damage accumulation, Trafikverket document recommends the calculation to be done by one of these two methods:

a) The stress range is determined by calculating stresses based on the load of equivalent trains, and the number of load cycles is determined based on the freight carried according to the load history.

b) The stress range is determined by measuring stresses for a limited period of train traffic and the number of cycles is estimated in proportion to transported freight during the measurement period and load history.

Table 4-3 Axel loads and wagon data for Swedish railways (excluding Malmbanan) reproduced from Table 10-9 in Trafikverket (2017).

Year	–1920	1921–1940	1941–1960	1961–1980	1981–2000	2001 Stax 22.5	2001 Stax 25	Mean
P_k	160	180	200	200	225	225	250	200
P_m	120	150	160	160	180	180	200	160
a	2	3	4	4	4	4	4	4
P_0	40	40	50	50	50	50	50	50

Year: time period concerned,

P_k : characteristic value for axel loads for calculation of stress ranges

P_m: mean axel loads for calculation of number of train passages

a : number of axels per wagon

P_0: weight of empty wagon

4.2.2 Traffic loads for Phase I

For the design of new bridge structures, fatigue verification using damage equivalent factors (λ −coefficient) is standard practice. Following the "control-as-new-design" approach of phase I assessment (see Chapter 2), damage equivalent factors can be used for this phase, too. Therefore, the action-side of the Equation (3-2) becomes:

$$\Delta\sigma_{E,2} = \lambda \cdot \Phi_2 \cdot \Delta\sigma_{FLM} \tag{4-1}$$

where

$\Delta\sigma_{FLM}$: the reference stress range from analysis of structure under code-based traffic loads,

λ : damage equivalent factor according to EN 1993-2 (2006) for steel bridges, or EN 1994-2 (2005) for shear connectors in the steel-concrete composite bridges,

Φ_2 : for road bridges $\Phi_2 = 1$; for Φ_2 values for railway bridges refer to EN 1991-2 (2003),

$\Delta\sigma_{E,2}$: equivalent stress range (2 indicates the value is calculated for 2 million cycles).

4.2.3 Traffic loads for Phase II

Damage accumulation method and its associated fatigue load models are intended for more accurate assessment of fatigue life. This means the so-called "Traffic mixes" (see 4.2.1.2) should be used to create stress-histories and subsequently stress spectrums (i.e. histograms) for the studied details. According to Kühn et al. (2008), the highest stress

ranges that occur in a low number of cycles due to passage of few super heavy trucks (these make up the highest 5-10% fractile in the stress spectrum) do not contribute significantly to the fatigue damage sum.

4.2.4 Traffic loads for phase III

Since "traffic mixes" are the most accurate code-based estimate available, they can be used for phase III assessments, similar to phase II. However, modifications can be made to improve the load estimates towards real values. These modifications can include the adjustment of annual freight tonnages to the historical data from the bridge. For road bridges fatigue load model 5 is a desirable choice, since it directly relies upon measurement of actual loads on the structure.

Arguably, the largest source of uncertainty in assessment of bridge structures comes from action-side factors. Because of these large uncertainties, conservative load models and dynamic amplification factors are used in the assessment which leads to an over-conservative assessment. A more accurate alternative would be the application of direct monitoring to acquire a reasonable measure of in-service actions on the structure (Mark Anthony Treacy 2014). The recent progresses in data acquisition technologies has facilitated the deployment of direct monitoring for existing bridges. On the other hand, the methodologies for incorporation of the measurements in structural assessment and management of generated "big data" are still under extensive development. Two of such ongoing efforts are European COST actions TU 1402 and TU 1406 (TU1402 and TU1406 2017).

When the load measurements are used, dynamic effects should not be overlooked. Annex A1 of EN 1993-1-9 (2005a) requires that for determining histories of load effects in structural details, the effects of dynamic magnification of the structural response should be considered in addition to the type and shape of the influence lines. Annex A1 also allows the use of dynamic calculations for structural response.

Stress range spectra may be modified by neglecting peak values of stress ranges representing less than 1% of the total damage and small stress ranges below the cut off limit.

For highway bridges, the measurements can be done by B-WIM (bridge weigh in motion) which are devices installed on the road surface and weigh the axel loads from passing trucks while they travel in full speed. Figure 4.4 presents an example of a B-WIM system. The advances in WIM technology has facilitated obtaining high-quality site-specific traffic data. For a review of advances in the field see (Lydon et al. 2016). Use of WIM data in assessments typically leads to less conservative results. Document D4.3.2 from sustainable bridges project (R. Karoumi, A. Liljencranz, and F. Carlsson 2007) gives the details of using WIM data for load measurements. WIM statistics can also be used for traffic simulations to estimate the traffic on a similar site or to extrapolate the traffic data to a time in future. One viable method is Monte Carlo simulations (Getachew and Obrien 2007; Maddah 2013)

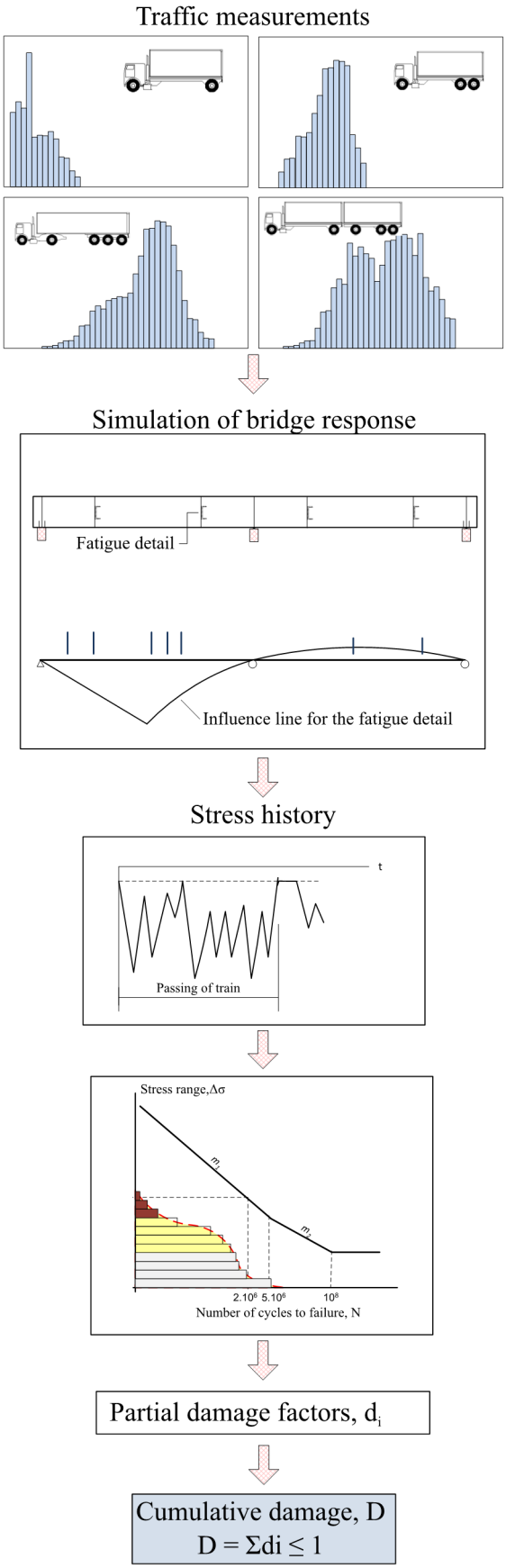

Figure 4.3 Fatigue damage assessment from traffic load measurements (Al-Emrani and Aygül 2013).

The workflow for implementing monitoring data is similar to the procedure that was used in producing fatigue load models in Eurocode EN 1991-2. The detailed explanation the latter can be found in Al-Emrani & Aygül (2013). As is shown in Figure 4.3, one procedure for implementing monitoring data is as follows:

1. Selection of critical structural details for fatigue analysis and their corresponding fatigue resistance curves
2. Determining influence lines or influence surfaces for the action effects for critical details of Step 1
3. Simulation of bridge response under measured traffic data using the influence lines/surfaces for the studied details. Determining stress histories pertinent for fatigue design of the detail.
4. Converting stress histories to stress range histograms using an appropriate cycle counting method.
5. Calculating partial damage indices for each of the constant amplitude stress ranges in the histogram to obtain the accumulated damage index using Palmgren-Miner rule.

Instead of load measurements, another possibility is to measure load effects and stresses, instead of loads themselves, in critical details in the bridge. Once the critical details have been identified (phase I), they can be instrumented by e.g. strain gauges. Traffic measurements combined with statistical methods to include load extremes, will lead to accurate assessments of action effects on those details. Treacy et al. (2014) show the methodology and example measurement (for the case of reinforcement in a concrete bridge) for such assessments.

In addition to direct monitoring of actions and action effects, the monitoring data can be used for validation and calibration of the structural models developed for phase III. Since the finite element models developed for the phase III are more complex and with various assumptions for material properties and boundary conditions (see next chapter), their validation is important to ensure the reliability of the analysis result. For the validation purposes, it is recommended to use controlled loading tests (e.g. a truck with known axel loads on a precisely determined location on the bridge), measure the action effects (e.g. strains in the girders), and compare the measured value against analysis results to validate the FE model. Subsequently, model parameters (e.g. degree of fixity at the supports) can be adjusted to better comply with the actual structure. Further extension of a model that closely corresponds to the actual structure, has recently given way to the idea of "digital twins" (Omenzetter 2015). A digital twin is a high-resolution, multi-scale model of the real structure which is validated and continuously updated by the data collected from structural health monitoring (SHM).

The model calibration can be done either by "manual" tuning or using optimization algorithms. An important step for validation is to choose the error function which indicates the difference between analytical response and measured data ('Instrumentation, Nondestructive Testing, and Finite-Element Model Updating for Bridge Evaluation Using Strain Measurements' 2012).

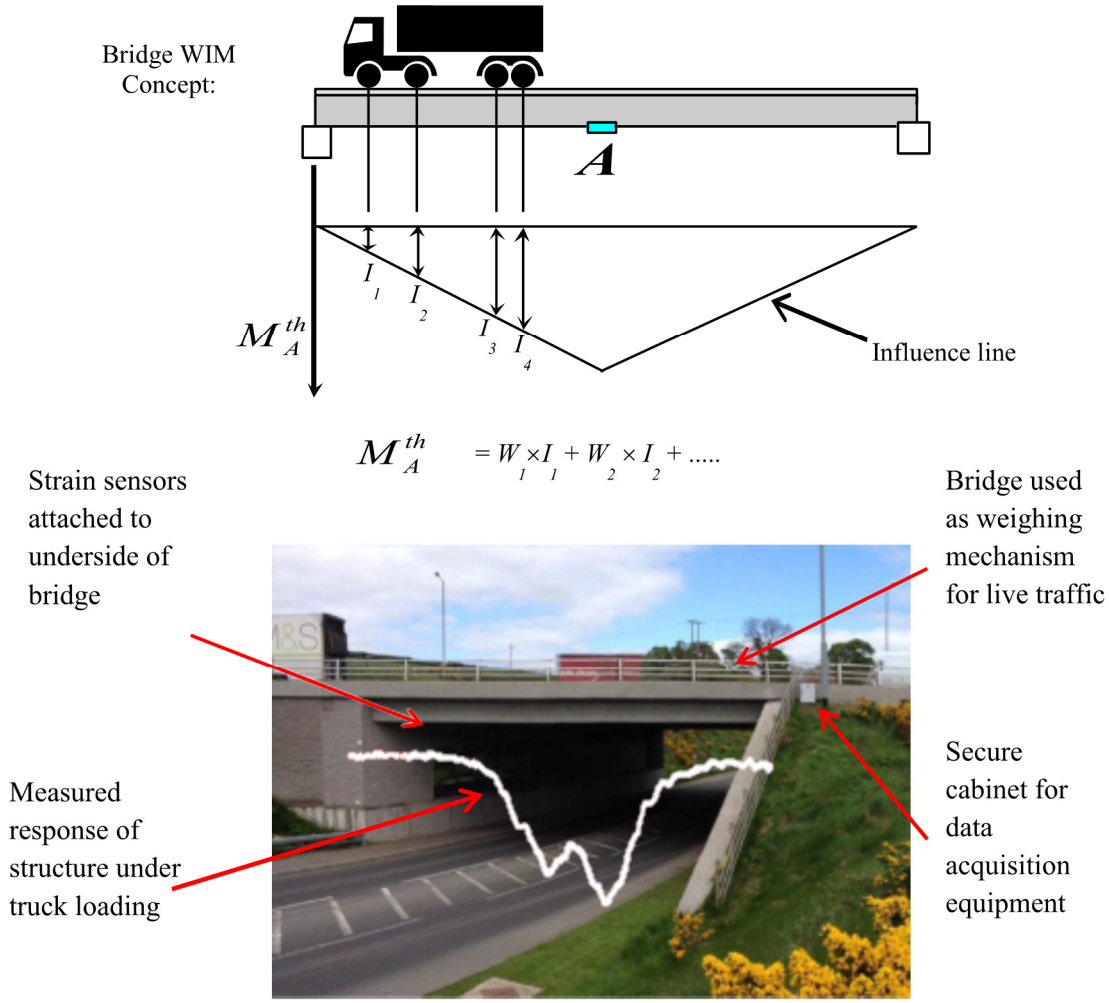

Figure 4.4 An example of a B-WIM instrumentation on a bridge (Lydon et al. 2016).

4.2.4.1 Available guidelines for structural health monitoring (SHM)

Currently a few technical guidelines for structural health monitoring exist. Hejll (2007) has conducted a comprehensive review of the available guidelines. A more recent review is carried out by Daum (2013).

The Canadian Network of Centres of Excellence on Intelligent Sensing for Innovative Structures (ISIS Canada) has published one of the leading comprehensive guidelines for structural health monitoring of civil infrastructure (Mufti 2001). The ISIS guidelines mainly deal with capabilities of SHM as a diagnostic tool. It also showcases the advantages of using SHM in the context of civil engineering structures.

European thematic network SAMCO (Structural Assessment, Monitoring and Control), comprised of industries and research institutes, has published another general guidelines for SHM (Rücker, Hille, and Rohrmann 2006). The SAMCO F08b guidelines has collected the existing state of the art methods and techniques with recommendations for effective application of those methods.

Drexel Intelligent Infrastructure and Transportation Safety Institute has proposed a SHM guidelines document specific to bridge structures (Aktan et al. 2003). The guidelines describe the methods for implementing the information from different sources (analysis, experiments, and monitoring) for diagnosis and condition appraisal

of bridge structures. Recommendations are given for planning and design of instrumentation and monitoring system. The proposal also includes best practice recommendations for numerical modelling and of bridges at different accuracy levels as well as the validation of those models from field monitoring data.

4.2.4.2 Monitoring systems

The monitoring system should collect the desired information in a reliable manner. It should be possible to operate the system and receive the collected data from a location outside the site. The large size of the bridge and the extension of construction work area around it, require that the monitoring might be needed in a large area of the bridge, but not in all locations at the same time. The latter is also important from data size management viewpoint. A good solution would be to adopt a scalable monitoring system which can be rapidly extended/moved to other parts of the bridge. The monitoring program can start in a limited number of locations where the construction work starts. Then it can be extended according to the needs of the project.

One viable option is the relatively new concept of wireless sensor networks (WSNs) for monitoring of large infrastructure. Wireless sensors and sensor networks are two emerging sensing technologies for the field of structural engineering as well as other engineering disciplines. One advantages of WSNs compared to traditional tethered networks is a price cut because extensive wiring is not needed between sensing nodes and data acquisition system. Besides, a part of processing of the structural response data can be done in the sensing nodes. This helps in screening the data for signs of structural damage (Lynch 2006). Figure 4.5 shows a simple layout of a WSN. Dispersed sensors are connected to nearby low-power wireless nodes. The nodes communicate wirelessly with the gateways. Finally, the wireless gateway sends data to the cloud for storage and processing by the end user.

While the majority of low-power wireless sensor technologies are developed for monitoring with quasi-static, low sampling rates (e.g. temperature and humidity), there are some solutions that are capable of high-frequency data transfer (Potter et al. 2012). One main obstacle for achieving high sampling rates is the increased power consumption, which makes these WSNs unsuitable for battery-operation.

In summary, comparing to traditional data acquisition systems, WSNs provide some advantages as following:

- **Rapid**: Light, small, and rapidly deployable sensing nodes.
- **Wireless**: Eliminating wiring (electricity and data) for the sensing nodes makes WSNs more desirable for monitoring of large structures. Sensor locations are only limited by the antenna ranges.
- **Costs**: Costs for the hardware is less than, or comparable to, that of traditional DAQ systems; The precise amount of saving depends on the costs of wiring (for traditional solution) versus battery-changing costs (WSN solution).

The shortcomings of WSNs originate from the trade-offs that should be made to optimize the battery life of the wireless sensing nodes:

- **Resolution**: In general, WSNs have lower, but still acceptable resolutions[3] compared to tethered networks. A wireless sensor node may have 16-bit or 18-bit resolution, while a high-end tethered acquisition instrument has 24-bit resolution.

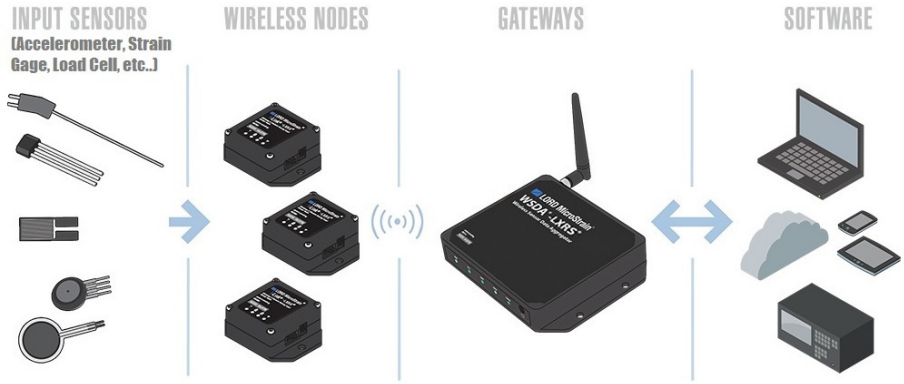

Figure 4.5. Overview of a Wireless Sensor Network (Source: http://goo.gl/BoQoA1).

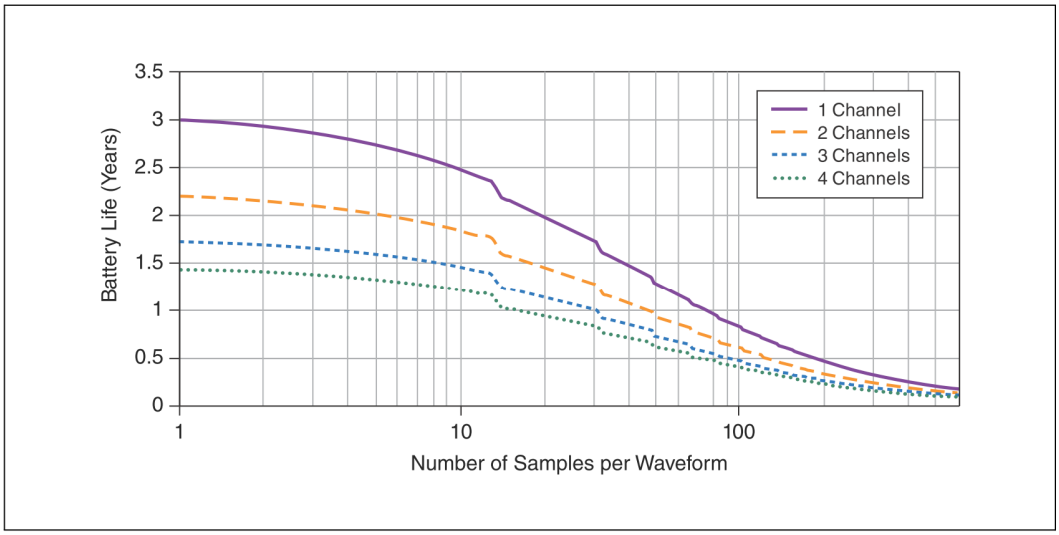

Figure 4.6 Battery life versus sampling rate for a wireless sensing node (model: NI WSN 3214).

- **Reliability**: A tethered instrument has a more powerful CPU and can carry out sampling with higher frequencies, compared to a wireless sensing node.

[3] The resolution of an analog-to-digital (ADC) converter indicates the number of levels that are used for digitizing an analog signal. A 16-bit resolution means that the ADC can represent the signal with 2^16=65536 discrete levels; i.e. our best resolution is 1 /2^16=0.0015%.

- **Bandwidth**: Wireless protocol IEEE 802.15.4 is designed for high power-efficiency, not the high data transfer rate. Therefore, special care is needed to reduce the amount of data transferred on the network to not to saturate the bandwidth.
- **Battery changing**: the more intensive monitoring (high sampling rates, longer measurement times), the shorter the battery life of the wireless node will be (See Figure 4.6 for an example).

5 Modelling options

Sufficiently accurate models are required for correct evaluation of action effects (stress and internal forces) in the structure. The complexity of the chosen structural model in each assessment phase is in tandem with how detailed is the assessment level.

It is common practice for the design of new bridges that the primary load-carrying system and the secondary load-carrying systems are analysed separately (Kühn et al. 2008). Any secondary effects from the interaction of those two systems are neglected. This simplified analysis can be used for Phase I assessments, too. Having in mind that secondary effects, namely cracking due to deformation-induced actions (Fisher 1984), will not be covered using this analysis method.

Thus, the modelling in Phase I can be as simple as 1D linear elastic beam models or analytical solutions for continuous beams. For phase II assessment the secondary effects should be included and thus 2-D or 3-D models can be used. If special structural features exist (e.g. skew bridge, or girders curved in plan), then 3-D models should be used to improve the evaluation of interaction effects between secondary and primary load-bearing elements. The 3-D global models of the whole structure will also be used for phase III, possibly with accompanying sub models of critical details for a more detailed study of the behaviour at the substructure level (see Section 5.1). Table 5-1 summarizes the recommended modelling for various assessment phases.

When a detailed model of the bridge structure is developed, accurate determination of model parameters becomes more important. This includes for example the degree of partial fixity for the joints: a simple joint that has undergone aging can show some friction resistance that affects the real behaviour, but remains unnoticed in the “ideal” model. Another example can be the degree of composite action between concrete and steel in a composite deck. This was the case for the case study bridge (see Chapter 6), where the number of shear studs was much lower than what is required in the modern standards. These types of modelling parameters can affect the results of the assessment. One way to determine these parameters and validate the structural model is to perform controlled measurements on the bridge, see section 4.2.4.

Table 5-1 Modelling options for various assessment phases.

<table>
<tr><th>Structure type</th><th>Phase I</th><th>Phase II</th><th>Phase III</th></tr>
<tr><td>Girder bridge</td><td>1-D linear elastic analysis (FEM or handbook solutions)</td><td>2-D grillage linear elastic analysis</td><td rowspan="4">3-D global model (beam and shell elements) + 3-D sub-model(s) consisting of shell or solid elements</td></tr>
<tr><td>Girder bridge (skewed or curved in plan)</td><td>2-D grillage allowing torsion effects</td><td>2-D or 3-D linear elastic analysis</td></tr>
<tr><td>Truss bridge</td><td>2D truss linear elastic analysis</td><td>3-D linear elastic analysis</td></tr>
<tr><td>Truss bridge (skewed)</td><td>3-D truss linear elastic analysis</td><td>3-D linear elastic analysis</td></tr>
</table>

For the detailed models in assessment phases II and III, following points need to be considered:

- EN 1994-2 (2005) requires that shear lag effects (i.e. effective widths) being considered in the global model (clause §5.4.1.1). See also next paragraph.
- When the bridge deck (composite slab or orthotropic steel deck) is modelled in 3-D global models, it is important to model the deck in correct distance from neutral axis of the whole composite section (slab/deck and girder). The steel girders can be modelled either by beam elements or shell elements. Either way, the deck will be modelled with shell elements being offset from the neutral axis such that the shell elements are in the centreline of the actual deck. See Figure 5.1 for clarification. Recall that all the members should be constrained appropriately such that "planes remain plane" assumption for global bending holds. This method of modelling has the advantage that the effects of shear lag are automatically (and accurately) considered in the global model.
- Furthermore, influence of cracking of the concrete deck on elastic stiffness of the composite beam in regions with negative moments should be considered. For simplicity, clause §5.4.2.3 of EN 1994-2 allows to consider the effect of composite deck cracking in the following manner: First, the envelope of internal forces and moments for the characteristic load combinations is calculated assuming un-cracked section properties; second, the stresses in the extreme fibres of concrete deck from first analysis (un-cracked analysis) are checked. In regions that these stresses exceed the twice the tensile strength of concrete ($2 \cdot f_{ctm}$) concrete is assumed fully cracked. A second analysis (cracked analysis) is performed assuming cracked concrete in the regions affected. The internal actions from cracked analysis can then be used for all ULS and SLS checks.
- If local detailed models are built for the critical details, it is preferable (and maybe even simpler) to use the local stress-based methods, namely hot-spot stress method and notch stress method (see Section 3.4.2). Note that these methods are only applicable for fatigue cracking in the weld regions. To achieve reliable results using these methods, special care should be taken in constructing the finite element model (e.g. element types and sizes, modelling of weld geometry, and so on). Detailed instructions can be found in (Al-Emrani and Aygül 2013) .

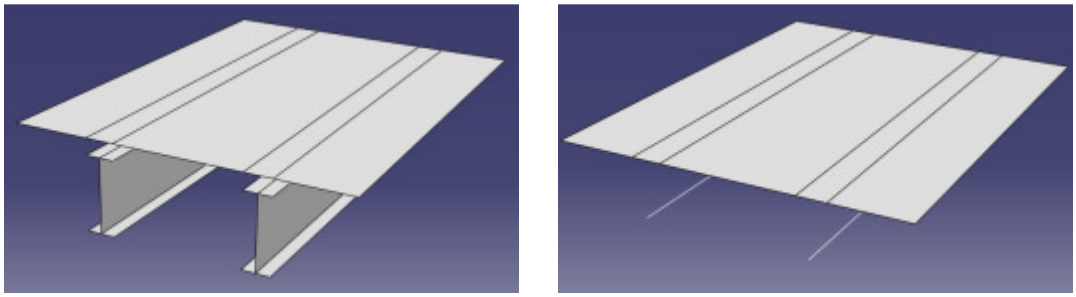

(a) (b)

Figure 5.1 Two methods for modelling of girder and deck system such that each element's axis coincides with the member's centreline in the actual structure; (a) shell elements for all members; (b) beam elements for girder and shell elements for the deck (Bengtsson and Widén 2010).

5.1 Modelling techniques for local strength assessment of large structures

Fatigue damage is a highly localized process. The service loads act on the whole structure while the resulted fatigue cracking occurs at the local details with high stress concentrations, such as welded connections of the structure. The detail level provided by the global models of bridge structures usually fail to predict the detailed stress state in the details. To overcome this limitation, four methods can be considered (von Selle, Doerk, and Scharrer 2009):

1. Using the standard tables and formulas for the stress concentration factors (SCFs)
2. Sub-modelling technique
3. Sub-structuring technique
4. Locally-refined global FE-models

Figure 5.2 depicts these methods for a cope hole detail. Using SCFs is fast and easy, but this is in case that SCF's be available for the studied detail.

Sub-modelling technique is a two-step analysis: the global model and the sub-model are two distinct FE models. First, the global model is analysed. Then, the results of global analysis at the location of boundaries of sub-model are extracted. These "driven variables" (displacements or stresses) at the boundaries of sub-model are then applied to the sub-model as boundary conditions. Finally, sub-model is analysed to get the local results. In short, the local model is driven by the deformations from global model applied on the boundaries of local model. This technique is implemented in major finite element analysis packages, e.g. ABAQUS and ANSYS. Sub-modelling technique provides easier control over the mesh in the local model. Besides, once the global model is analysed, several sub-models (i.e. details) can be analysed without need to re-analyse the global model.

A useful feature implemented in sub-models in some software (e.g. ABAQUS) is shell-to-solid sub-modelling. The global model can be constructed of shell elements, while the local model being made of solid models. The program generates the necessary constraint equations at the boundaries to maintain the compatibility between the global and two models.

Sub-structuring is a modelling technique belonging to the earlier days of finite element analysis. It is used only for linear analysis of structures and is particularly useful in cases when repetitive patterns of parts exist in the structure. The program calculates the sub-structure (formerly known as super element) stiffness matrix at the beginning of analysis and retains only 'external DOFs while eliminating internal DOFs. Thus, the whole substructure will be threatened as a single element. Thus, the analysis will perform faster.

Direct mesh refinement of global FE-model can result in a large model with lots of details. This may cause difficulties in working with model, as well as long analysis times. Therefore, it is not generally recommended for detailed analysis of structural details in the bridges.

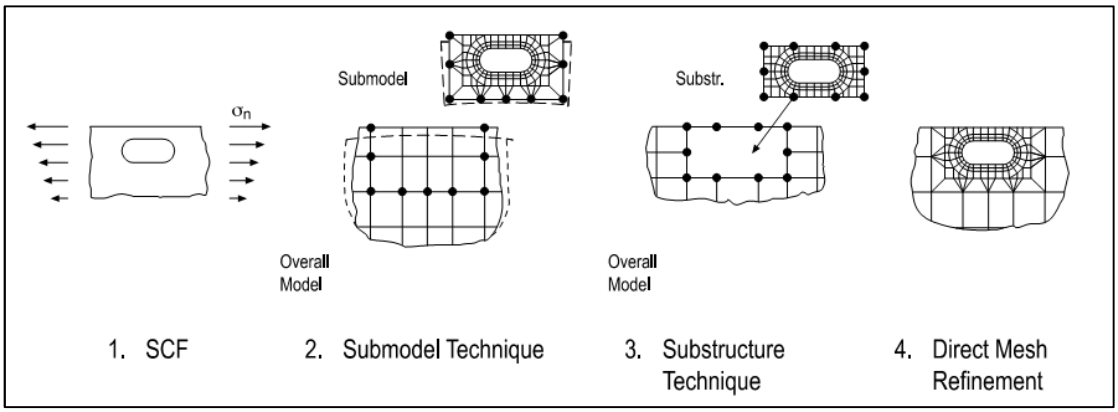

Figure 5.2 Methods for local stress evaluation in a Large FE model (von Selle, Doerk, and Scharrer 2009).

6 Case study

6.1 Introduction

The Göta river bridge (Götaälvbron) connects the Hisingen island to the central part of the Gothenburg. The bridge is an important connection mainly for local traffic and public transport from central Gothenburg and Hisingen. It is the only tramway link to Hisingen and is planned to be replaced soon (between years 2020 and 2021) by the new Hisingen bridge. Figure 6.1 shows a panorama image of the bridge.

Götaälvbron is a welded steel bridge. The cross section is composite multi-girder structure with concrete slab (thicknesses varying in different locations between 180 to 270mm). However, composite action is not fully achieved because of the lack of enough number of shear studs according to modern standards. The girders are designed as continuous multi-span beams. Total length of the bridge is ~950 m with the maximum span size of 42 m. There is an opening part (bascule type, Swedish: Klaffbro) located in the middle of the river, see Figure 6.2. The main part of Götaälvbron was built in the period 1936 – 1939. The welding technology was at its early development at the time of the construction. The bridge is one of the first welded bridges built in Sweden (L. Wallin 1973). Later, in 1956, the bridge was widened to accommodate for the increased traffic at the time. Cross sections shown in Figure 6.3 show the current state of the bridge. Note the extended parts in the cross section (bicycle and pedestrian, B&P lanes) which are attached to the original construction. Allowable vehicle charge is load class 3 (Bärighetsklass BK 3) which includes trucks up to 37.5 tonnes gross weight (max. axel weight 8 tonnes). For the two outermost lanes, only vehicles with maximum gross weight of 3.5 tonnes can pass. Average daily traffic is 20,100 passages per day (Trafikkontoret 2013).

Figure 6.1 Panoramic image of Götaälvbron.

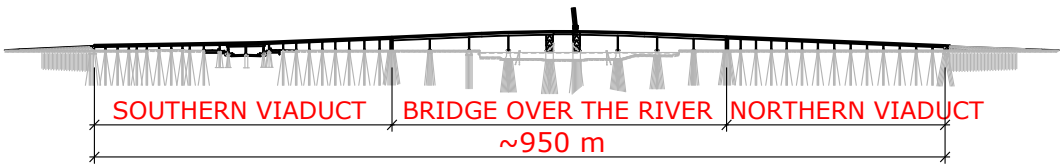

Figure 6.2 Side view of the bridge.

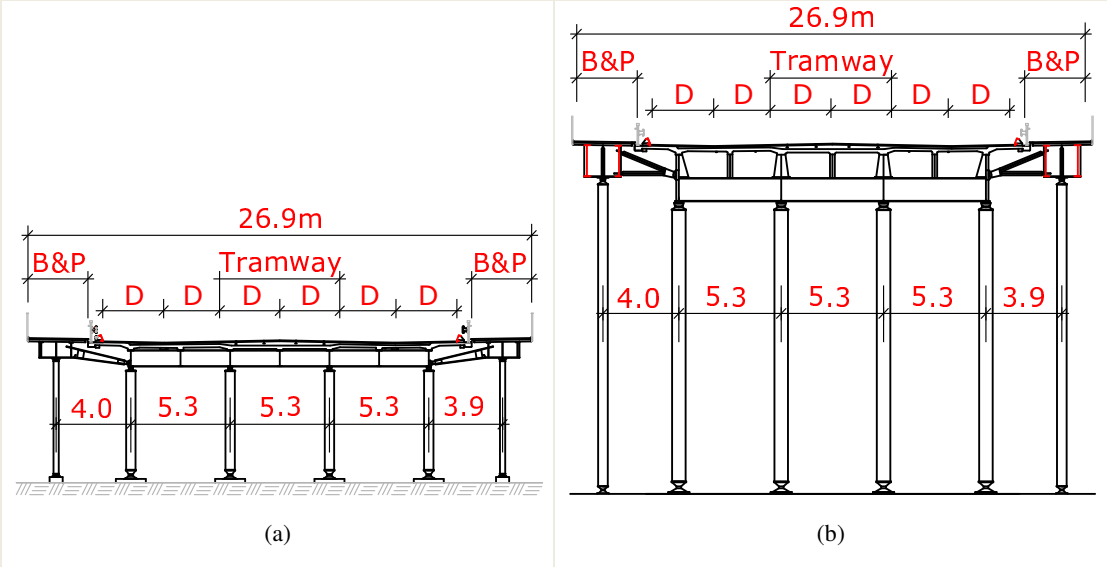

Figure 6.3 Cross sections of the bridge. B&P (bicycle and pedestrian) lanes were added later to accommodate for increased vehicle traffic in the 1956.

6.1.1 Materials

For the main girders in superstructure, two steel grades according to old German DIN 17100 have been used: St 44 (Equivalent[4] to S275) for the "viaduct" parts, and St 52 (Equivalent to S355) for the "river" part. The steel used in the bridge was produced by Thomas process. A coated electrode with designation E52h was used for welding. Concrete of class C28/35 has been used for the deck slab. The plain steel rebars are St44 grade.

A summary of all the previous material tests for the bridge is given in Table 6-1. The only available fracture toughness tests were carried out in 2003 and only for one steel grade (St 44). The design speed of $v = 50\ km/h$ in the Table was used to determine the loading speed of specimens in the fracture tests according to Equation (C-18). The treatment of fracture test data for determining of master curve is presented in Table 6-5, Section 6.4.1 (Phase III assessment). Charpy V-notch energy data are used for evaluating transition temperature, applicable for phases I and II of assessment.

6.1.1.1 Chemical composition of steel material

Table 6-2 presents the chemical composition. The data is a collection of test results from three different measurements in 1939, 1956, and 2003. As the upper-bound values show, high carbon percentages were observed in some specimens of both St44 and St52 steels. Typical values from a modern steel grade S355JR (R stands for reduced toughness) is given in the table for comparison. High carbon content together with the fact that the material is Thomas steel are indicators of the low fracture toughness of steel material. One typical aspect of Thomas steels is their high nitrogen content. Unfortunately, the nitrogen content had not been measured during any of the past chemical analysis tests of bridge material.

[4] For finding equivalent modern steel grades of old European steel material, following sources can be consulted: Annex A of EN 10025-2 (2004) and Annex A of EN 10025-3 (2004)

Table 6-1 Summary of the past tests on the bridge.

Test	Laboratory (Date) / Standard	No. of specimens	Sampling location and material	Comments
Fracture toughness	SP (2003) / BVS 583.12 & ASTM 813	9 pcs	Viaduct, ST-44	$V = 50\ km/h$ $T = -30°C$
Chemical analysis	SP (2003) / BVS 583.12	3 pcs	Viaduct, ST-44	
Tensile test	SP (2003) / SS-EN 10002-1	9 pcs	Viaduct, ST-44	$T_{plate} = 10{\sim}24mm$
Chemical analysis	Kemiska Kontrollbyrån (1939)	2 pcs	ST-52 T=12mm	High sulphur content in one specimen
Tensile test	Kemiska Kontrollbyrån (1939)	6 pcs BM 4 pcs HAZ 4 pcs WM	ST-52 T=12mm	Report is missing
Charpy V-notch test	EASB (1956)	6 pcs	ST-52	Main girders and transverse girders in I and X
Chemical analysis	KTH (1956)	4 pcs	River part ST-52 & ST-44	Specimens from web and flange
Charpy V-notch test	KTH (1956) / SIS 112350	4 pcs	River part ST-52 & ST-44	

Table 6-2 Chemical composition of steel material from measurements in 1939, 1956, and 2003. Values are given in weight percentage of the alloy. Typical values for S355JR are given in the table only for comparison.

Grade	Qty	C	Mn	Si	P	S	Cr	Ni	Cu
St44	5	0.12–0.26	0.40–0.67	0.00–0.16	0.009–0.065	0.014–0.045	0.01–0.08	0.02–0.03	0.03–0.12
St52	4	0.16–0.22	0.87–1.10	0.28–0.36	0.019–0.043	0.015–0.086	0.23–0.32	–	0.26–0.49
S355JR	–	*0.24*	*1.5*	*0.55*	*0.035*	*0.035*	–	*0.012*	*0.55*

6.1.2 Fatigue-critical detail

During regular inspections in 1999, two cracked welded connections in the northern viaduct part of the bridge were detected. The cracking had occurred in two similar details over two bridge supports. Figure 6.4 shows the details of observed cracks. As it is seen, the negative moment at the support is transferred by means of two cover plates, with the top cover plate transferring the tensile force of the couple. The cracking had occurred at this plate in two different support locations in the "northern viaduct" part

of the bridge. It is not clear for how long the cracks had formed. Larsson (2004) concluded two potential reasons for this cracking:

- Fatigue due to traffic loads with large stress ranges (considering the dynamic effects) and a high number of loading cycles,
- Brittle fracture due to insufficient toughness of the steel material in combination with thermal effects and large traffic loads. Also, the contribution form differential support settlements to increase the tensile stresses in the supports might have played a role.

The detail shown in Figure 6.4 has a peculiar geometry, and does not conform to modern fatigue design guidelines that encourage more smooth transition geometry between main load-bearing components. Besides, site inspections of the bridge showed generally inferior welding quality compared to modern welded structures. This is understandable due to less onerous early welding regulations, compared to modern execution standards. These two factors are reflected in the choice of detail category, as is discussed in the following section.

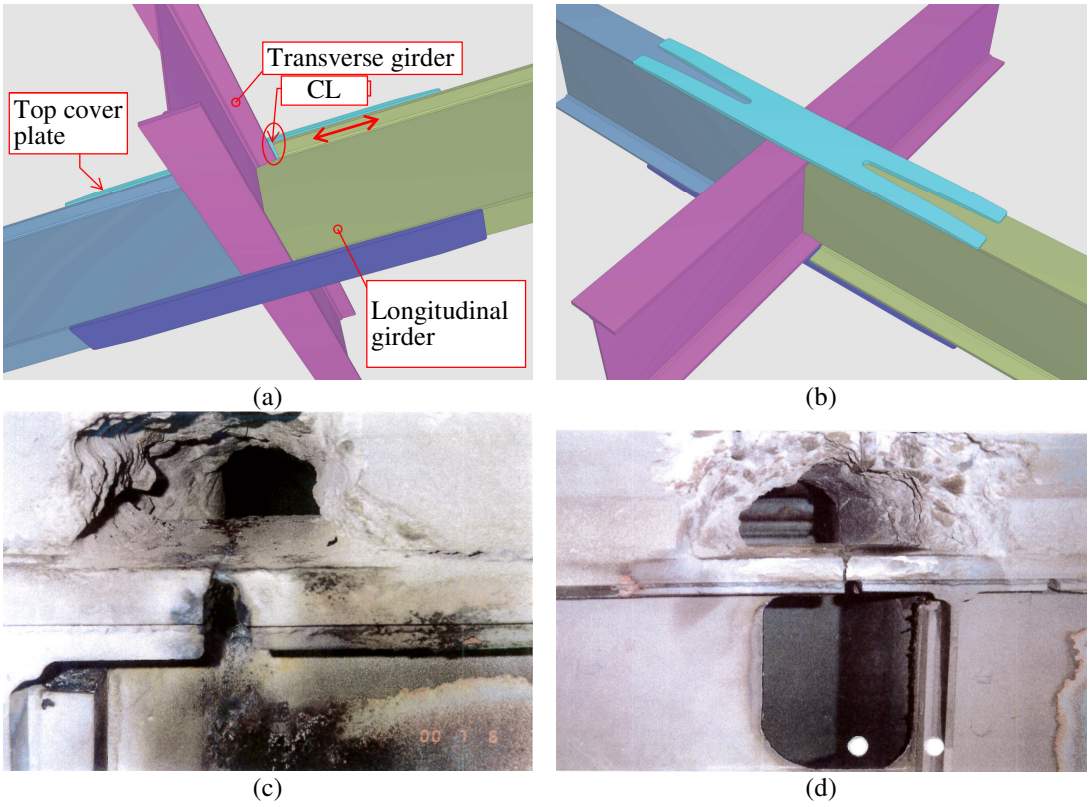

Figure 6.4 *Critical detail at viaduct part of the bridge. (a) continuity of longitudinal girder is interrupted at the support location by transverse girder. Top and bottom cover plates are provided to transfer the moment. Cracking location is shown as "CL" (view from below the deck); (b) View from top; (c)&(d) Cracked top cover plates at support locations N7 and N9.*

6.2 Phase I

Phase I evaluation was carried out earlier by Larsson (2004). Swedish national standard was used because at the time Eurocode was not the governing standard in Sweden. Therefore, No phase I evaluation was carried out and the assessment started at phase II. For examples of Phase I assessment (fatigue evaluation using equivalent stress range), see Al-Emrani and Aygül (2013).

6.3 Phase II

In this phase, the collected data about traffic loads and material tests are used to assess the Palmgren-Miner index for damage due to fatigue. For brittle fracture assessment, permissible thickness table (see Section 2.2.1) is used.

6.3.1 Resistance-side data

6.3.1.1 Choice of detail category

An exact representation of this detail cannot be found in detail category tables of EN 1993-1-9. However, it is similar to the detail 1 (Tee joint, See Figure 6.5) in Table 8.5 of EN 1993-1-9, with a large support length ($l > 120\,mm$). The conservative assumption for l can be justified by the fact that the flange plate is stiffened by the I-beam's web plate. Given the plate thickness $T_{plate} = 28\,mm$, the detail category would be C-class 50. However, this value corresponds to a modern welded detail fabricated according to EN 1090-2 (2008) and free form discontinuities and misalignments outside the tolerance limits of that standard. Therefore, for assessments in Phase I (and Phase II) further reductions (two detail categories) are considered; i.e. C-class 36 is selected, which is the lowest C-class available in EN 1993-1-9.

Detail category	Constructional detail			Description
80	ℓ<50 mm	all t [mm]	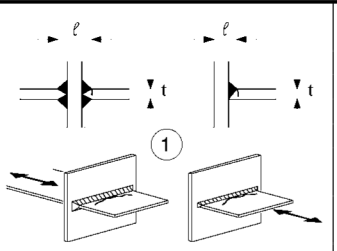	Cruciform and Tee joints: 1) Toe failure in full penetration butt welds and all partial penetration joints.
71	50<ℓ≤80	all t		
63	80<ℓ≤100	all t		
56	100<ℓ≤120	all t		
56	ℓ>120	t≤20		
50	120<ℓ≤200 ℓ>200	t>20 20<t≤30		
45	200<ℓ≤300 ℓ>300	t>30 30<t≤50		
40	ℓ>300	t>50		

Figure 6.5 Detail 1 from Table 8.5 of EN 1993-1-9.

6.3.1.2 Charpy impact energy data

The Charpy data from the past tests were analysed to assess the temperatures T_{27J} and T_{40J}. Figure 6.6 shows the data points from one of the tests by ESAB (see Table 6-1) and fitted curve to the data according to Equation (C-5). The temperatures corresponding to 27J and 40J impact energies are evaluated from the fitted curve as $T_{27J} = 9℃$ and $T_{40J} = 20℃$.

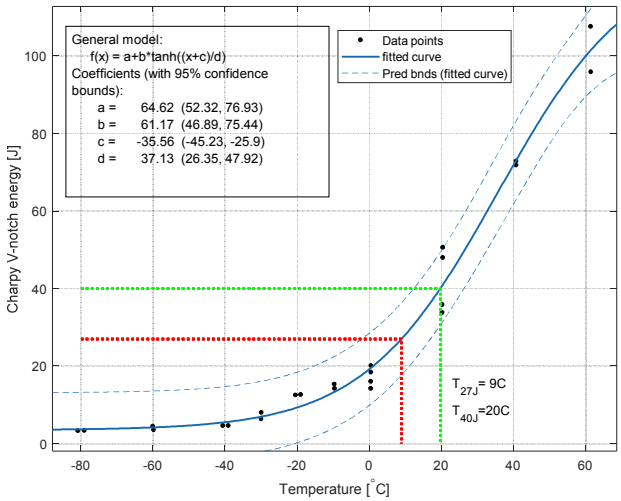

Figure 6.6 Charpy test data and fitted transition curve in the form of a tanh function.

6.3.2 Action-side data

The temperature is the main action for brittle fracture assessment in T-method. The minimum service temperature by Swedish National Annex to Eurocode (Trafikverket 2012) is $T_{min} = -29℃$. The temperature data registered for the past 6 years is given in Figure 6.7 for comparison. The temperatures were registered by the fibre optic continuous measurement system installed on longitudinal steel girders of the bridge. Glisic et al. (2007) and Enckel (2011) have provided a complete review of the installed fibre optic system. In summary, the minimum service temperature $T_{min} = -29℃$ is considered for this study.

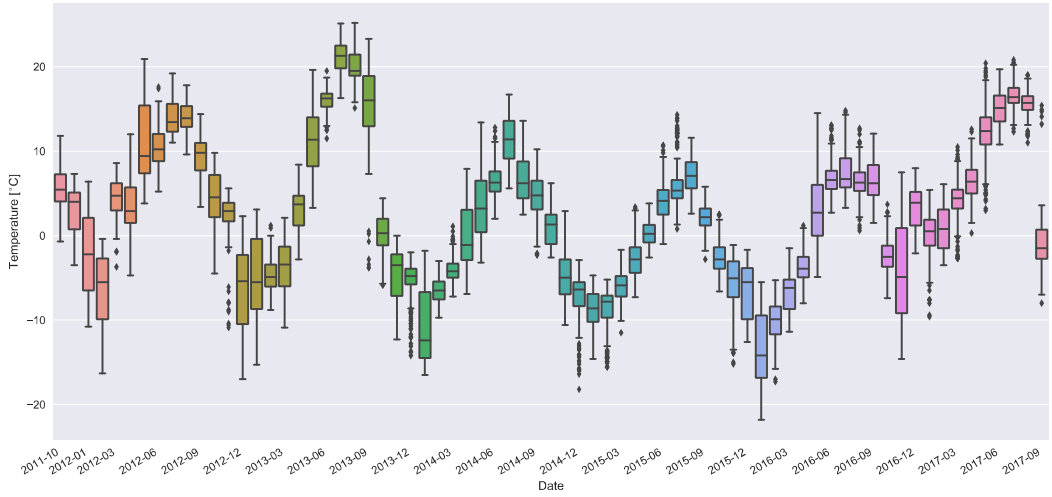

Figure 6.7 Box plot of temperature data from measurements (4 times per day) on the bridge, aggregated by month.

6.3.2.1 Traffic loads

From the available traffic data, Larsson (2004) carried out an estimation of traffic on the bridge for the period 1939—2020. The results are shown in Figure 6.8, categorized by the vehicle type (tramway, bus, truck, and personal car) and the gross weight of the vehicle. As can be seen, the vehicle weights on the bridge have been below 80 tonnes and largest loads were due to passage of tramways.

Various types of tramways have been in service over the bridge during the past 79 years. The two most frequent types were models M21 and M31. The axel arrangement and maximum nominal axel loads for these tramways are shown in Figure 6.9. The heaviest loads on the bridge (vehicles with weight above 75 tonnes in Figure 6.8) were the result of passage of two M21 tramways with a short headway. That is why the combination "2xM21" is included in Figure 6.9.

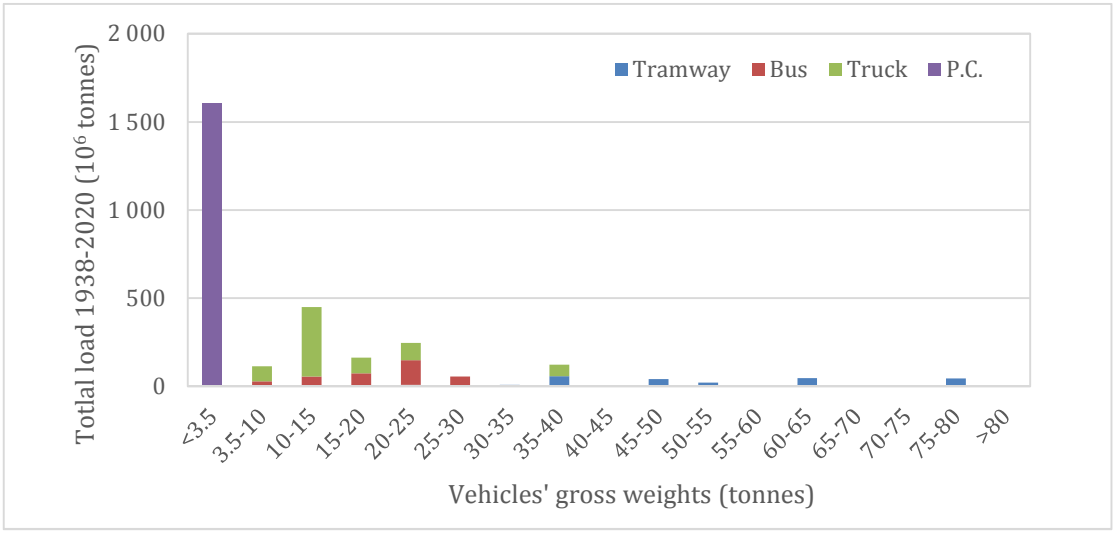

Figure 6.8 Estimated Traffic loads on the bridge (one direction) for the period 1939-2020, according to Larsson (2004).

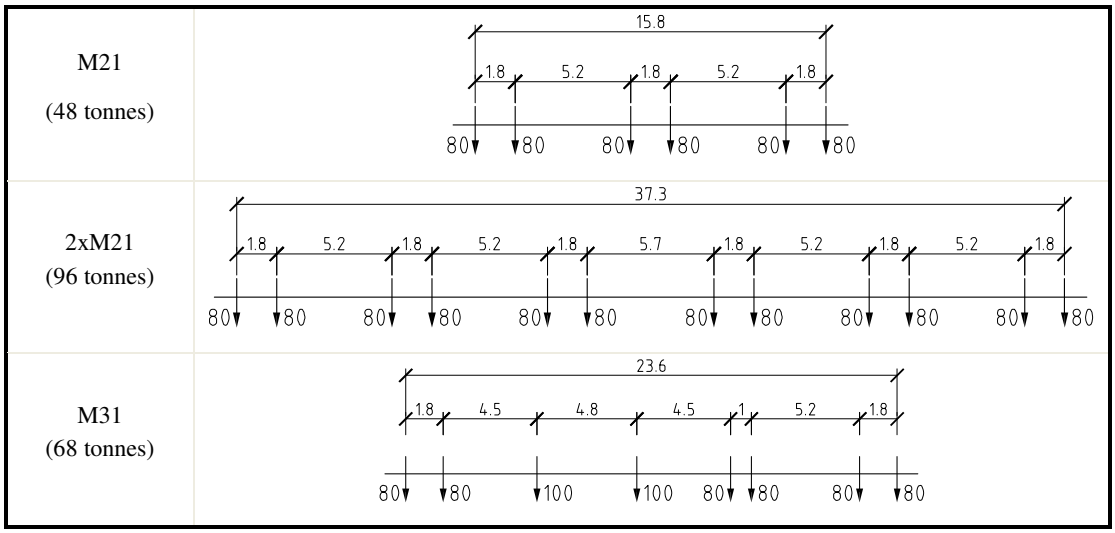

Figure 6.9 Axel arrangement and maximum nominal axel loads for M21 and M31 tramways. Axel loads are in [kN] and axel distances are in [m].

To simplify the calculations, all the tramway loads on the bridge from Figure 6.8 are modelled using one of the three tramway loads shown in Figure 6.9. The tramway types used for each weight range are indicated in Table 6-3. A reduction factor is multiplied by maximum nominal weight of the Tramway to adjust its weight to the corresponding weight range. For example, for the first row of the table the nominal weight of 2xM21 trams (96 tonnes) is multiplied by a reduction factor of $77.5/98 = 0.81$ in fatigue calculations.

Dynamic amplification factor: dynamic effects for the passage of tramways are considered according to article 2.3.3.2.5 from Trafikverket's "Krav" document (2017) which gives similar regulations to Annex C of Eurocode EN 1991-2. The calculations are as follows:

Total length of spans in continuous beam:	$\Sigma L = 137.6\ m$
Number of spans:	$\mathrm{n_{spans}} = 10$
Mean span length:	$L_m = \frac{\Sigma L}{n_{spans}} = 13.76\ m$
The determinant length from article 10.5 in "Krav" document:	$L_\Phi = 1.5 \cdot L_m = 20.64\ m$
Maximum permitted speed:	$v = 50\ km/h = 13.9\ m/s$
First natural vibration frequency of the bridge (from FE model):	$n_0 = 1.64\ Hz$
α coefficient depending on the speed:	$\alpha = v/22 \leq 1 \rightarrow \alpha = 0.63$
Parameter K:	$K = \frac{v}{2L_\Phi \times n_0} = 0.205$

Now the parameters ϕ' and ϕ'' can be calculated:

$$\phi' = \frac{K}{1-K+K^4} = 0.258$$

$$\phi'' = \frac{\alpha}{100}\left[56e^{-\left(\frac{L_\Phi}{10}\right)^2} + 50\left(\frac{L_\Phi n_0}{80} - 1\right)e^{-\left(\frac{L_\Phi}{20}\right)^2}\right] \geq 0 \rightarrow \phi'' = 0$$

Finally, the dynamic amplification factor will be:

$$DAF = 1 + \phi' + 0.5 \cdot \phi'' \rightarrow DAF = 1.258$$

6.3.3 Fatigue assessment

Influence line for moment at support C13 (critical detail location) due to movement of a 1kN axel along the rail track closest to the support is shown in Figure 6.10. To evaluate the time history of bridge response under traffic load effects, the axle loads (including dynamic amplification factor) of each of the vehicles in Table 6-3 are moved along the influence line in small steps and the action effect is calculated for each step. To evaluate bending stresses from bending moments, section properties $I = 6.39 \times 10^9 mm^4$ and $c = 464\ mm$ are used. Figure 6.19 shows the geometry of the girder at critical location. This sequence of action effects forms the time history of response under each vehicle loading, from which the stress range histogram is derived using rainflow cycle counting. Having the stress cycles from each vehicle, corresponding partial damage can be calculated for that vehicle according to Section 2.2.2. The partial factors are also presented in Table 6-3. The stress spectrum from all the traffic loads in the table, is shown in Figure 6.11. The S-N curve for detail category C36 is also shown

in the figure. As can be seen, the majority of stress cycles are below ~14 MPa and do not contribute to the fatigue damage. Total Accumulated fatigue damage is calculated according to Equation (2-5):

$$D = \Sigma d_i = 2.80 > 1$$

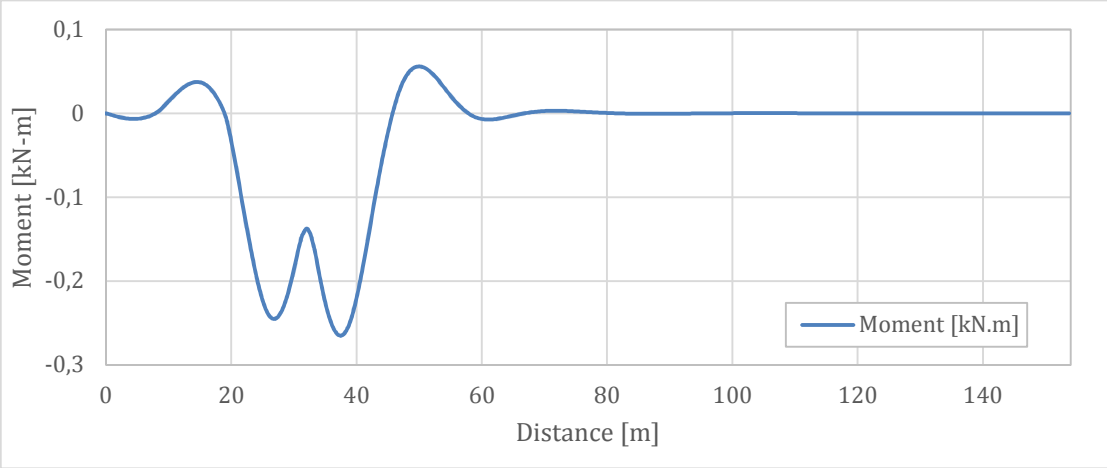

Figure 6.10 Influence line for moment at support C13 for a 1kN axel moving on the rail track closest to the support location.

Table 6-3 Tramway traffic loads on the bridge, categorized by vehicle weight and type. Last column shows the partial fatigue damage from each vehicle type.

Tramway weight [t]	Average Weight [t]	Type	AADT	Total number of trains	Partial damage, d_i
75-80	77.5	2xM21	19	565,619	1.45201
65-70	67.5	M31	2	58,629	0.18509
60-65	62.5	M31	24	715,269	0.89531
50-55	52.5	M31	14	398,063	0.15380
45-50	47.5	M31	28	831,661	0.09243
40-45	42.5	M21	4	109,929	0.00824
35-40	37.5	M21	48	1,415,652	0.01622
30-35	32.5	M21	9	262,147	0
25-30	27.5	M21	4	114,326	0
20-25	22.5	M21	10	303,989	0
Total Fatigue Damage				Σd_i:	2.80

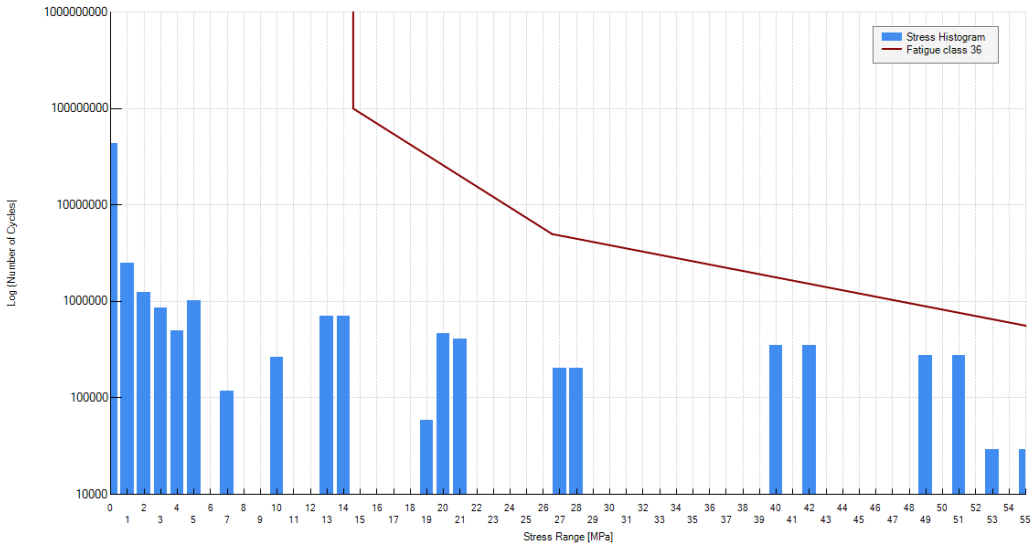

Figure 6.11 Stress spectrum for the tramway traffic on the bridge in the period 1939—2020. The S-N curve for detail category C36 is also shown.

The damage index being larger than 1 indicates that the service life of the detail is exhausted. There is no remaining fatigue life according to this method! This is even without consideration of the road traffic (buses and trucks) on the bridge with which the Palmgren-Miner damage will be even larger.

6.3.4 Brittle fracture assessment

For brittle fracture assessment, first the reference temperature is calculated:

Minimum air temperature:	$\mathrm{T}_{\mathrm{min,d}} = -29℃$
Radiation loss (EN 1991-1-5 for a steel and concrete composite bridge)	$\Delta T_r = -5℃$
The influence of stress, member geometry, and crack:	$\Delta T_\sigma = 0℃$
The additive safety element:	$\Delta T_R = 0℃$
Other factors (cold working and high strain rate):	$\Delta T_{\dot{\epsilon}} = \Delta T_{\epsilon pl} = 0℃$

Thus, according to Equation (2-2) the reference temperature is:

$$T_{Ed} = -34℃$$

Then the ratio $\frac{\sigma_{Ed}}{f_y(t)}$ should be evaluated, as follows:

Plate thickness (cf Figure 6.12):	$\mathrm{T}_{\mathrm{Plate}} = 28\ mm$
Yield stress (Equation (2-3)):	$f_y(t) = 275 - 0.25 \cdot 28 = 268\ \mathrm{MPa}$

The maximum resultant stress acting on the section is evaluated from the finite element model as:

Self-weight:	$\sigma_G = 37\ MPa$
Variable action (Traffic):	$\sigma_Q = 33\ MPa$, $\psi_1 = 0.75$ (TRVFS 2011, 7kap-5§)

Design value: $\sigma_{Ed} = \sigma_G + \psi_1 \cdot \sigma_Q = 62\ MPa$

Finally, the stress-to-yield ratio is: $\frac{\sigma_{Ed}}{f_y(t)} = \frac{62}{268} = 0.23$

From the Charpy energy data ($T_{27J} \geq 9$ °C), the steel grade is equivalent to S275JR. The permissible plate thickness can now be calculated from the data in Table 3-7. The part of the table that is used here is shown in Table 6-4, with the pertinent numbers being highlighted. The permissible plate thickness is normally evaluated by double interpolation of the pertinent rows and columns in the table. But since $\sigma_{Ed} = 0.23 f_y(t) < 0.25 f_y(t)$, only a single interpolation between the two highlighted values is required. For $T_{Ed} = -34$°C, the permissible plate thickness is $64\ mm$ which is considerably larger than $T_{plate} = 28\ mm$. This means that, had the studied detail were built following modern execution standards (e.g. EN 1090-2), it would have had enough resistance against brittle fracture. But since the quality control standards were not followed for the execution of the weldments in the studied bridge, the risk of brittle fracture cannot be entirely ruled out. See also the discussion at the end of this chapter (Section 6.5).

Table 6-4 Part of Table 3-7 used for the case study. The relevant numbers in S275JR row are highlighted.

Steel grade	Sub-grade	Charpy energy CVN at T [°C]	Charpy energy CVN J_{min}	Reference temperature T_{Ed} [°C]																								
				10	0	-10	-20	-30	-40	-50	10	0	-10	-20	-30	-40	-50	10	0	-10	-20	-30	-40	-50
				$\sigma_{Ed} = 0{,}75\ f_y(t)$							$\sigma_{Ed} = 0{,}50\ f_y(t)$							$\sigma_{Ed} = 0{,}25\ f_y(t)$						
S235	JR	20	27	60	50	40	35	30	25	20	90	75	65	55	45	40	35	135	115	100	85	75	65	60
	J0	0	27	90	75	60	50	40	35	30	125	105	90	75	65	55	45	175	155	135	115	100	85	75
	J2	-20	27	125	105	90	75	60	50	40	170	145	125	105	90	75	65	200	200	175	155	135	115	100
S275	JR	20	27	55	45	35	30	25	20	15	80	70	55	50	40	35	30	125	110	95	80	70	60	55
	J0	0	27	75	65	55	45	35	30	25	115	95	80	70	55	50	40	165	145	125	110	95	80	70
	J2	-20	27	110	95	75	65	55	45	35	155	130	115	95	80	70	55	200	190	165	145	125	110	95
	M,N	-20	40	135	110	95	75	65	55	45	180	155	130	115	95	80	70	200	200	190	165	145	125	110
	ML,NL	-50	27	185	160	135	110	95	75	65	200	200	180	155	130	115	95	230	200	200	200	190	165	145

6.4 Phase III

According to previous phase II (damage accumulation calculations) the studied detail is unsafe against fatigue. The analysed connection is a crucial link in maintaining the integrity of the structure. Given the large consequences (risks and costs) of the failure of the studied detail, an expert investigation (phase III assessment) is deemed necessary. The details of the assessment are presented in this section.

6.4.1 Resistance-side data

6.4.1.1 Detail geometry

The geometry of the detail, which is in the viaduct part of the bridge (close to support S13, see Figure 6.17), is shown in Figure 6.4a and b. The dimensions for use in SIF calculation are as follows (see Figure 6.12 for explanation of parameters):

Cover Plate thickness:	$T_{plate} = 28$ mm
Plate width:	$B_{plate} = 290$ mm
Flange thickness:	$T_{flange} = e = 18$ mm
Fillet weld leg size:	$z = 7$ mm

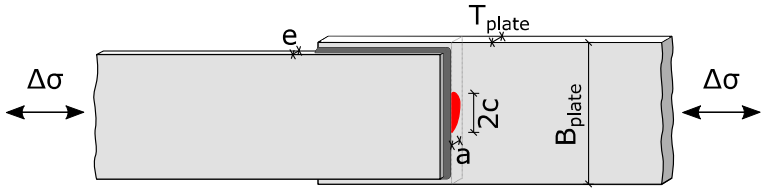

Figure 6.12 Dimensions of the cover plate detail and assumed crack for fracture mechanical analysis. The leg size of the fillet weld (designated by z in the text) is not shown here.

6.4.1.2 Fracture toughness

The fracture energy (J_c) test data from SP (2003) at test temperature $T_{test} = -30$ ℃ is presented in Table 6-5. The transformation of the results to plain strain fracture toughness is also presented in the table:

- linear-elastic fracture toughness for given specimen's thickness, K_{Jc}^{x}, calculated using Equation (C-10).
- limit value of elastic fracture toughness, $K_{Jc,limit}$, according to Equation (C-11)
- fracture toughness for a specimen with the thickness of $1\text{T} = 1$ in.$=$ 25.4mm, K_{Jc}^{1T}, for which the stress state at the large part of crack front will be plane strain (See A.1.1), according to (C-12)

The verification $K_{Jc}^{x} < K_{Jc,limit}$ in Table 6-5 is to make sure that the fracture in the test has occurred in a brittle manner. This can be observed from fracture surface in Figure 6.13, too. The fracture toughness values above $K_{Jc,limit}$ indicate ductile fracture of the test specimen, which makes it of little significance for brittle fracture assessment.

Table 6-5 Fracture test data (test temperature $= -30$ ℃) and transformation of the results to plain strain fracture toughness ($1T = 1\ in. = 25.4mm$).

Sampling location	Flange	Flange	Flange	Web	Web	Web	Flange	Flange	Flange
Thickness $[mm]$	23	22.5	23	10.5	10.6	10.5	24	24.1	24
$J_c\left[\frac{kN}{m}\right]$	16.5	11.8	12.3	13.2	11.9	13.4	16.4	15.5	15
$K_{Jc}^{x}\left[MPa\sqrt{m}\right]$	84.1	71.1	72.6	75.2	71.4	75.8	83.8	81.5	80.2
$K_{Jc,limit}\left[MPa\sqrt{m}\right]$	234.9	232.4	234.9	158.7	159.5	158.7	240.0	240.5	240.0
$K_{Jc}^{x} < K_{Jc,limit}$?	OK	OK	OK	OK	OK	OK	OK	OK	OK
$K_{Jc}^{1T}\left[MPa\sqrt{m}\right]$	82.5	69.6	71.3	64.3	61.3	64.7	82.9	80.7	79.3

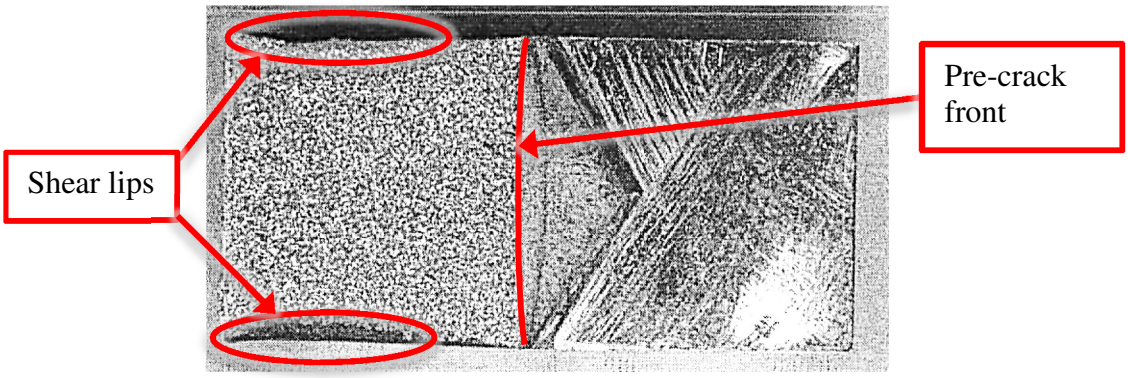

Figure 6.13 Fracture surface of a fracture toughness test specimen. The rough fracture surface and small shear lips indicate negligible ductile deformations, i.e. occurrence of brittle fracture.

Determining master curve using Equations (C-13) and (C-14):

$$K_0 = 74.7\ MPa\sqrt{m}$$

$$K_{Jc,med} = 69.9\ MPa\sqrt{m}$$

Reference temperature T_{K100}, for which $K_{Jc}(T)$ is equal to $100\ MPa\sqrt{m}$, is calculated from master curve, Equation (C-15), having only T_{K100} as unknown

$$T_{K100} = -0.4\ ℃$$

Now that one point on the master curve is known, point $(T_{K100}, K_{Jc} = 100)$, the whole master curve for the temperature range $[T_{K100} - 50℃, T_{K100} + 50℃]$ can be constructed. Using Equation (C-7) and having the T_{K100} value from above, characteristic ($P_f = 5\%$), median ($P_f = 50\%$), and upper bound ($P_f = 95\%$) curves for K_{Jc} versus temperature are estimated. These curves are shown in Figure 6.14.

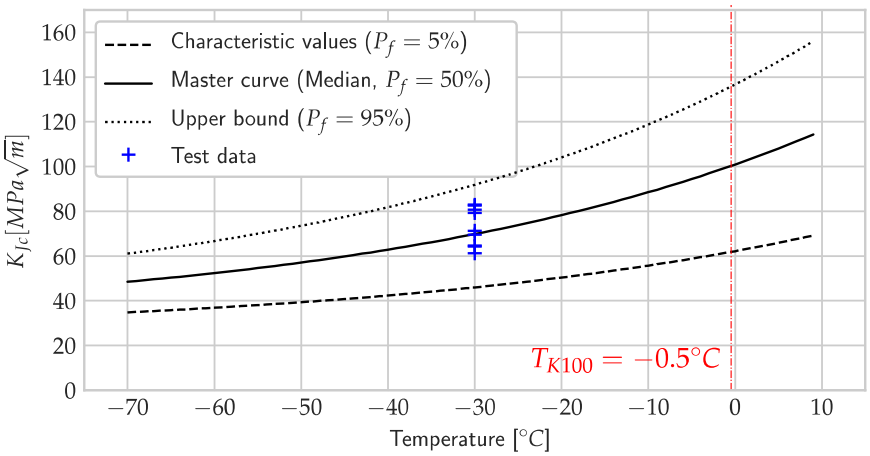

Figure 6.14 Calculated master curve from fracture test data.

As will be seen in the next section on action-side data, the design value of service temperature is $T_{Ed} = -70$ ℃. So, the design value of $K_{mat}(T_{Ed})$, corresponding to 5% fractile fracture toughness (lowest curve in Figure 6.14), will be:

$K_{mat}(-70\ ℃) = K_{Jc,5\%}(-70\ ℃) = 34.9\ MPa\sqrt{m}$

6.4.1.3 Design value of crack size at brittle fracture

According to Equation (2-10), design value of crack size is composed of two parts: initial crack size a_0, and fatigue crack growth size Δa_{FCG}.

6.4.1.3.1 Initial crack size a_0

Initial crack size:	$a_0 = 0.5 \cdot \ln\left(\frac{T_{plate}}{1\text{mm}}\right) = 1.67$ mm
Initial crack width:	$c_0 = \frac{13.3}{2} \cdot a_0 = 11.1$ mm

The choice of relatively large value for a_0 is due to conservative assumption for defects originating from manufacturing (welding). A more realistic (and possibly smaller) value is attained via the use of non-destructive inspections. A limited-extent non-destructive campaign for characterization of crack size in the studied details (using Magnetic Particle Inspection method) did not show any cracks in the cover plates, although only an arrested crack in a fillet weld was observed. In summary, the conservative value of initial crack size shown above was chosen for the calculations in this phase.

6.4.1.3.2 Crack growth due to cyclic loading Δa_{FCG}

Fatigue crack growth calculations are performed according to the methods summarized in Section A.2 and described in a previous report (Zamiri, Leander, and Al-Emrani 2016).

Assuming crack aspect ratio as constant: $a/c = a_0/c_0 = 2/13.3 = 0.15$

Correction factors for evaluation of stress intensity factor can be calculated:

- Correction factor for crack shape (empirical data):

$$F_e(a) = \left[\int_0^{\frac{\pi}{2}} \left(1 - \left(1 - \frac{a^2}{c^2} sin^2\,\phi\right)\right)^{\frac{1}{2}} d\phi\right]^{-1}$$

- Correction factor for a free surface crack:

$$F_s(a) = 1.211 - 0.186\left(\frac{a}{c}\right)^{\frac{1}{2}}$$

- Correction factor for a finite width plate:

$$F_w(a) = \left[sec\left(\frac{\pi a}{B_{plate}}\right)\right]^{\frac{1}{2}}$$

- Correction factor for stress gradient (see Table A-2):

$$\alpha(a) = \frac{a}{T_{plate}}, d = 0.1473\,, q = 0.4398$$

$$K_t = -3.539\,log\left(\frac{z}{T_{plate}}\right) + 1.981\,log\left(\frac{T_{flange}}{T_{plate}}\right) + 5.798$$

$$F_G(a) = \frac{K_t}{1+\frac{(\alpha(a))^q}{d}}$$

Correction factors F_e, F_e, F_S, F_w, and F_G are shown in Figure 6.15(a) as functions of crack size.

To evaluate stress intensity factor range, fatigue stress range is required. Details of calculation of $\Delta\sigma_{eq,CL}$ are given in Section 6.4.2. The SIF range $\Delta K(a)$ corresponding to $\Delta\sigma_{eq,CL} = 9.1\ MPa$ is then calculated from following relation and is shown in Figure 6.15(b):

$$\Delta K(a) = F_s(a) \cdot F_w(a) \cdot F_e(a) \cdot F_G(a) \cdot \Delta\sigma_{eq,CL} \cdot \sqrt{\pi a}$$

With ΔK(a) calculated above and using Paris crack growth Equation (A-8), the crack growth curve is determined. Crack growth parameters are:

Initial crack size:	$a_0 = 1.67$ mm
Paris' relation parameters:	$C = 1.3 \times 10^{-11}$, $m = 3$, [units: MPa and $\sqrt{m}$]

The resulted crack growth curve is shown in Figure 6.16. As will be shown in Section 6.4.2, total number of cycles to next inspection is estimated as:

$$N_f = N_{tot,inspection} = 9.385 \times 10^5 \text{ cycles}$$

Therefore, the crack growth due to cyclic loading will be (see Figure 6.16):

$$\Delta a_{FCG} = 3.8\,mm$$

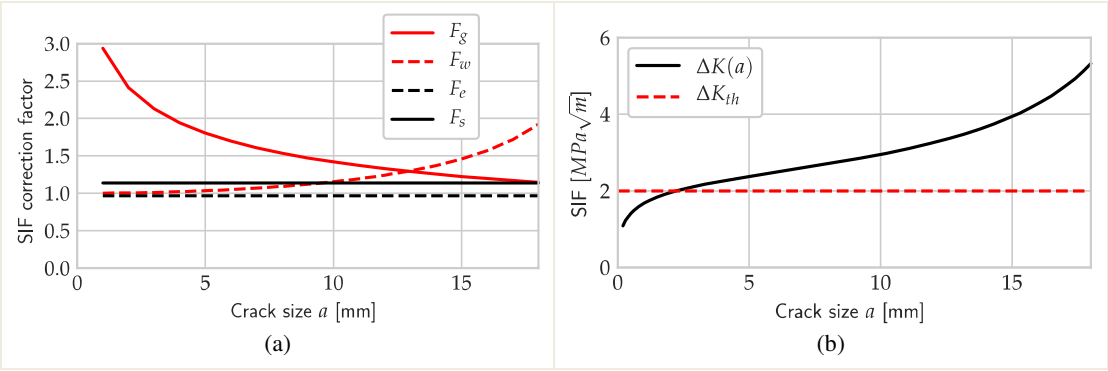

Figure 6.15 (a) Plot of correction factors as functions of crack size; (b) Stress intensity factor range due to fatigue loading $\Delta\sigma_{eq,CL} = 9.1\ MPa$; Threshold stress intensity factor ΔK_{th} is also shown on the diagram.

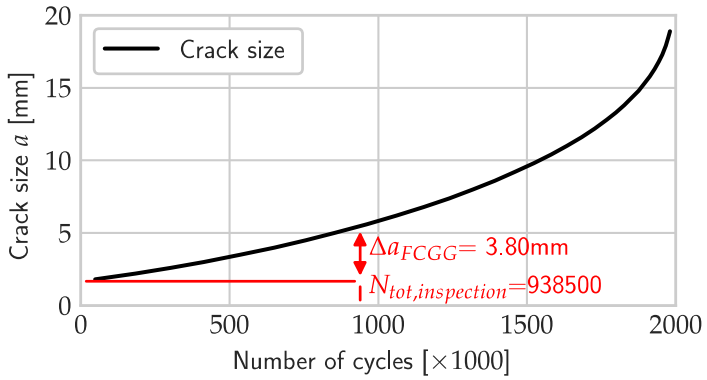

Figure 6.16 Crack growth curve for the studied detail; Initial crack size $a_0 = 1.67\ mm$.

6.4.1.3.3 Design crack size a_d

Finally, the design crack size for brittle fracture assessment will be:

$$a_d = a_0 + \Delta a_{FCG} = 1.67 + 3.8 = 5.5\ mm$$

and the crack width is:

$$c_d = \frac{13.3}{2} a_d = 36.6\ mm$$

6.4.2 Action-side data

To have a more realistic understanding of the action effects in the critical structural members, including the specific detail studied here, the stresses in the structure were measured under controlled loading (continuous monitoring for calibrating FE model) and then normal traffic loading (to estimate the traffic action effects). The details of measurement campaign are given by Leander (2015). Plan of measurement zone I and the details of the instrumentation (strain gauges) are shown in Figure 6.18 and Figure 6.18, respectively. Continuous monitoring took place for more than 9 hours during busy traffic hours. The recorded stress time history was then transferred to the stress ranges spectrum using rainflow cycle counting method (Leander, Trillkott, and Kullberg 2015).

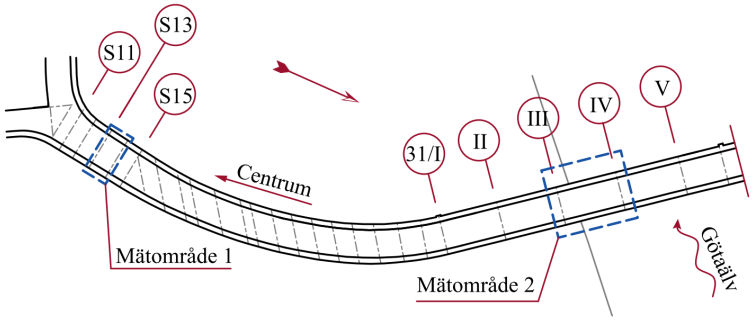

Figure 6.17 Two monitoring locations which were previously used for the calibration of analysis model (Leander, Trillkott, and Kullberg 2015).

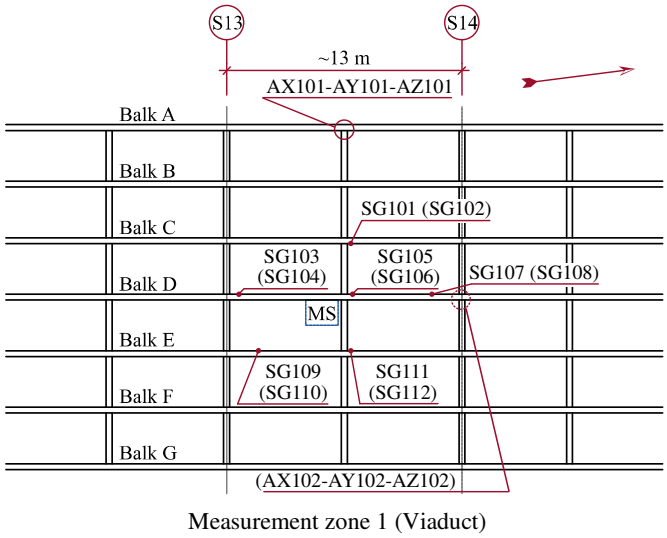

Figure 6.18 Locations of strain gages according to (Leander, Trillkott, and Kullberg 2015).

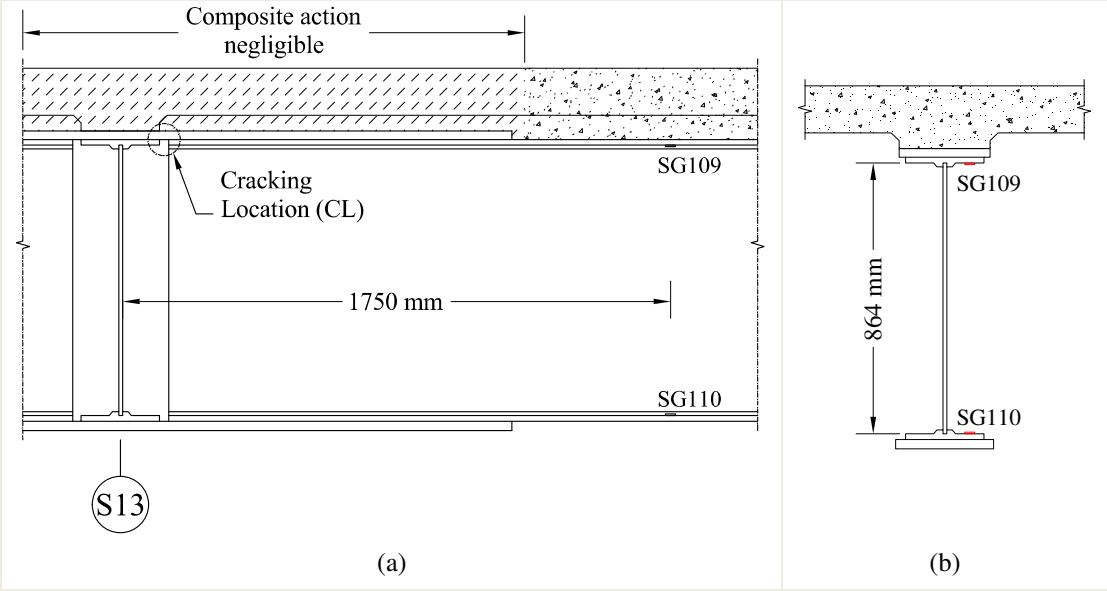

Figure 6.19 Location of strain gages on longitudinal girder C (span: 13m); (a) Elevation view, showing the estimated extent of span for which the composite action is negligible due to negative moments; (b) Cross section.

Because of physical space limitations, it was not possible to install strain gages near the potential cracking site, i.e. the longitudinal girder connections in the supports (Figure 6.4). Therefore, strain gages were installed at various distances from cracking location. For example, as shown in Figure 6.19, strain gages SG109 and SG110 were installed at ~1750 mm distance from the support. Because of composite action existing in the measurement location, the stresses reported by SG109 were low. As a conservative assumption, the stresses from SG110 (installed on the lower flange) are used for calculations here, since they better represent the stresses in the cracking location, where composite action is negligible. The stress range spectrum for strain gage SG110 is shown in Figure 6.20. In summary:

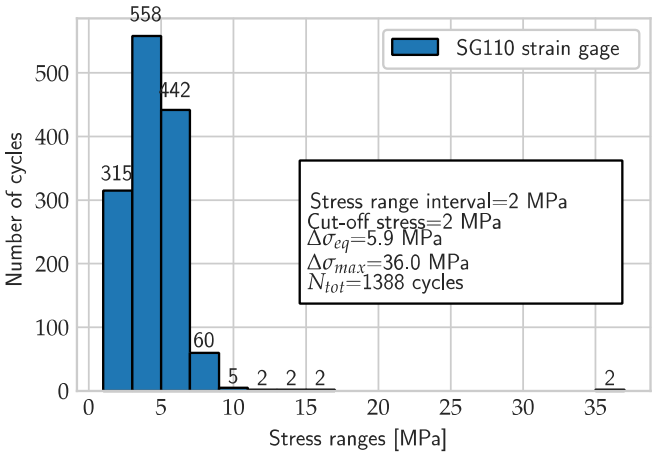

Figure 6.20 Measured stress range spectrum at the location of SG110 strain gage

Equivalent stress range from Equation (A-10):	$\begin{cases} \Delta\sigma_{eq,SG110} = \left[\frac{\sum_i (n_i \cdot \Delta\sigma_i^3)}{n_{tot,G110}}\right]^{\frac{1}{3}} \\ \Delta\sigma_{eq,SG110} = 5.9\ MPa \end{cases}$
Total number of cycles in measured spectrum:	$N_{9h,SG110} = 1388$

This equivalent stress is corresponding to stress spectrum measured at strain gauge location, which is located 1750 mm apart from the crack location. Kwon et al. (2010) have suggested a so-called spatial adjustment factor (SAF) to transfer the results from neighbouring sensor locations to the cracking location. Kwon and colleagues derived SAF as the ratio of stresses at the two locations (sensor location and potential cracking location) from analysis of a finite element model under static loading (vehicle axel load). However, this ratio will change if the location of axel load changes along the bridge.

To better account for the variation of load location on SAF, a different approach based on the influence lines is used in this study. Figure 6.21 shows the influence lines for the moments in the two locations (measurement location and cracking location). The influence lines are calculated using analysis of the FE model of bridge deck for the passage of a 2-wheel ($2 \times 50\ kN$) axel load moving along the rail track located close to the studied detail. Since the bending stresses in the flanges are proportional to the bending moments, the influence lines for the stresses in indicated locations will have the same shape. Considering the influence line as the stress history in the detail due to

the passage of a single axel load, corresponding stress range histograms are evaluated using rain flow counting algorithm, see Figure 6.22.

Comparing the two stress range histograms in Figure 6.22, apparently the passage of a single unit axel load on the lane over beam C has resulted different equivalent stress ranges and number of cycles in the two locations SG110 and CL. The following spatial adjustment factors (SAFs) are suggested for equivalent stress range and number of cycles, respectively:

SAF for stresses:	$SAF_{srtress} = \frac{\Delta\sigma_{eq,\mathrm{CL,mon}}}{\Delta\sigma_{eq,SG110}} = \frac{52.7}{33.8} = 1.56$
SAF for number of cycles:	$SAF_{\mathrm{ncycles}} = \frac{N_{infline,CL}}{N_{infline,SG110}} = \frac{3}{2} = 1.50$

Having the equivalent stress range and number of cycles from measurement in SG110 location, the corresponding values for the cracking location (CL) can be deduced using SAFs:

Equivalent stress range in CL:	$\Delta\sigma_{eq,CL} = SAF_{Stress} \cdot \Delta\sigma_{\mathrm{eq,SG110}} = 9.1\ MPa$
Number of cycles in CL for the duration of measurement:	$n_{9h,CL} = SAF_{\mathrm{ncycles}} \cdot n_{9h,G110} = 2082$

Dynamic effects are already included in the measurement of real traffic; hence no need to apply dynamic amplification factors. The estimated values of equivalent stress range and number of cycles in cracking location will be used in the fatigue crack growth calculations in 6.4.1.3.2. Monitoring was done for a period of 575 minutes. To assess the crack growth until the next inspection period, the measured stress block should be extrapolated:

$$T_{inspection} = 6\ month \cdot 30\ \mathrm{day} \cdot 24\ \mathrm{hour} \cdot 60\ \mathrm{min} = 2.592 \times 10^5 \mathrm{min}$$

$$N_{tot,inspection} = \frac{T_{inspection}}{575\ \mathrm{min}} \cdot n_{9h,CL} = 9.385 \times 10^5\ \mathrm{cycles}$$

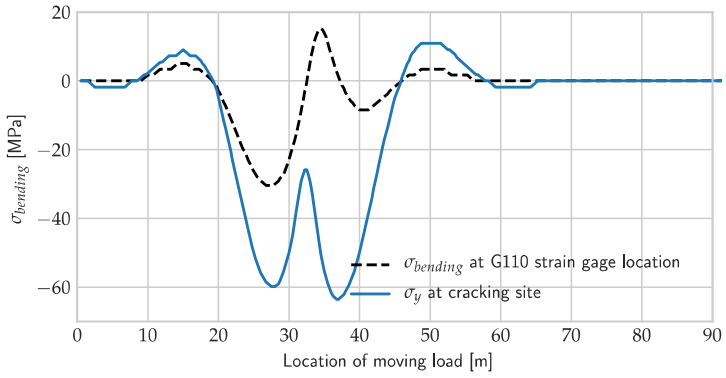

Figure 6.21 Bending stress influence lines for two close locations located on Girder C, calculated from FE model under a moving axel load ($2 \times 50kN$).

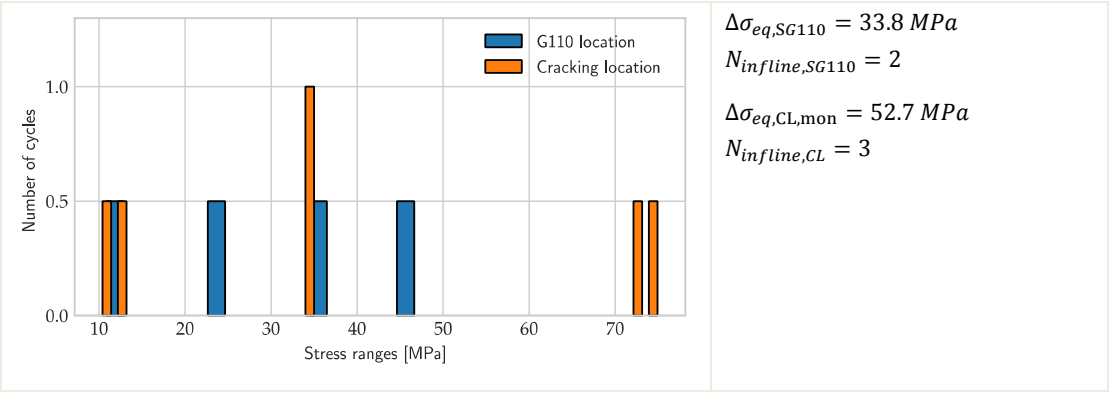

Figure 6.22 Stress ranges spectrums due to passage of unit axel load, deduced from influence lines shown in Figure 6.21.

6.4.3 Brittle fracture assessment

For assessment of brittle fracture, temperature is the main action. Moreover, the safety element is of the additive type, instead of the usual multiplicative (γ-factors) type:

Minimum service temperature:	$T_{min,d} = -30\ ℃$
Temperature shift (safety element):	$\Delta T_R = -40\ ℃$
Design temperature:	$T_{Ed} = T_{min,d} + \Delta T_R = -70\ ℃$

Accompanying actions include stresses due to self-weight, traffic and residual stresses. The value of residual stress is conservatively taken as $\sigma_{res} = 100\ MPa$. Similar to phase II assessment, the values of other action effects are taken from FE analysis:

Residual stresses (assumed):	$\sigma_{res} = 100\ MPa$
Self-weight action effects:	$\sigma_G = 37\ MPa$
Variable action (Traffic) effects:	$\sigma_Q = 33\ MPa$, $\psi_1 = 0.75$ (TRVFS 2011, 7kap-5§)
Design value:	$\sigma_{Ed} = \sigma_G + \psi_1 \cdot \sigma_Q + \sigma_{res} = 162\ MPa$

Design value of plasticity-corrected stress intensity factor (Action side)

K_{Ed}^* is calculated according to Equation (2-12): $K_{Ed}^* = \frac{K_{Ed}}{k_{R6}-\rho}$

Value of elastic stress intensity factor K_{Ed} is:

$$K_{Ed} = F_s(a_d) \cdot F_w(a_d) \cdot F_e(a_d) \cdot F_g(a_d) \cdot \sigma_{Ed} \cdot \sqrt{\pi a_d} \rightarrow K_{ed} = 42.7\ MPa\sqrt{m}$$

The values of k_{R6} and ρ are evaluated according to the formulas given in commentary document (G. Sedlacek, Feldmann, et al. 2008). A summary of these calculations is given below.

Calculation of k_{R6} : the plasticity correction factor is applied to account for local plasticity at the crack tip. It is evaluated as follows:

- Yield stress at room temperature: $f_y(20℃) = \sigma_y = 260\ MPa$
- Yield stress at service temperature:

$$f_y(T_{Ed}) = f_y(20℃) + \frac{55555}{T_{Ed}+273.15} - 189 - 0.25 \cdot \frac{T_{plate}}{1mm}$$
$$f_y(T_{Ed}) = 337\ MPa$$

- From Table (2-5) in commentary document, yield stresses at net cross section is:

$$\sigma_{gy} = f_y(T_{Ed}) \cdot \left[1 - \frac{\pi \cdot 2.5 \cdot a_d^2}{2 \cdot T_{plate} \cdot (5a_d + T_{plate})}\right] = 312\ MPa$$

- Ligament yielding parameter (a measure of proximity to plastic yielding):

$$L_r = \frac{\sigma_{Ed}}{\sigma_{gy}} = 0.519$$

- Finally, k_{R6} is calculated as: $$k_{R6} = \frac{1}{\sqrt{1 + 0.5 \cdot L_r^2}} = 0.939$$

Calculation of ρ: the correction factor for local residual stresses (ρ = 0 only for non-welded details) is calculated as:

- Secondary stresses: $\sigma_S = \sigma_{res} = 100\ MPa$
- Primary stresses: $\sigma_P = \sigma_{Ed} - \sigma_S = 62\ MPa$
- Calculating ρ from Table 2-6 in commentary document:

$$\Psi = \frac{\sigma_S \cdot L_r}{\sigma_P} = 0.876$$

$$\rho_1 = \begin{cases} 0 & \text{if } 0 \geq \Psi \\ 0.1 \cdot \Psi^{0.714} - 0.007 \cdot \Psi^2 + 0.00003 \cdot \Psi^5 & \text{if } 0 < \Psi \leq 5.2 \\ 0.25 & \text{if } 5.2 < \Psi \end{cases}$$

$$\rho_1 = 0.083$$

$$\rho = \begin{cases} \rho_1 & \text{if } 0.8 > \mathrm{L_r} \\ 4\rho_1(1.05 - L_r) & \text{if } 0.8 \leq L_r \leq 1.05 \\ 0 & \text{if } 1.05 < \Psi \end{cases}$$

$$\rho = 0.083$$

Thus, K_{Ed}^* will be: $$K_{Ed}^* = \frac{K_{Ed}}{k_{R6} - \rho} \rightarrow K_{Ed}^* = 49.9\ MPa\sqrt{m}$$

Safety verification:

$$Resistance\ side \geq Action\ side\ ?$$

$$K_{mat}(-70\ ℃) = 34.9\ MPa\sqrt{m} \ngeq K_{Ed}^* = 49.9\ MPa\sqrt{m}$$

This means with current traffic loads, assuming an initial crack size of $a_0 = 1.67\ mm$, an inspection interval equal to 6 months would not be enough to ensure safe operation. If in the above calculations the rather conservative assumption of residual stresses ($\sigma_{res} = 100\ MPa$) is replaced by more realistic value of $\sigma_{res} = 50\ MPa$ (due to relaxation), then the inspection interval of 6 months for the same detail will prove sufficient.

Also note that the fracture toughness at $T_{Ed} = -70$ ℃ is probably underestimated (on the safe side), since the design temperature is lower than the application interval of master curve, which is: $$[T_{K100} - 50℃, T_{K100} + 50℃] = [-50.4℃, +49.6℃]$$

6.4.3.1 Alternative method (estimation of safe service period)

K_{mat} for service temperature $T_{min,d} = -30℃$ can be evaluated form master curve:

$$K_{mat}(-30℃) = 46.0\ MPa\sqrt{m}$$

In the safe service period method, the variable traffic load is the dominant action, not the thermal effects. Therefore:

$$\sigma_{Ed} = \sigma_G + \sigma_Q + \sigma_{res} = 170\ MPa$$

The critical crack size a_d can be found from the following design equation:

$$K^*_{Ed}(a_d) = K_{mat}(-30℃) = 46.0\ MPa\sqrt{m}$$

Calculations similar to the previous section yield the critical crack size as:

$$a_d = 3.12mm$$

Which is a small critical size for the crack depth in a 28-mm thick plate. Again, this is mainly due to poor fracture toughness of the material, besides the conservative assumption for the welding residual stresses.

From the crack growth curve (1) in Figure 6.23, the number of cycles corresponding to $a_d = 3.12mm$ is estimated as:

$$N_{service} = 443'779$$

Using Equation (2-13), number of cycles between inspection intervals will be:

$$N_{insp} = 1.5 * N_{service} \approx 300'000\ cycles$$

Which corresponds to an inspection interval of $T_{insp} \approx 2\ months$.

One way to increase this estimated safe service period is to increase the NDT efforts, so that minimum crack size at detection (consequently a_0 value) is reduced. For the studied case, considering the initial crack size of $a_0 = 1mm$, which corresponds to detection threshold of visual inspection (see Appendix B), leads to crack growth curve (3) in Figure 6.23 and $N_{service} \approx 741000\ cycles$ and an inspection interval of $T_{insp} \approx 3\ months$. In order to use this value for the inspection interval, more intense inspection program of critical details using VT (or a more accurate NDT method) should be implemented.

Another possibility is, like previous section, to consider the relaxation in residual stresses due to variable-amplitude loading on the bridge, e.g. $\sigma_{res} = 50\ MPa$. Unfortunately, accurate measurement of residual stresses is difficult, both due to technical complexities and high variability of the residual stress field from one location to another. Nonetheless, this assumption can still provide an upper-bound estimate of the inspection intervals. From curve (2) in Figure 6.23, $N_{service} = 1.69 \times 10^6\ cycles$, which corresponds to an inspection interval of $T_{insp} \approx 7\ months$. The service life of the detail in this case is 3.8 times the service life of the detail in the base case. This shows the potential for service life improvement of the detail by modifying the residual stresses at the crack-prone locations, which will be briefly discussed in the following Section 6.5.

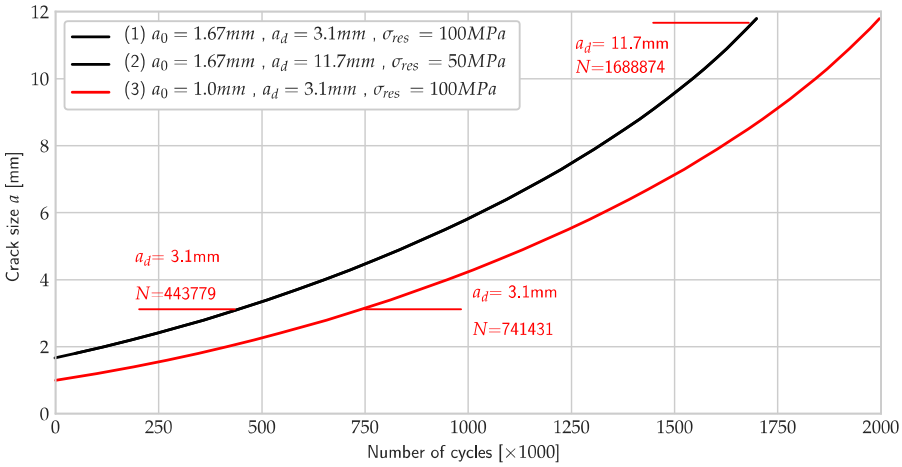

Figure 6.23 Crack growth curves for the studied detail with different assumptions for initial crack size a_0 under cyclic stress range $\Delta\sigma_{eq,CL}$; curves (1) and (2) are identical.

6.5 Summary

In this chapter, the application of the multi-step assessment methodology was demonstrated on one of the most critical details of the case study bridge.

- No phase I assessment was performed because firstly, a similar assessment was done earlier by Larsson (2004), and secondly, the detailed traffic data were available.
- The result of Phase II assessment using damage accumulation was that the bridge has surpassed its theoretical fatigue life. Due to Inadequate safety of the studied detail from phase II, phase III assessment was carried out.
- A difficulty in doing phase II assessments is that the historic traffic data are not available for the whole lifetime of the bridge. This limitation is overcome by using appropriate but conservative assumptions fort the missing parts in the load history. In contrast, an apparent advantage of the phase III (LEFM) method is that it does not require the past loading data. Instead, its focus is on the current status of the detail (in terms of cracks and defects) and future loading on the bridge, which can be controlled or measured more accurately.
- Using maximum permissible thickness table in phase II is a rapid means for screening of the structure to find critical members prone to brittle fracture. But as was seen in this chapter, if the plate thickness of the detail is below permissible thickness, still the brittle fracture is probable as the actual defects in the member might be larger than the defect sizes that were assumed in producing the Table 3-7 data. Most notable of such assumptions was that the welded detail is produced in accordance with EN 1090, which is not the case for many old bridges.
- Using phase III assessment detailed information about damage prognosis can be acquired. This in turn can lead to more informed decisions about subsequent interventions. These interventions include:
    - Intensify inspections and/or monitoring
    - Estimating impact of using more accurate NDT techniques (i.e. smaller initial crack size) on inspection intervals
    - Repairing (for example drilling stop holes)

- The effect of Given the detrimental effect of welding residual stresses and their high variability, modifying residual stress field in the welded detail can have a considerable impact on the remaining service life of the structure. One of the latest developed techniques, high frequency mechanical impact treatment (HFMI), has demonstrated promising results while it also has the advantage of being both rapid and economic, compared to other methods (Marquis and Barsoum 2014). These methods have not been examined on older steel structures, but research efforts are ongoing for assessing their impact on fatigue life of welded bridge details (Shams-Hakimi 2017). In future, it will be beneficial to evaluate the impact of HFMI on residual service life of the older bridges.

7 References

AASHTO. 1994. *Manual for Condition Evaluation of Bridges*. 2nd ed. Washington, D.C.: American Association of State Highway and Transportation O□cials.

Aktan, A. Emin, F. Necati Catbas, Kirk A. Grimmelsman, and Mesut Pervizpour. 2003. 'Development of a Model Health Monitoring Guide for Major Bridges'. DTFH61-01-P-00347. United Kingdom: Drexel Intelligent Infrastructure and Transportation Safety Institute.

Al-Emrani, Mohammad, and Mustafa Aygül. 2013. 'Fatigue Design of Steel and Composite Bridges'. 2014:10. Göteborg, Sweden: Chalmers University of Technology.

Al-Emrani, Mohammad, and Robert Kliger. 2009. 'Fatigue Prone Details in Steel Bridges'. In . Malmö, Sweden.

Anderson, Ted L. 2004. *Fracture Mechanics: Fundamentals and Applications, Third Edition*. 3rd ed. CRC Press.

ASME. 1998. *Boiler and Pressure Vessel Code, Section III, Rules for Construction of Nuclear Power Plant Components*. New York, United States: The American Society of Mechanical Engineers.

ASTM E415. 2017. 'Standard Test Method for Analysis of Carbon and Low-Alloy Steel by Spark Atomic Emission Spectrometry'. E415-17. United States: American Society for Testing Materials. http://www.astm.org/Standards/E1820.htm.

ASTM E647. 2015. 'Test Method for Measurement of Fatigue Crack Growth Rates (E 647)'. E647–15E. United States: American Society for Testing Materials. http://www.astm.org/doiLink.cgi?E647.

ASTM E1820. 2015. 'Standard Test Method for Measurement of Fracture Toughness'. E1820 – 15a. United States: American Society for Testing Materials. http://www.astm.org/Standards/E1820.htm.

ASTM E1921. 2015. *Standard Test Method for Determination of Reference Temperature, To, for Ferritic Steels in the Transition Range*. E1921 – 15ae1. United States: American Society for Testing Materials. http://publications.sckcen.be/dspace/handle/10038/435.

Banverket. 2003. 'Brottseghet hos konstruktionsstål i järnvägsbroar'. BVS 583.12. Swedish Rail Administration (Banveket).

Barsom, John M., and Stanley Theodore Rolfe. 1999. *Fracture and Fatigue Control in Structures: Applications of Fracture Mechanics*. ASTM International.

Bengtsson, Robert, and Mikael Widén. 2010. 'FE-Analysis of Vårby Bridge. Investigation of Fatigue Damage in a Composite Bridge'. Chalmers University of Technology. http://publications.lib.chalmers.se/records/fulltext/132144.pdf.

Bosshard, Max, and Marléne Plätzer. 2013. 'Histoire, identification et reconstruction'. *steeldoc 03+04/13 - Centre suisse de la construction métallique (SZS)*, 26–31.

Boström, Staffan. 1999. 'Crack Location in Steel Structures Using Acoustic Emission Techniques'. Sweden: Luleå University of Technology. http://www.diva-portal.org/smash/record.jsf?pid=diva2:989771.

Boverket. 1994. *Dimensionering genom provning: handbok (Handbook of design by testing)*. Sweden: National Board of Housing, Building and Planning (Boverket).

Bowness, D., and M. M. K. Lee. 2000. 'Prediction of Weld Toe Magnification Factors for Semi-Elliptical Cracks in T–butt Joints'. *International Journal of Fatigue* 22 (5): 369–87. https://doi.org/10.1016/S0142-1123(00)00012-8.

Boyd, Geoffrey Murray, ed. 1970. *Brittle Fracture in Steel Structures*. London, UK: Butterworths.
Broek, D. 1986. *Elementary Engineering Fracture Mechanics*. Springer.
Broek, David. 1989. *The Practical Use of Fracture Mechanics*. Springer.
BS 7910. 2013. *Guide to Methods for Assessing the Acceptability of Flaws in Metallic Structures*. British Standards Institution (BSI).
Bucak, Ö., and F. Mang. 1998. 'Erfahrungen Mit Alten Stahlkonstruktionen (Experiences with Old Steel Structures)'. *Stahlbau* 67 (1): 46–60. https://doi.org/10.1002/stab.199800070.
Daum, Werner. 2013. 'Guidelines for Structural Health Monitoring'. In *Handbook of Technical Diagnostics*, 539–41. Springer, Berlin, Heidelberg. https://doi.org/10.1007/978-3-642-25850-3_27.
Davaine, Laurence, F. Imberty, and J. Raoul. 2007. 'SETRA - Eurocode 3 and 4: Application to Steel-Concrete Composite Road Bridges - Guidance Book'. France: Service d'Études techniques des routes et autoroutes (Sétra). http://www.infra-transports-materiaux.cerema.fr/IMG/pdf/US_0720A_Calculationcomposite_Eurocode3_4.pdf.
DNV GL. 2015. 'Probabilistic Methods for Planning of Inspection for Fatigue Cracks in Offshore Structures'. DNVGL-RP-0001. Norway: DNV GL.
Easterling, K. E. 1992. *Introduction to the Physical Metallurgy of Welding*. 2nd ed. Butterworth-Heinemann.
EN 1090-2. 2008. *Execution of Steel Structures and Aluminum Structures - Part 2: Technical Requirements for Steel Structures*. EN 1090-2:2008:E. European Committee for Standardization.
EN 1991. 2005. 'Eurocode 1: Actions on Structures — Part 1-4: General Actions — Wind Actions'. EN 1991-1-4:2005. Brussels, Belgium: European Committee for Standardization (CEN).
EN 1991-1-5. 2009. 'Eurocode 1: Actions on Structures — Part 1-5: General Actions - Thermal Actions'. EN 1991-1-5:2003/AC 2009. Brussels, Belgium: European Committee for Standardization (CEN).
EN 1991-2. 2003. 'Eurocode 1: Actions on Structures — Part 2: Traffic Loads on Bridges'. EN 1991-2:2003/AC 2010. Brussels, Belgium: European Committee for Standardization (CEN).
EN 1993. 2005a. *Eurocode 3: Design of Steel Structures - Part 1-9: Fatigue*. Brussels: European Committee for Standardization (CEN).
———. 2005b. 'Eurocode 3: Design of Steel Structures. Part 1-10: Material Toughness and through-Thickness Properties'. EN 1993-1-10:2005. Brussels, Belgium: European Committee for Standardization (CEN).
———. 2005c. *Eurocode 3: Design of Steel Structures. Part 1-10: Material Toughness and through-Thickness Properties*. Brussels, Belgium: European Committee for Standardization (CEN).
———. 2006. *Eurocode 3: Design of Steel Structures - Part 2: Steel Bridges*. Brussels, Belgium: European Committee for Standardization (CEN).
EN 1994-2. 2005. 'Eurocode 4: Design of Composite Steel and Concrete Structures – Part 2: General Rules and Rules for Bridges'. EN 1994-2:2005/AC:2008. Brussels, Belgium: European Committee for Standardization (CEN).
EN 10025-1. 2004. *Hot Rolled Products of Structural Steels – Part 1: General Technical Delivery Conditions*. European Standard.

EN 10025-2. 2004. *Hot Rolled Products of Structural Steels – Part 2: Technical Delivery Conditions for Non-Alloy Structural Steels*. European Standard.

EN 10025-3. 2004. *Hot Rolled Products of Structural Steels – Part 3: Technical Delivery Conditions for Normalized/Normalized Rolled Weldable Fine Grain Structural Steels*. European Standard.

EN ISO 148-1. 2016. 'Metallic Materials. Charpy Pendulum Impact Test. Test Method'. EN ISO 148-1:2016. Geneva, Switzerland: International Organization for Standardization. https://www.iso.org/standard/63802.html.

EN ISO 17635. 2010. 'Non-Destructive Examination of Welds--General Rules for Metallic Materials'. ISO 17635:2010. International Organization for Standardization.

Enckell, Merit. 2011. 'Lessons Learned in Structural Health Monitoring of Bridges Using Advanced Sensor Technology'. Stockholm, Sweden: KTH. http://www.diva-portal.org/smash/record.jsf?pid=diva2:456855.

Eriksson, Kjell. 2011. 'An Overview of Older Structural Steel and Their Properties'. In . Luleå, Sweden: Luleå tekniska universitet. http://ltu.diva-portal.org/smash/record.jsf?pid=diva2:1004564.

ESDEP. 1993a. 'European Convention for Constructional Steelwork (ESDEP), Chapter 12'. http://www.esdep.org/members/master/toc.htm.

———. 1993b. 'European Convention for Constructional Steelwork (ESDEP), Chapter 16'. http://fgg-web.fgg.uni-lj.si/~/pmoze/ESDEP/master/wg16/l0500.htm.

FHWA. 2001. 'Reliability of Visual Inspection for Highway Bridges Volume I: Final Report'. FHWA-RD-01-020. United States: Federal Highway Administration (FHWA). https://ntl.bts.gov/lib/11000/11100/11133/.

Fisher, John W. 1984. *Fatigue and Fracture in Steel Bridges: Case Studies*. Wiley.

Fujimoto, Yukio, Swilem A. M. Swilem, and Mitsumasa Iwata. 1990. 'Estimation of Probabilities of Crack Detection and False Indication in Visual Inspection of Structures'. *Journal of the Society of Naval Architects of Japan* 1990 (168): 487–95. https://doi.org/10.2534/jjasnaoe1968.1990.168_487.

Getachew, A., and E. J. Obrien. 2007. 'Simplified Site-Specific Traffic Load Models for Bridge Assessment'. *Structure and Infrastructure Engineering* 3 (4): 303–11. https://doi.org/10.1080/15732470500424245.

Glišić, Branko, Daniele Posenato, and Daniele Inaudi. 2007. 'Integrity Monitoring of Old Steel Bridge Using Fiber Optic Distributed Sensors Based on Brillouin Scattering'. In *3rd International Conference on Structural Health Monitoring of Intelligent Infrastructure*. Vancouver, Canada. https://doi.org/10.1117/12.716055.

Günther, Hans-Peter, ed. 2005. *Use and Application of High-Performance Steels for Steel Structures*. Structural Engineering Documents SED 8. Switzerland: International Association for Bridge and Structural Engineering (IABSE).

Gurney, T. R. 1979. *Fatigue of Welded Structures*. United Kingdom: CUP Archive.

Härkegård, Gunnar. 2010. 'Software for Fatigue Life Assessment – Features and Challenges'. presented at the UTMIS meeting, Örebro, Sweden. https://www.evernote.com/shard/s15/nl/1630529/e6779482-5061-4537-ba37-6d54c6450b9c.

Hejll, Arvid. 2007. 'Civil Structural Health Monitoring: Strategies, Methods and Applications'. PhD thesis, Luleå, Sweden: Luleå University of Technology.

Helmerich, R., J. Bień, and Paulo J. S. Cruz. 2007. 'A Guideline for Railway Bridge Inspection and Condition Assessment Including the NDT Toolbox', October. http://repositorium.sdum.uminho.pt/handle/1822/8349.

Helmerich, Rosemarie, ed. 2005. *Alte Stähle und Stahlkonstruktionen: Materialuntersuchungen, Ermüdungsversuche an originalen Brückenträgern und Messungen von 1990 bis 2003*. Forschungsbericht 271. Berlin, Germany: Bundesanstalt für Materialforschung und -prüfung (BAM).

Helmerich, Rosemarie, and Ernst Niederleithinger. 2007. 'Deliverable D3.16 - NDT Toolbox'. Deliverable D3.16. Berlin, Germany: Sustainable Bridges-A project within EU FP6. http://www.transport-research.info/sites/default/files/project/documents/20120302_093934_60082_SB3.4.pdf.

Hobbacher, A. 1993. 'Stress Intensity Factors of Welded Joints'. *Engineering Fracture Mechanics* 46 (2): 173–82. https://doi.org/10.1016/0013-7944(93)90278-Z.

———. 2000. 'Evolution of Design and Fabrication of Steel Structures'. In , 65–87.

———. 2008. 'Recommendations for Fatigue Design of Welded Joints and Components'. IIW-1823-07. International Institute of Welding (IIW).

———. 2011. 'The Use of Fracture Mechanics in the Fatigue Analysis of Welded Joints'. In *Fracture and Fatigue of Welded Joints and Structures*, edited by K. A MacDonald, 91–112. Cambridge, UK: Woodhead Pub.

'Instrumentation, Nondestructive Testing, and Finite-Element Model Updating for Bridge Evaluation Using Strain Measurements'. 2012. *Journal of Bridge Engineering* 17 (1): 130–38. https://doi.org/10.1061/(ASCE)BE.1943-5592.0000228.

Irwin, George R. 1957. 'Analysis of Stresses and Strains near the End of a Crack Traversing a Plate'. *Journal of Applied Mechanics* 24 (3): 361–364.

ISO 15653. 2010. *International Standard: Metallic Materials–Method of Test for the Determination of Quasistatic Fracture Toughness of Welds*. 1st Edition. Switzerland: International Organization for Standardization.

JCSS. 2001. *Probabilistic Model Code*. Denmark: Joint Committee on Structural Safety.

Klinger, C., M. Mehdianpour, D. Klingbeil, D. Bettge, R. Häcker, and W. Baer. 2011. 'Failure Analysis on Collapsed Towers of Overhead Electrical Lines in the Region Münsterland (Germany) 2005'. *Engineering Failure Analysis*, The Fourth International Conference on Engineering Failure Analysis Part 2, 18 (7): 1873–83. https://doi.org/10.1016/j.engfailanal.2011.07.004.

Klinger, Christian. 2013. 'Failure Analysis: Case Studies'. In *Handbook of Technical Diagnostics*, edited by Horst Czichos, 355–85. Springer Berlin Heidelberg. http://link.springer.com/chapter/10.1007/978-3-642-25850-3_18.

Kühn, Bertram. 2005. *Beitrag zur Vereinheitlichung der europäischen Regelungen zur Vermeidung von Sprödbruch*. Schriftenreihe Stahlbau 54. Aachen: Shaker.

———. 2013. 'Assessment of Existing Steel Structures – Recommendations for Estimation of the Remaining Fatigue Life'. *Procedia Engineering*, Fatigue Design 2013, International Conference Proceedings, 66: 3–11. https://doi.org/10.1016/j.proeng.2013.12.057.

Kühn, Bertram, Mladen Lukić, Alain Nussbaumer, H. P Günther, Rosemarie Helmerich, Stefan Herion, Menke Henderikus Kolstein, et al. 2008. *Assessment of Existing Steel Structures-Recommendations for Estimation of Remaining Fatigue Life*.

Larsson, Ingvar. 2004. 'Evaluation of remaining service life of Götaälv bridge (Swedish title: Utredning avseende sannolik återstående livslängd)'. 309/03. Gothenburg, Sweden: Gatubolaget Konsult.

Larsson, T., and O. Lagerqvist. 2009. 'Material Properties of Old Steel Bridges'. In *Nordic Steel Construction Conference 2009*. http://nordicsteel2009.se/pdf/888.pdf.

Larsson, Tobias. 2009. 'Fatigue Assessment of Riveted Bridges'. Luleå, Sweden: Luleå University of Technology. http://vpp.sbuf.se/Public/Documents/ProjectDocuments/7336BECF-5CFB-4B6A-B0A2-177C547C0E2D%5CFinalReport%5CSBUF%2012049%20Doktorsavhandling%20Fatigue%20assessment%20of%20riveted%20bridges.pdf.

Leander, John, Mustafa Aygül, and Bert Norlin. 2013. 'Refined Fatigue Assessment of Joints with Welded In-Plane Attachments by LEFM'. *International Journal of Fatigue* 56 (November): 25–32. https://doi.org/10.1016/j.ijfatigue.2013.07.013.

Leander, John, Stefan Trillkott, and Claes Kullberg. 2015. 'Götaälvbron–Töjningsmätningar för kalibrering av beräkningsmodell (Götaälv bridge–Strain measuremnts for calibration of the analysis model)'. Stockholm, Sweden: Royal Institute of Technology (KTH).

Lindroth, Pasi, Gary Marquis, and Grzegorz Glinka. 2013. 'Fatigue Crack Growth of Arbitrary Planar Cracks in Welded Components'. *Welding in the World* 57 (3): 425–35. https://doi.org/10.1007/s40194-013-0029-3.

Lukić, Mladen, Mohammad Al-Emrani, Shota Urushadze, Mathias Nilsson, Björn Eichler, and Boulent M. Imam. 2011. 'Bridge Fatigue Guidance (BriFaG)'. Technical Report No. 6. Research Programme of the Research Fund for Coal and Steel (RFCS).

Lüthi, Thomas. 2013. 'Non-Destructive Evaluation Methods (Course Book)'. Dübendorf, Switzerland: EMPA.

Lydon, Myra, S. E. Taylor, D. Robinson, A. Mufti, and E. J. O. Brien. 2016. 'Recent Developments in Bridge Weigh in Motion (B-WIM)'. *Journal of Civil Structural Health Monitoring* 6 (1): 69–81. https://doi.org/10.1007/s13349-015-0119-6.

Lynch, J. P. 2006. 'A Summary Review of Wireless Sensors and Sensor Networks for Structural Health Monitoring'. *The Shock and Vibration Digest* 38 (2): 91–128. https://doi.org/10.1177/0583102406061499.

Maddah, Nariman. 2013. 'Fatigue Life Assessment of Roadway Bridges Based on Actual Traffic Loads'. Switzerland: Ecole Polytechnique Fédérale de Lausanne (EPFL). http://infoscience.epfl.ch/record/183277/files/EPFL_TH5575.pdf.

Maddox, S. J. 1975. 'An Analysis of Fatigue Cracks in Fillet Welded Joints'. *International Journal of Fracture* 11 (2): 221–43. https://doi.org/10.1007/BF00038890.

Madsen, H. O., R. K. Skjong, A. G. Tallin, and F. Kirkemo. 1987. 'Probabilistic Fatigue Crack Growth Analysis of Offshore Structures, with Reliability Updating through Inspection'. In . Virginia, US: The Society of Naval Architects and Marine Engineers. http://trid.trb.org/view.aspx?id=397000.

Marquis, Gary, and Zuheir Barsoum. 2014. 'Fatigue Strength Improvement of Steel Structures by High-Frequency Mechanical Impact: Proposed Procedures and Quality Assurance Guidelines'. *Welding in the World* 58 (1): 19–28. https://doi.org/10.1007/s40194-013-0077-8.

Moan, Torgeir, and Ruxin Song. 2000. 'Implications of Inspection Updating on System Fatigue Reliability of Offshore Structures'. *Journal of Offshore Mechanics and Arctic Engineering* 122 (3): 173–80. https://doi.org/10.1115/1.1286601.

Moan, Torgeir, Ole T. Vårdal, Nils-C. Hellevig, and Knut Skjoldli. 2000. 'Initial Crack Depth and POD Values Inferred From In-Service Observations of Cracks in North Sea Jackets'. *Journal of Offshore Mechanics and Arctic Engineering* 122 (3): 157–62. https://doi.org/10.1115/1.1286676.

Mufti, Aftab. 2001. 'Guidelines for Structural Health Monitoring'. Canada: The Canadian Network of Centres of Excellence on Intelligent Sensing for Innovative Structures (ISIS Canada). http://simtrec.ca/publications/design-manuals/.

Murakami, Y., ed. 2005. *Stress Intensity Factors Handbook*. Amsterdam: Elsevier Science Ltd.

Naumann, Joachim. 2011. 'Brückenertüchtigung Jetzt – Ein Wichtiger Beitrag Zur Sicherung Der Mobilität Auf Bundesfernstraßen'. DBV-Heft 22. Berlin, Germany: Deutscher Beton- und Bautechnik-Verein e.V.

Newman, J. C., and I. S. Raju. 1981. 'An Empirical Stress-Intensity Factor Equation for the Surface Crack'. *Engineering Fracture Mechanics* 15 (1): 185–192.

Niemi, E., W. Fricke, and S. J. Maddox. 2006. 'Fatigue Analysis of Welded Components: Designer's Guide to the Structural Hot-Spot Stress Approach'. IIW-1430-00. International Institute of Welding (IIW).

Nussbaumer, Alain, Luis Borges, and Laurence Davaine. 2012. *Fatigue Design of Steel and Composite Structures*. Berlin, Germany: Ernst & Sohn Verlag für Architektur und technische Wissenschaften GmbH & Co. KG. https://doi.org/10.1002/9783433601181.

Ogle, M. H., F. M. Burdekin, and I. Hadley. 2013. 'Material Selection Requirements for Civil Structures'. In *Materials Selection Requirements for Civil Structures, 56th IIW Annual Assembly*. Bucharest, Romania. http://www.twi-global.com/technical-knowledge/published-papers/material-selection-requirements-for-civil-structures-july-2003/.

Omenzetter, Piotr. 2015. 'Piotr Omenzetter, The LRF Centre for Safety and Reliability Engineering'. In *Workshop on Quantifying the Value of Structural Health Monitoring - Cost Action TU1402*, edited by Sebastian Thöns. Denmark.

Ponge, D. 2005. 'Structural Materials - Steels'. presented at the Marie Curie Summer School, Hürtgenwald. http://materialsknowledge.org/docs/Steels%20Ponge%20Marie-Curie%20Summer%20School.pdf.

Potter, David, Jeremiah Fasl, Todd Helwig, Sharon L. Wood, and Rich Lindenberg. 2012. 'Development of a Rapidly Deployable Wireless Monitoring System for Bridges'. In *Civil Structural Health Monitoring Workshop (CSHM-4)*.

Prokop, Ines. 2012. *Vom Eisenbau zum Stahlbau: Tragwerke und ihre Protagonisten in Berlin 1850 – 1925*. 1 edition. Berlin: Mensch & Buch.

Pyttel, B., I. Varfolomeyev, M. Luke, C. Berger, and D. Siegele. 2007. 'FKM Guideline "Fracture Mechanics Proof of Strength for Engineering Components" — Overview and Extension Topics'. *Welding in the World* 51 (5–6): 85–93. https://doi.org/10.1007/BF03266576.

R. Karoumi, A. Liljencranz, and F. Carlsson. 2007. 'D4.3.2 Background Document - Assessment of Actual Traffic Loads Using B-WIM, Site Specific Characteristic Load from Collected Data & Statistical Evaluation of Dynamic Amplification Factors'. D4.3.2. Sweden: Sustainable Bridges-A project within EU FP6.

Rice, J. R. 1968. 'A Path Independent Integral and the Approximate Analysis of Strain Concentration by Notches and Cracks'. *Journal of Applied Mechanics* 35 (2): 379–86. https://doi.org/10.1115/1.3601206.

Righiniotis, Timothy D. 2006. 'A Comparative Study of Fatigue Inspection Methods'. *Journal of Constructional Steel Research* 62 (4): 352–58. https://doi.org/10.1016/j.jcsr.2005.08.008.

Roy, S., Y.C. Park, and B. Valeti. 2015. 'Toughness Requirements for Heat-Affected Zones of Welded Structural Steels for Highway Bridges'. NCHRP 10-95 (interim report). United States: ATLSS, Lehigh University.

Rücker, W., F. Hille, and R. Rohrmann. 2006. 'Guideline for Structural Health Monitoring'. SAMCO Final Report F08b. Berlin, Germany: SAMCO. http://www.samco.org/network/download_area/mon_guide.pdf.

Sattari-Far, Iradj, and Kim Wallin. 2005. 'Application of Master Curve Methodology for Structural Integrity Assessments of Nuclear Components'. SKI Report 2005:55. Sweden: Statens kärnkraftinspektion. http://www.stralsakerhetsmyndigheten.se/Global/Publikationer/SKI_import/060323/35f67d3300e2153391581e12192285c7/SKI%20Rapport%202005_55%20weboriginal.pdf.

Schijve, Jaap. 2009. *Fatigue of Structures and Materials*. 2nd ed. Springer. http://dx.doi.org/10.1007/978-1-4020-6808-9.

Schneider, C. R. A., and S. J. Maddox. 2006. 'Best Practice Guide on Statistical Analysis of Fatigue Data'. XIII-2138-06. International Institute of Welding. http://www.math.ntnu.no/~bo/stat2/welding.pdf.

Sedlacek, G., M. Feldmann, B. Kühn, D. Tschickardt, S. Höhler, C. Müller, W. Hensen, et al. 2008. 'Commentary and Worked Examples to EN 1993-1-10 "Material Toughness and through Thickness Properties"'. Joint report JRC – ECCS JRC EUR 23510 EN-2008. Luxembourg: European Commission / Joint Research Centre. http://www.eurocodes.fi/1993/1993-1-10/background/EUR_23510_EN[1].pdf.

Sedlacek, G., G. Merzenich, M. Paschen, A. Bruls, L. Sanpaolesi, P. Croce, J.A. Calgaro, et al. 2008. 'Background Document to EN 1991- Part 2 - Traffic Loads for Road Bridges - and Consequences for the Design'. EN 1991-2. Joint Research Center (JRC).

Sedlacek, Gerhard, Christian Kammel, Bertram Kühn, and Wolfgang Hensen. 2005. 'Condition Assessment and Inspection of Steel Railway Bridges, Including Stress Measurements in Riveted, Bolted and Welded Structures'. Deliverable D3.4. Sustainable Bridges-A project within EU FP6. http://www.sustainablebridges.net/.

———. 2007. 'Condition Assessment and Inspection of Steel Railway Bridges, Including Stress Measurements in Riveted, Bolted and Welded Structures'. Background document SB3.4. Sustainable Bridges-A project within EU FP6. http://www.transport-research.info/sites/default/files/project/documents/20120302_093934_60082_SB3.4.pdf.

Selle, Hubertus von, Olaf Doerk, and M Scharrer. 2009. 'Global Strength Analysis of Ships with Special Focus on Fatigue of Hatch Corners'. In *Analysis and Design of Marine Structures*, 255–60. CRC Press. http://dx.doi.org/10.1201/9780203874981.ch29.

SENSIMA. 2012. 'Advanced Eddy Current Devices - Extracting More Information from NDT Devices for Material Characterisation'. presented at the Sensima Inspection Sàrl, Gland, Switzerland.

Seyedianchoobi, Rasa. 2012. 'Long Term Health Monitoring of Anthony Wayne Bridge Main Cable with Acoustic Emission Technique'. Master's thesis, United

States: University of Toledo. http://utdr.utoledo.edu/cgi/viewcontent.cgi?article=1447&context=theses-dissertations.
Shafie, Mohd. Azhar, and Lailatun N. Sabardin. 1997. 'Ageing and Brittle Fracture in Steel'. Master's Thesis, Gothenburg, Sweden: Chalmers University of Technology. http://chans.lib.chalmers.se/record=b1119533.
Shams-Hakimi, Poja. 2017. 'Performance of High-Frequency Mechanical Impact Treatment for Bridge Application'. Licentiate thesis, Gothenburg, Sweden: Chalmers University of Technology.
SIA. 2013. 'SIA 263 - Steel Structures'. SIA 263:2013. Zurich, Switzerland: Swiss society of engineers and architects(SIA).
Simulia. 2014. *ABAQUS Analysis: User's Manual, Version 6.14*. United States: Dassault systèmes.
Socie, Darrell F., and Gary B. Marquis. 2000. *Multiaxial Fatigue*. Warrendale, Pa: Society of Automotive Engineers.
Stephens, Ralph I., Ali Fatemi, Robert R. Stephens, and Henry O. Fuchs. 2000. *Metal Fatigue in Engineering*. Wiley.
Sustainable Bridges. 2007. 'Improved Assessment Methods for Static and Fatigue Resistance of Old Steel Railway Bridges'. Background document D4.6. Sustainable Bridges-A project within EU FP6. http://www.sustainablebridges.net/.
Tada, Hiroshi, Paul Croce Paris, and George Rankin Irwin. 2000. *The Stress Analysis of Cracks Handbook*. 3rd ed. New York: ASME Press.
Thelning, Karl-Erik. 1984. *Steel and Its Heat Treatment*. 2. ed. London: Butterworth.
Topp, David. 2014. 'The ACFM Inspection Method'. presented at the TSC inspection systems, United Kingdom.
Trafikkontoret. 2013. 'Trafik På Götaälvbron'. Göteborgs Stad Trafikkontoret. 2013. http://goo.gl/5nsyNn.
Trafikverket. 2012. 'Swedish National Annex to Eurocode EN 1993-1-9'. TRVFS 2011:12. Sweden: Trafikverket (Swedish road administration). http://webapp.trafikverket.se/TRVFS/pdf/2011nr012.pdf.
———. 2014a. 'Brottseghet och kemisk analys av konstruktionsstål'. TDOK 2012:23. Sweden: Trafikverket (Swedish road administration).
———. 2014b. 'Requirements for Inspection of Construction Works (Krav På Inspektion Av Byggnadsverk)'. TRV 2014:95667. Borlänge, Sweden: Trafikverket (Swedish Transport Administration). https://batman.trafikverket.se/batinfo/Batman/BiblioteketPDF/01_Dokument%20Batman/Krav%20Insp%20Byggnadsverk%20inkl%20Beslut.pdf?
———. 2015a. 'Swedish Road Administration's Guidelines for Bridge Maintenance (Swedish: Brounderhåll - Råd) - Version 2.0'. TDOK 2013:0416. Sweden: Trafikverket (Swedish road administration). http://webapp.trafikverket.se/TRVFS/pdf/2011nr012.pdf.
———. 2015b. 'Swedish Road Administration's Requirements for Bridge Maintenance (Swedish: Brounderhåll - Krav) - Version 2.0'. TDOK 2013:0415. Sweden: Trafikverket (Swedish road administration). http://webapp.trafikverket.se/TRVFS/pdf/2011nr012.pdf.
———. 2016. 'Additional Requirements for Swedish Bridge Structures -Version 1.0 (Swedish: Krav Brobyggande)'. TDOK 2016:0204. Sweden: Trafikverket (Swedish road administration). http://webapp.trafikverket.se/TRVFS/pdf/2011nr012.pdf.

———. 2017. ‘Krav - Bärighetsberäkning Av Broar (Version 4.0)’. TDOK 2013:0267. Sweden: Trafikverket (Swedish road administration).
Trafikverket [The Swedish Transport Administration]. 2017. ‘BaTMan (Bridge and Tunnel Management) – Swedish Bridge Management System’. 2017. https://batman.trafikverket.se/.
Treacy, Mark A., Eugen Brühwiler, and Colin C. Caprani. 2014. ‘Monitoring of Traffic Action Local Effects in Highway Bridge Deck Slabs and the Influence of Measurement Duration on Extreme Value Estimates’. *Structure and Infrastructure Engineering* 10 (12): 1555–72. https://doi.org/10.1080/15732479.2013.835327.
Treacy, Mark Anthony. 2014. ‘The Use of Monitored Data in the Verification of Structural and Fatigue Safety of Existing Post-Tensioned Concrete Highway Bridges (Thesis No. 6207)’. Lausanne, Switzerland: Ecole Polytechnique Fédérale de Lausanne (EPFL). https://doi.org/10.5075/epfl-thesis-6207.
TU1402, and TU1406. 2017. *The Value of Structural Health Monitoring for the Reliable Bridge Management - Proceedings of the Joint TU1402-TU1406-IABSE Workshop*. Zagreb, Croatia: European Cooperation in Science and Technology (COST).
TWI. 2015. ‘FAQ: What Is a Fracture Toughness Test?’ The Welding Institute. 2015. http://www.twi-global.com/technical-knowledge/faqs/structural-integrity-faqs/faq-what-is-a-fracture-toughness-test/.
Wallin, Kim. 2002. ‘Master Curve Analysis of the “Euro” Fracture Toughness Dataset’. *Engineering Fracture Mechanics* 69 (4): 451–81. https://doi.org/10.1016/S0013-7944(01)00071-6.
Wallin, Lars. 1973. ‘Att Bygga i Stål – Modern Teknik Med Gamla Anor’. Stockholm, Sweden: Dædalus, Tekniska museets årsbok. http://digitalamodeller.se/arsbocker/daedalus-1973/lars-wallin-att-bygga-i-stal-modern-teknik-med-gamla-anor/.
Wenzel, Helmut. 2009. *Health Monitoring of Bridges*. United Kingdom: Wiley.
Yu, Jia. 2007. ‘Development of Data Sheets for Statistical Evaluation of Fatigue Data’. Lappeenranta, Finland: Lappeenranta University of Technology.
Zamiri, Farshid. 2009. ‘Fatigue Life Assessment of Welded Bridge Details Using Structural Hot Spot Stress Method’. Göteborg, Sweden: Chalmers University of Technology.
Zamiri, Farshid, John Leander, and Mohammad Al-Emrani. 2016. ‘Fatigue Assessment of Steel Bridges Using Probabilistic Fracture Mechanics - A Feasibility Study’. BBT 2013-004. Sweden: Chalmers University of Technology / Royal Institute of Technology (KTH).
Zerbst, U., R. A. Ainsworth, H. Th. Beier, H. Pisarski, Z. L. Zhang, K. Nikbin, T. Nitschke-Pagel, S. Münstermann, P. Kucharczyk, and D. Klingbeil. 2014. ‘Review on Fracture and Crack Propagation in Weldments – A Fracture Mechanics Perspective’. *Engineering Fracture Mechanics* 132 (December): 200–276. https://doi.org/10.1016/j.engfracmech.2014.05.012.
Zettlemoyer, N., and J. W. Fisher. 1977. ‘Stress Gradient Correction Factor for Stress Intensity at Welded Stiffeners and Cover Plates’. *AWS Welding Journal - Welding Research Supplement* 56 (12): 393s–398s.
Zhao, X. L., S. Herion, J. A. Packer, R. S. Puthli, G. Sedlacek, J. Wardenier, K. Weynard, A. M. Van Wingerde, and N. F. Yeomans. 2000. *Design Guide for Circular and Rectangular Hollow Section Joints under Fatigue Loading*. CIDECT, Comité International pour le Développement et l’Etude de la

Construction Tubulaire. Construction with Hollow Steel Sections 8. Köln, Germany: TÜV-Verlag.

Appendix A Short summary of LEFM

In this appendix, key concepts of linear elastic fracture mechanics needed for fatigue and brittle fracture of welded details is presented. There are many references that treat the vast topic of fracture mechanics extensively, e.g. (Anderson 2004; David Broek 1989; Barsom and Rolfe 1999).

Fracture mechanics deals with the failure of the flawed (cracked) components. As it is known from the linear elasticity theory, the stress state is singular in the crack tip of a cracked body, i.e. at the point with coordinates (0,0) in Figure A.1. Simply put, the main idea of LEFM is to describe the stress state near the crack tip with a single parameter called Stress Intensity Factor (SIF). This was shown by Irwin (1957) using the so-called Westergaard's stress functions. The stress fields were presented as series functions with a singular term and several non-singular terms. The non-singular omitted terms are vanished for the locations at the crack tip (singularity) region. The stress functions at the crack region are as follows:

$$\begin{cases} \sigma_x(r,\phi) = \dfrac{K_I}{\sqrt{2\pi r}}\cos\dfrac{\phi}{2}\cdot\left(1-\sin\dfrac{\phi}{2}\sin\dfrac{3\phi}{2}\right) \\ \sigma_y(r,\phi) = \dfrac{K_I}{\sqrt{2\pi r}}\cos\dfrac{\phi}{2}\cdot\left(1+\sin\dfrac{\phi}{2}\sin\dfrac{3\phi}{2}\right) \\ \tau_{xy}(r,\phi) = \dfrac{K_I}{\sqrt{2\pi r}}\cos\dfrac{\phi}{2}\cdot\sin\dfrac{\phi}{2}\cdot\cos\dfrac{3\phi}{2} \end{cases} \quad \text{(A-1)}$$

Where the definitions of stresses and the two coordinate systems (Cartesian and polar coordinate systems) are presented in Figure A.1. K_I is the stress intensity factor which is independent of r and ϕ, but it does depend on the remote (i.e. nominal) stresses and crack size, see Equation (A-2). Index "I" in K_I refers to the way that the crack is strained/stretched. Three identical modes can be identified, as shown in Figure A.2 for the case of a planar (2D) crack with a straight crack front (red line) in a three-dimensional body:

- Mode I – opening crack: points on the two sides of the crack plane displace away from crack plane (xy-plane in the Figure),
- Mode II – shearing/sliding crack: points on the two sides of the crack plane displace in the crack plane in the direction perpendicular to the crack front,

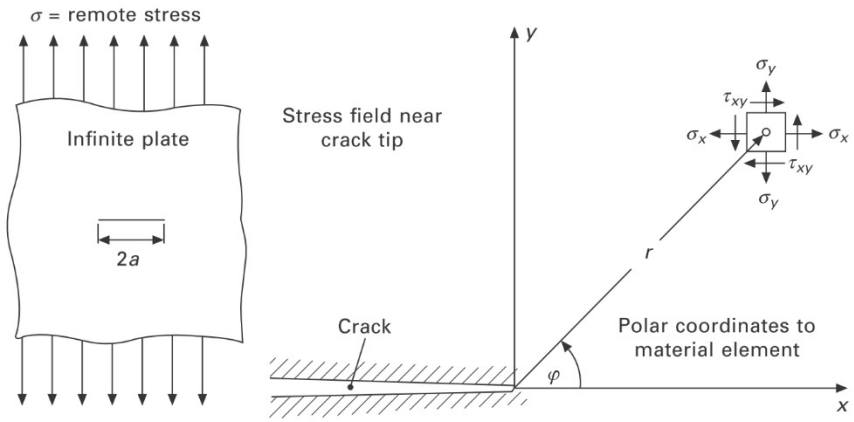

Figure A.1 Infinite plate with a crack. Notations for the stress field in the vicinity of the crack are given in the diagram on the right; from (Hobbacher 2011).

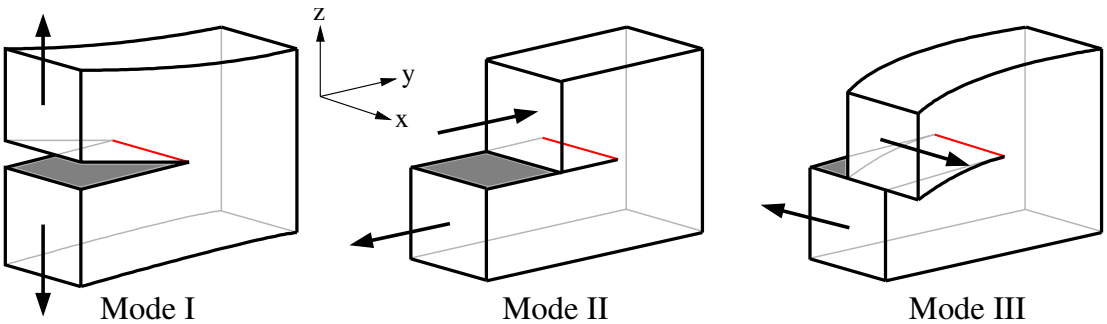

Figure A.2 Crack straining modes.

- Mode III – tearing mode: points on the two sides of the crack plane displace in the crack plane in the direction parallel to the crack front.

In practice, cracking rarely happens purely in only one of these modes; rather, a combination of these three modes happens. But normally the effect of mode I on fracture (and on fatigue) is far greater than the other two modes. Therefore, the discussion here is limited to mode I cracking. For mixed mode cracking calculations refer to (Socie and Marquis 2000).

For the thin plate shown in Figure A.1, Stress intensity factor K_I is calculated as follows (Tada, Paris, and Irwin 2000). The plate has infinite in-plane dimensions and a through-thickness crack of size a. Loading is static and uniform axial tensile remote stress σ:

$$K = \sigma\sqrt{\pi a} \tag{A-2}$$

The two internationally recognized units for SIF are $N/mm^{3/2}$ and $MPa\sqrt{m}$ (or $MN/m^{\frac{3}{2}}$)[5]. For all other situations where a cracked body is analysed, the same equation with the addition of a correction factor Y is used:

$$K = Y(a) \cdot \sigma\sqrt{\pi a} \tag{A-3}$$

The correction factor is a function of crack size a. According to Equation (A-3), the calculation of SIF for a crack reduces to calculation of the geometry correction factor $Y(a)$ for that specific geometry and stress distribution. There are many ways for estimation of SIFs for a crack:

- Stress Intensity Factor Handbooks, e.g. (Murakami 2005; Tada, Paris, and Irwin 2000),
- Weight function method (Lindroth, Marquis, and Glinka 2013)
- Finite element method or associated methods derived from FEM, namely Boundary element method (BEM) or extended finite element method (XFEM).

The resistance side counterpart of stress intensity factor is called *critical stress intensity factor* or *fracture toughness*. Given certain conditions are satisfied (see A.1.1) It is a property of material and is defined as the maximum stress intensity factor that can be tolerated by a cracked body of material in plane strain condition before unstable crack growth (fracture) occurs.

[5] $1\ N/(mm\text{^}(3/2)\ ) = 1MPa\sqrt{mm} = 0.032\ MPa\sqrt{m}$

Considering lengthy calculations involved in LEFM, several software tools have been developed to facilitate the crack growth life computations. Some of them rely on internal external finite element packages, while others calculate the crack growth using handbooks' analytical formulas or empirical formulas. A summary of more popular software in this field is given in Table A-1. The next section describes the method for hand calculation of stress intensity factors.

Table A-1 Facture mechanics analysis software; Adapted from (Härkegård 2010).

Software	Note	Crack growth calculation	Reference
ABAQUS	XFEM (older methods also available)	-	(Simulia 2014)
AFGROW[6]	Handbook formulas + Weight functions	+	
ANSYS	XFEM (older methods also available)	-	
BEASY	BEM	+	
CrackWise	Analytical/empirical formulas for a range of geometries found in BS7910	+	
Franc 3D	BEM and FEM calculations.	+	
Glinka	Weight functions	+	
p-FAT	Weight functions. Works as a post-processor for Abaqus	+	
ProSACC	Probabilistic and deterministic analyses / not welds	+	
Zencrack	FEM post processor	+	

[6] AFGROW was free software up to version 4. The newer version 5 is commercial. The latest free version (AFGROW 4.12.15.0) can be downloaded from "Internet Archive" from the following address: https://goo.gl/1ibHRx (scroll to the end of page and download the "Lite" version).

A.1.1 Plane strain versus plane stress

For a crack in a plate, such as the one shown in Figure A.3, there is a cylindrical part of material at the crack tip that is under large tensile stresses (and part of is plasticised) in x and y directions (σ_x and σ_y in Equation (A-1)). Under these high tensile stresses, the material in the hypothetical cylinder tends to contract in the axial direction of the cylinder (Poisson's law), but is constrained by its surrounding material.

Assume that cylinder's radius is r and plate thickness is B. Considering the through crack in Figure A.3a, if the cylinder is sufficiently thick ($r \ll B$), then the constrained contraction causes a tension σ_z in the direction perpendicular to the plate surface. This means that now the cylinder's material is under triaxial tensile stress state in the interior of plate, while the stress state near the plate surface is biaxial. On the other hand, if the plate is relatively thin, then the contraction of the theoretical cylinder can take place freely and no stress state is biaxial all along the crack tip.

For part-through cracks shown in Figure A.3b (labelled surface flaw and corner crack), apparently the length of the cylinder (hence the triaxiality of stress state a t the crack tip) does not have any relation to the plate thickness. For these cases, it is on the safe side to always consider plane strain conditions.

As mentioned in the previous section, the critical stress intensity factor, K_c, is considered a material constant only if the stress state at the crack tip is triaxial (i.e. plane strain). The triaxial stress state, means almost complete constraint of the material and limited plastic deformation at the crack tip. Figure A.4 shows the schematic results of critical stress intensity factor, K_c, measurements on specimens with various plate thicknesses. When the plate thickness becomes larger than a certain value, K_c reaches its lowest limit because of stress triaxiality. This lower limit of critical stress intensity factor is a material constant and is shown by K_{Ic} where index I refers to mode I loading.

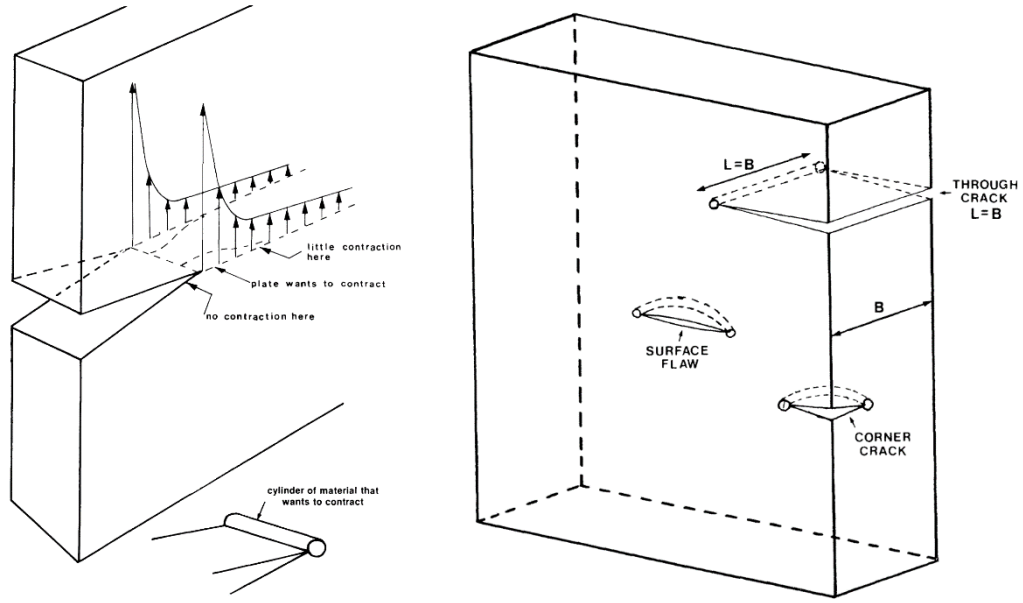

Figure A.3 Constraint conditions for different types of crack (David Broek 1989).

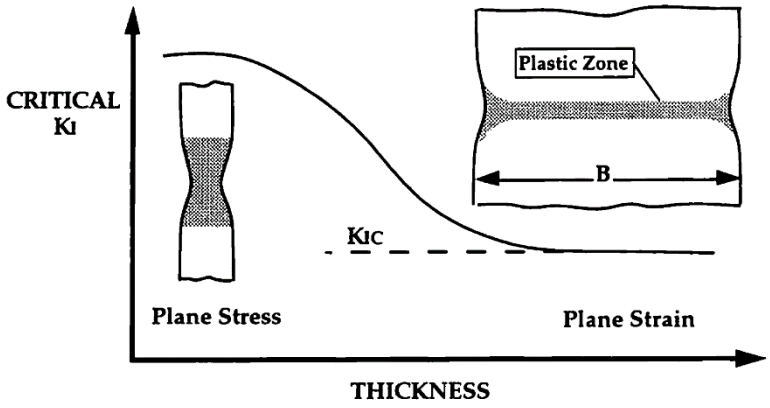

Figure A.4 Effect of specimen thickness on Mode I fracture toughness (Anderson 2004). B indicates the plate thickness.

A.1.2 J-Integral

Another description for material toughness is proposed by Rice (1968). It represents the energy required for fracture per unit surface area of the crack. For a crack in a planar plate, the J-Integral is defined as:

$$J = \int_{\Gamma} \left(W dy - \vec{T} \cdot \frac{\partial \vec{u}}{\partial x} ds \right) \tag{A-4}$$

Where $W(x, y)$ is the strain energy density, (x, y) are the coordinates, $\vec{T} = [\sigma]\vec{n}$ is the surface traction vector, $\vec{n}$ is the normal to the curve Γ, $[\sigma]$ is the stress tensor, and $\vec{u}$ is the displacement vector, see Figure A.5.

Like stress intensity factor, J-Integral for applied stresses on a cracked body can be taken from handbooks or calculated by FEM. Conversely, the material resistance counterpart, namely J_{Ic}, can be experimentally determined in the laboratory.

For a material with linear elastic material behaviour, i.e. the size of plastic region ahead of the crack tip is small (see A.4), under Mode I loading, a simple relation between J_I and K_I holds (D. Broek 1986):

$$\begin{cases} J_I = \dfrac{K_I^2}{E}, & \text{plane stress condition} \\ J_I = (1 - \nu^2)\dfrac{K_I^2}{E}, & \text{plane strain condition} \end{cases} \tag{A-5}$$

Similar relations exist for loading modes II and III. In comparison to stress intensity factor, J-Integral is a better descriptor of the material behaviour when the fracture transitions from LEFM to elastic-plastic fracture mechanics (EPFM).

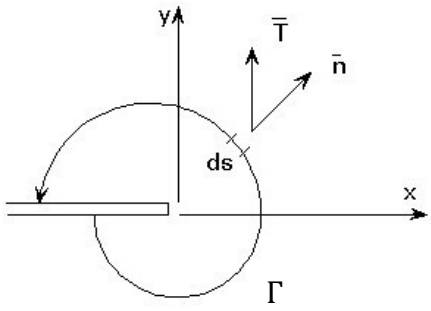

Figure A.5 Definition of J-integral (ESDEP 1993b).

A.2 Analytical determination of stress intensity factors

The method suggested by Newman and Raju (1981) provides a series of empirical formulas for calculation of SIFs for semi-elliptical surface cracks in plates under bending and axial stresses. The method is described in detail in a previous BBT report (Zamiri, Leander, and Al-Emrani 2016).

Newman and Raju method gives the SIFs for plain (un-welded) plates. To estimate stress intensity factors for welded connections, a so-called weld magnification factor M_k, is multiplied to the former SIF values. The M_k factor indicates the change in stress intensity factor due to the presence of weld and welded attachment, compared to a plain non-welded plate (Maddox 1975):

$$M_k = \frac{K_{welded\ plate}}{K_{corresponding\ non-welded\ plate}} \tag{A-6}$$

A few parametric formulae from literature are presented in the previous BBT report (Zamiri, Leander, and Al-Emrani 2016), including those proposed by (Maddox 1975; Hobbacher 1993; Bowness and Lee 2000; Leander, Aygül, and Norlin 2013). Table A-2 gives a summary of formulas for estimation of M_k values with acceptable accuracy in typical welded bridge details.

Table A-2 SIF solutions for bridge details. $K_{plain\ plate}$: SIF for cracked plate without weld; $M_{k,app}$: Weld magnification factor for applied stresses; Sources of figures: cases1-4 (ESDEP 1993a), case 5 (Leander, Aygül, and Norlin 2013).

	Case	$M_{k,app}$	Ref.
1	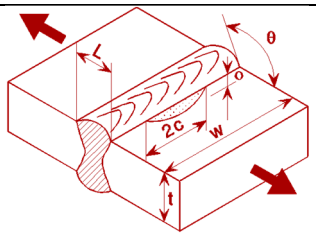 Transverse butt weld	For membrane loading: $M_k = F_G = \frac{5a^q}{t}$ Where: $q = \frac{\log(11.584 - 0.0588\phi)}{2.301}$	(Gurney 1979)

2	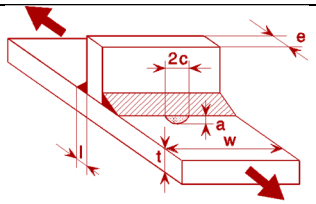 Transverse stiffener weld (non-load-carrying fillet welds)	For bending and membrane loading: See (Zamiri, Leander, and Al-Emrani 2016) Appendix A	(Bowness and Lee 2000)
3	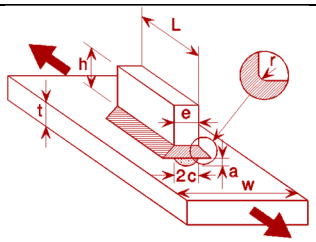 Gusset plate	Only for membrane loading: See (Zamiri, Leander, and Al-Emrani 2016): Appendix A	(Hobbacher 1993)
4	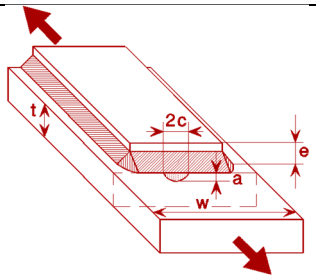 Cover plate	$M_k = F_G = \frac{K_t}{1+\frac{a^q}{d}}$ Where: $K_t = -3.539\log\frac{z}{t} + 1.981 log\frac{e}{t} + 5.798$ $a = a/t$, $d = 0.1473$, $q = 0.4398$ z: fillet weld's footprint size	(Zettlemoyer and Fisher 1977)
5	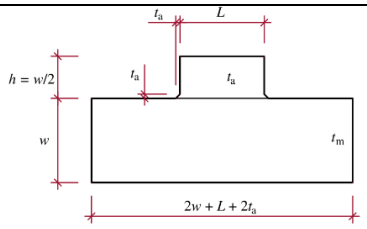 Edge detail	Only for membrane loading: See (Zamiri, Leander, and Al-Emrani 2016) Appendix A	(Hobbacher 1993; Leander et al. 2013)

A.3 Fatigue crack growth calculation

The service life of a component under cyclic loading can be divided into two distinct stages: initiation and propagation. During the fatigue crack initiation life, a macro-crack which is detectable by normal non-destructive methods, has not taken shape. The fatigue process in this stage is taking place in the lattice/microstructure level (accumulation of dislocations) to form micro cracks. After a number of loading cycles, when the micro-cracks have grown large enough, a macro-crack forms that grows with a much higher speed, compared to micro cracks in the initiation phase. Thus, the total fatigue life N_t of the component can be given as:

$$N_t = N_i + N_p \tag{A-7}$$

Where N_i and N_p are number of load cycles spent in initiation and propagation phases, respectively. Figure A.6 shows the two stages of fatigue life in relation to the crack size. Failure takes place when the critical stress intensity factor is reached in the crack tip which corresponds to critical crack size, a_c.

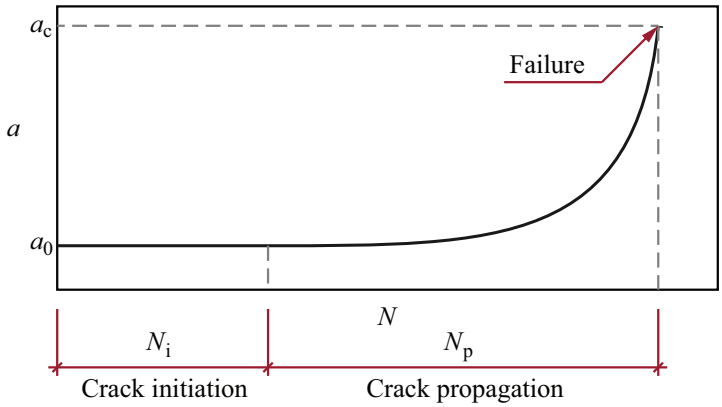

Figure A.6 A schematic figure of the relation between fatigue life N and crack size a.

Crack initiation life is a function of material characteristics, surface finish conditions and several other parameters. According to (Schijve 2009), majority of the fatigue life of a welded connection (up to 90%) is spent in the propagation phase. This is because almost universally pre-existing crack-like defects (such as undercuts or inclusions) can be found in the welds. Thus, neglecting the initiation life is an acceptable assumption which also is on the safe side because it leads to underestimation of the total fatigue life.

Figure A.7 shows a typical fatigue crack growth diagram for carbon steels. As can be seen from this figure, in phase II (propagation phase), an approximately linear relation exists between stress intensity factor range ΔK and the crack growth speed $\frac{da}{dN}$. This relation can be described as (BS 7910 2013):

The crack growth in the propagation stage is usually calculated using

$$\begin{cases} \frac{da}{dN} = C(\Delta K)^m & \text{for } \Delta K > \Delta K_{th} \\ \frac{da}{dN} = 0 & \text{for } \Delta K \leq \Delta K_{th} \end{cases} \quad \text{(A-8)}$$

Where:

a	: Crack size [mm];
N	: Number of cycles;
da/dN	: Crack propagation rate [mm/cycle];
ΔK	: Stress intensity factor range,
ΔK_{th}	: Stress intensity factor range below which no crack growth happens,
C and m	: So-called Paris-Erdogan constants (material parameters).

The fatigue crack propagation life N_p can be calculated by numerical integration of above equation:

$$N_p = \int_{a_o}^{a_d} \frac{da}{C \cdot \Delta K^m} \quad \text{(A-9)}$$

Note again that this approach is in contrast to the S-N approach, where stress range $\Delta\sigma$ is correlated to the total fatigue life.

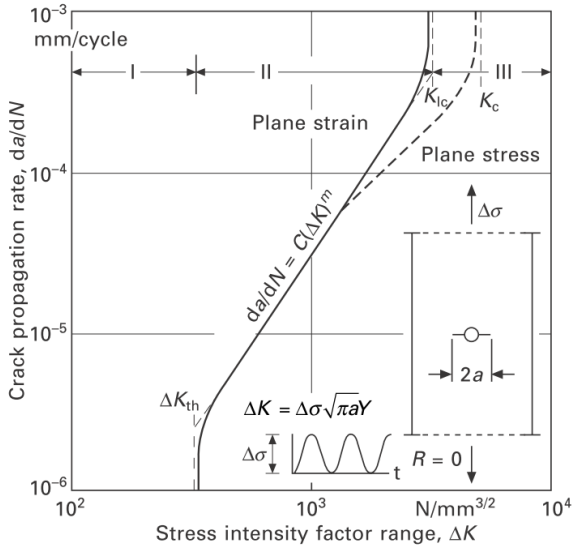

Figure A.7 Fatigue crack propagation diagram (Hobbacher 2011).

A.3.1 Crack growth under variable amplitude loading

As Annex A of Eurocode 3 part 1-9 (EN 1993 2005a) specifies, stress history in the studied detail should be converted to the form of stress range spectrum by means of a cycle counting method (e.g. rainflow method). Evidently, some information is lost in the conversion process, namely the sequence in which the loading was exerted into structure.

In theory, the loading sequence can affect the crack propagation process either in a beneficial or in a detrimental manner. This is mainly due to the effect from high load peaks (overloads); in the cycles following a high tensile overload, plastically stretched material in the crack tip tends to keep the crack closed and resists further opening. Crack closure can significantly affect the fatigue crack growth, especially in the near-threshold load cycles at low stress ratios. See (Schijve 2009; Stephens et al. 2000; Zamiri, Leander, and Al-Emrani 2016) for more details.

However, it has been shown (Zamiri, Leander, and Al-Emrani 2016) that for the case of steel bridges under random traffic loading, the effect from loading sequence is either negligible or on the safe side. Therefore, the stress spectrum can be used in a multistep integration of Equation (A-8). Each block of stress ranges in the spectrum is considered as a number of load cycles with constant amplitude. The crack growth for each block is calculated based on the final crack size at the end of previous block. The whole load spectrum is repeated k times over the service life of the structure (or between inspection intervals), therefore the block-by-block load integration should be repeated k times to predict the crack size at the end of intended residual life of the detail.

For a faster but less accurate estimation of crack growth, the whole stress spectrum can be replaced with a single equivalent constant amplitude stress range calculated from EN 1993 part 1-9 (2005a) as:

$$\Delta\sigma_{eq} = \left(\frac{\sum_{i=1}^{p}(\Delta\sigma_i^m \cdot n_i)}{\sum_{i=1}^{p} n_i}\right)^{1/m} \quad \text{(A-10)}$$

Where:

$\Delta\sigma_{eq}$	: equivalent constant-amplitude stress range,
p	: number of stress range blocks in the spectrum,
$m = 3$	: slope of S-N curve (and power coefficient in Paris' equation),
n_i and $\Delta\sigma_i$	: number of cycles and stress range for load block I in the spectrum, respectively.

A.4 Ductile vs. brittle fracture

A structural component with a crack may fail in different failure modes, depending on the crack size, amount of applied stresses, and material's resistance to crack extension (fracture toughness). Figure A.8 shows the two modes of fracture, namely ductile and brittle fracture. Brittle fracture occurs when the toughness of material is lower than stress intensity factor from applied loads, while the stresses are well below the yield stress, and the size of plastic region at the crack tip (hatched area in the Figure A.8) is relatively small at the time of fracture. For the plane strain conditions, this can be stated as:

$$K \geq K_c \quad \text{(A-11)}$$

Where K_c is the critical stress intensity factor. If certain conditions are satisfied, K_c can be considered as a property of material (see C.3.1). Combining above relation with Equation (A-3) yields:

$$a_{cr} = \frac{1}{\pi}\left(\frac{K_c}{Y\sigma_0}\right)^2 \quad \text{(A-12)}$$

Where a_{cr} is the critical crack depth, $Y = Y(a)$ is the geometry correction factor, and σ_0 is the nominal stress in the detail.

Since net section yielding does not occur during brittle fracture, a redistribution of stresses will not occur. This means residual stresses will not vanish at the time of fracture and their effect on fracture should be considered.

Yielding pattern	Failure mode	Design values

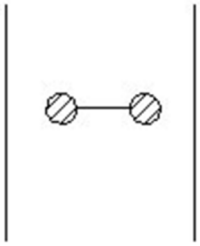	Fracture before net-section yielding **Brittle**	Applied stress distribution in the net section + residual stresses + restraints
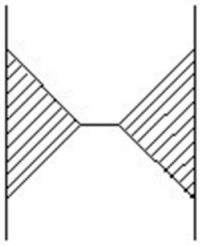	Fracture after net section yielding **Ductile**	Applied nominal stress distribution in the net-section

Figure A.8 Failure modes and applied design values of stresses depending on the ductility level, reproduced from (ESDEP 1993b).

Appendix B Non-destructive testing (NDT)

Non-destructive inspection (NDI) methods can identify flaws and/or material properties in structural members without affecting their performance. For the case of bridges, a benefit of keeping the structure intact is that the bridge can remain in service during inspection period and thus the traffic flow is not disrupted.

The accuracy of the non-destructive inspections depends on several factors (Kühn et al. 2008):

- Chosen NDT technique,
- Material of the inspected structure,
- Qualifications of personnel who perform inspections,
- Quality and correct calibration of the equipment,
- Position of the inspected details and the environmental conditions during inspection,
- Applied acceptance criteria; given the difficulty that majority of available guidelines are given for fabrication of new structures and may not be suitable for old structures.

Some NDI techniques that can be used for detection and characterization of cracks and pre-existing flaws in steel and composite bridge details are listed in the following sections. Table B-1 gives a summary of applicability of these NDT methods for various flaw detection situations. A comprehensive review of NDT methods for all types of bridges (including steel and composite bridges) can be found in the documentation of "Sustainable Bridges" project (R. Helmerich, Bień, and Cruz 2007).

Table B-1 Suitability of NDI techniques for flaw detection in various situations; adopted from (AASHTO 1994).

NDT method	Abbreviation	Minute Surface Cracks	Deeper Surface Cracks	Embedded Cracks	Fatigue Cracks	Internal Voids	Porosity and Slag in Welds	Measuring plate Thickness
Radiography	RT	N	F	F	P	G	G	F
Magnetic particle (Wet)	MT	G	G	N	G	N	N	N
Eddy current	ET	F	G	N	N	N	P	P
Dye-Penetrant	PT	F	G	N	G	N	N	N
Ultrasonic testing	UT	P	G	G	G	G	F	G
G:Good ; F:Fair ; P:Poor ; N:Not suitable								

B.1.1 Visual testing (VT)

Visual inspection is the predominant NDE inspection method for bridge structures, and should always be done before more advanced inspection methods. It is fast and more economical compared to other inspection methods and does not ned special equipment except for suitable lighting.

A large drawback of the method is its subjectivity and difficulty to quantify results reliably. The probability that a crack can be detected using this method depends on many factors, such as duration of inspection, ease of access, lighting conditions, eyesight of the operator (as well as use of any magnifying instruments) (Lukić et al. 2011). According to Lukić et al. (2011), other factors that affect the probability of crack detection include: orientation and location of the crack, gap opening of the crack mouth, the surface condition (e.g. rusted surface), and the environmental conditions, in which the inspection takes place all influence the chance of detection.

Several attempts have been made in the past to quantify the detectability of the cracks by the visual inspection. One important contribution is the work of Fujimoto et al. (1990) in the context of shipbuilding industry. They performed an extensive field inspection by various inspectors to estimate probability of detection (PoD) curves (see Section B.2) for various "classes" of surface cracks. They had classified the cracks based on various factors such as the crack mouth opening and the surface conditions, see Figure B.1a. The estimated PoD curves for three first crack classes (the ones that were free from rust and corrosion) from their work is shown in Figure B.1b. As can be seen, the probability of detection rapidly decreases for cracks with smaller mouth opening. This is true even for cracks as large as 50 mm in length.

Another project aimed at evaluation of "reliability of visual inspection for highway bridges" was conducted in United States by FHWA (2001). The study proposed qualitative measures for reliability and accuracy of the visual inspections and gave several factors that can influence the detectability of the surface cracks, as was mentioned above. Despite the research efforts conducted so far, a conclusive result for reliability of visual inspection does not exist. This is mainly due to subjective and non-quantitative nature of the method (Lukić et al. 2011).

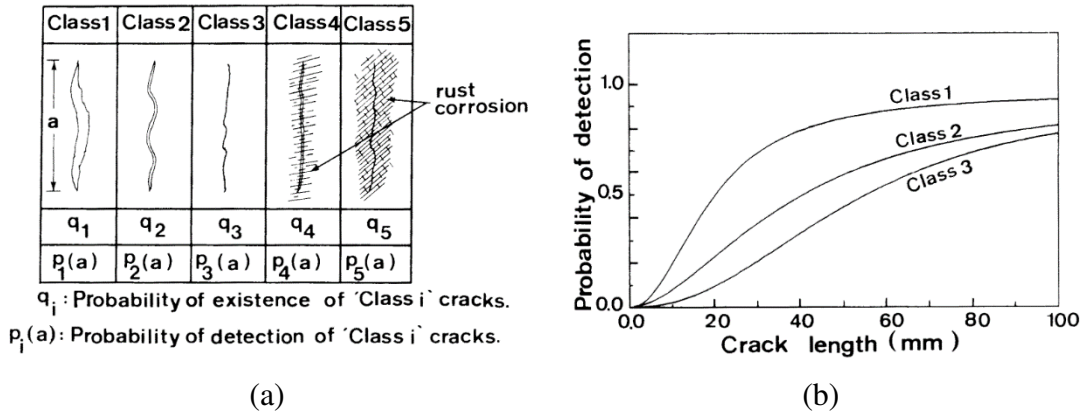

Figure B.1 Quantification of visual testing for detection of surface cracks by Fujimoto et al. (1990); (a) Various classes of cracks; (b) Estimated probability of detection (PoD) curves for classes 1, 2, and 3.

B.1.2 Penetrant testing (PT)

The method is also called dye penetrant inspection. A coloured penetrant with low surface tension is applied on the surface to be inspected and is given time (~30 minutes) to penetrates the surface breaking cracks and other surface flaws. Afterwards, the surface is carefully cleaned such that only the excess penetrant on the surface is removed, but the coloured penetrant that has accumulated in the cracks and cavities is not cleaned. Finally, developer is applied to the surface which causes that the dye that is trapped in the cracks coming back to the surface and rendering the cracks visible.

The method is relatively low cost and easy to apply. Surface preparation (removal of rust or paint layer) is necessary, e.g. with wire brush. If grinding is used, it should be done carefully. Sandblasting is not recommended as it generally reduces the detectability of the crack. PT method is applicable to all types of metals (and even non-metallic materials). Apparently, it cannot be used to detect subsurface defects, see Table B-1.

B.1.3 Magnetic particles inspection (MT)

In this method, the inspected detail is magnetized by either a permanent magnet or an Electromagnet. To visualize the magnetic field, a suspension containing steel particles is sprayed on the surface. A surface-breaking defect, e.g. a fatigue crack, changes the magnetic field on the metal surface. This causes the accumulation of steel splinters (particle size in the range of $3 - 10\mu m$) in the crack region which leads to higher likelihood of crack detection. As a more sensitive alternative of MT method, the splinters are painted with fluorescent material and the detection takes place under UV light. Figure B.2 demonstrates application of MT method on a welded detail in Göta river bridge.

MT method can be used to detect surface cracks only in ferromagnetic materials. It has a high accuracy (see Figure B.8); small hairline surface cracks (up to crack mouth width of $0.2\mu m$) and length of 0.5—0.2 mm can be detected (Kühn et al. 2008). The requirement for surface preparation is similar to PT method; the paint layer should be removed and surface should be cleaned with a wire brush. Permanent magnets are easier to use for site applications, compared to electromagnetic yokes. Based on the type of magnetic suspension used, visualisation can be made under visible or UV light.

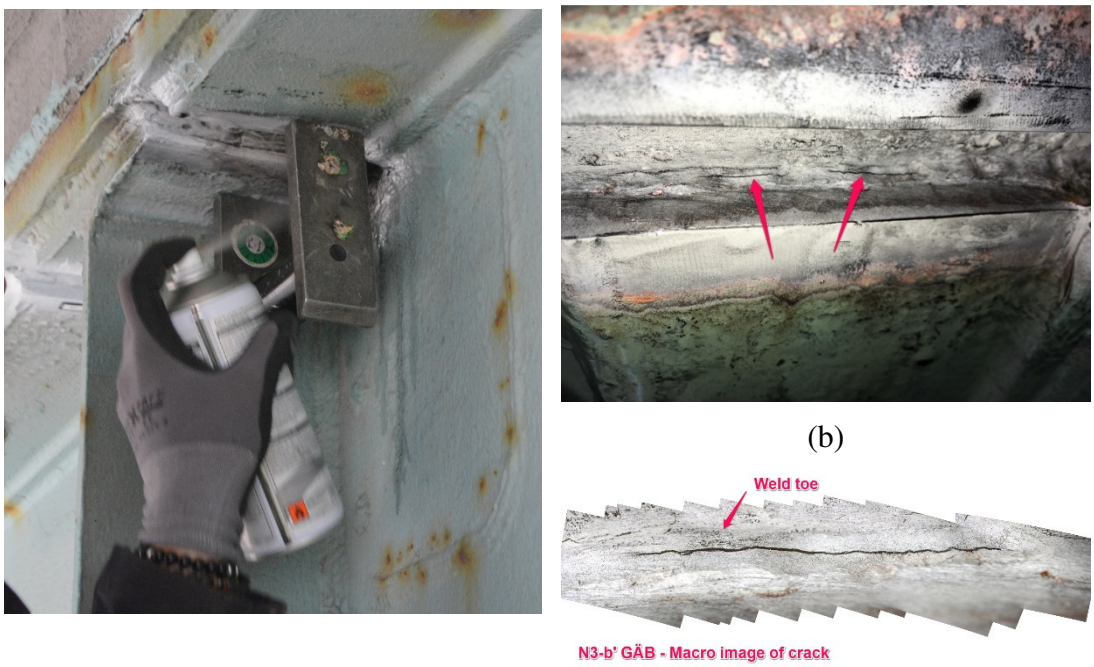

Figure B.2 *(a) Magnetic particles in a suspension are sprayed on the surface of studied detail on the bridge. The welded details are magnetized by attaching the permanent magnet; (b) cracks are revealed by accumulation of black-coloured steel splinters. White paint was sprayed beforehand to improve contrast; (c) Close-up of the crack made by stitching 11 images taken by a handheld USB-microscope.*

B.1.4 Ultrasonic testing (UT)

An ultrasonic wave is sent to the homogenous material using piezoelectric transducers. The wave travelling in the material is reflected by inhomogeneities (cracks, cavities, plate boundaries). Measuring the time of flight (TOF) of the wave (the time it takes for the emitted wave to reach the receiving transducer) can be analysed for finding and sizing the defects. A newer variant of UT employs an array of transducers bundled in a probe block instead of a single transducer. The transducers send their signals with various predefined angles and with accurately prescribed timings. The registered reflected signals give a 2-D scan of the internal defects with a just a single measurement. Figure B.3 shows the principles of both UT and phased array UT methods.

UT method is very powerful method capable of detecting both surface flaws and internal defects. It can be used on all types of materials. The cost of the test is higher than VT and MT methods and needs highly trained personnel for reliable implementation. For application of UT method, the paint layer should be removed and the surface being ground.

Since the time-of-flight calculations are based on geometry of the component, complex geometries (e.g. orthotropic decks) with a lot of reflected waves from different external surface could make it too difficult for reliable interpretation of results. On the other hand, if a relatively simple geometry is being studied, use of UT would be very effective in finding all types of defects, including cracks, with high accuracy. Figure B.4 shows an example of this condition. An overlap joint at the end of cover plate on the upper

flange of a bridge girder was inspected using ultrasonic testing. No other method could be used for this inspection, since the cover plate and the upside of the flange were buried in the concrete deck. The only access available was from the backside (below) of the plate.

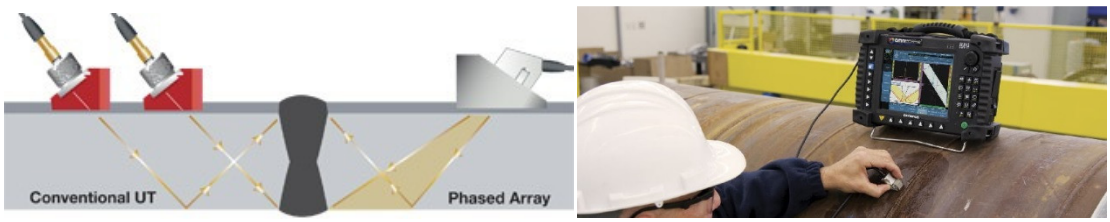

(a) (b)

Figure B.3 Conventional UT checks a single point in each scan while Phased array UT (PA UT) can scan a region in each scan; (b) crack visualization using modern PA UT equipment.

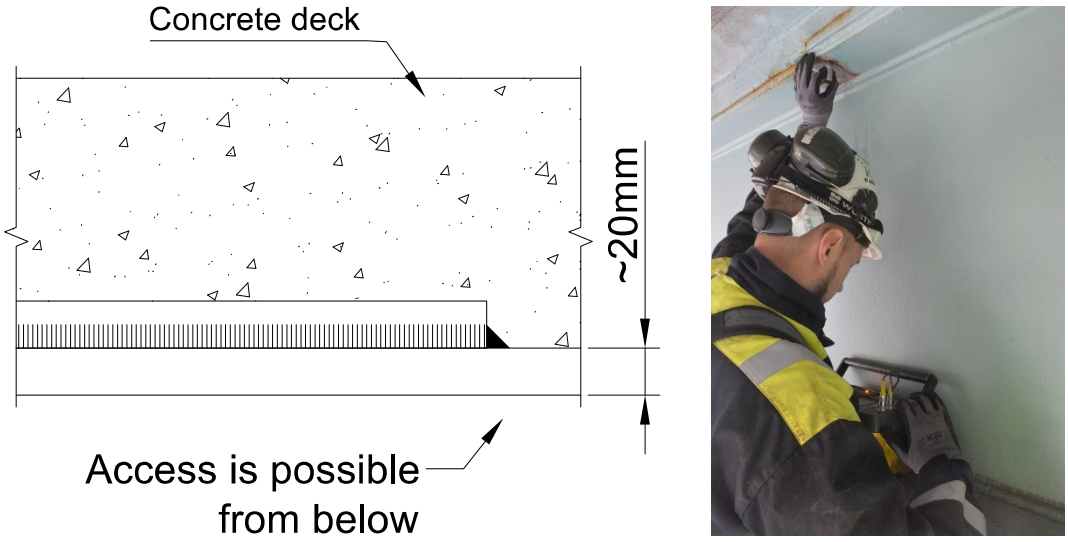

(a) (b)

Figure B.4 Crack detection in the back side of the plate (side buried in the concrete) sung UT; (a) surface preparation; (b) Operator working from the accessible side (below) of the plate.

B.1.5 Eddy current method (ET)

In the ET method, a coil is used to generate a highly varying magnetic field near surface of the metallic part which is studied. The excitation by magnetic field induces eddy currents in the studied metal surface. Due to skin effect, the eddy currents are mainly concentrated in the region close to the metal surface. If a defect exists, it disturbs the pattern of eddy currents. This change in the pattern of the currents affects the magnetic field which in turn can be sensed by the same coil that acts as excitatory and sensor at the same time. The fact that there is no contact between the sensor and the metal implies

that the non-conductive protective coating (within conventional thickness range) does not need to be removed for application of this method.

The method has a high accuracy, but it is also sensitive to changes in microstructure (such as those occurring in the HAZ at the welds). Therefore, calibration is burdensome and should be undertaken carefully. Also, if the distance of the coil from the surface changes, false indications will show up in the output signal (lift-off error). Therefore, the method is well suited for repetitive and automated weld inspections, e.g. welds on silos and pipes. According to Kühn et al. (2008), ET is not implemented for the steel bridges so far, but they report a feasibility study being conducted in Germany for built-up riveted sections.

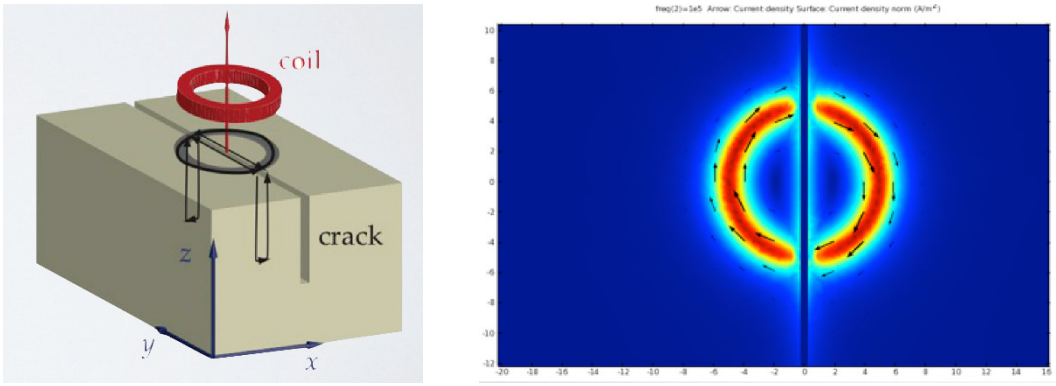

(a) (b)

Figure B.5 Principle of ET method; (a) A coils with high frequency AC current is held near the metal surface being studied to induce Eddy Currents; (b) Simulated Eddy currents at the cracked region (SENSIMA 2012).

B.1.5.1 Alternate current field measurement (ACFM)

The method is developed as a superior alternative to ET method, although with the same principle of action. Like ET, ACFM is a "current perturbation" technique. The method works by quantitively measuring the disturbance in the magnetic field induced by eddy currents. One distinct difference of ACFM from ET is that it maintains a uniform magnetic field which helps in increasing measurement accuracy. In addition to the length of the crack on the surface, the depth of the crack can be measured using this method.

ACFM sensors do not need direct contact to the metal surface, therefore they have the advantage that removal of protective coating is not necessary. The price of equipment is high and extensive training for personnel is required. They are currently used mainly in the fields of oil and gas industry and offshore structures.

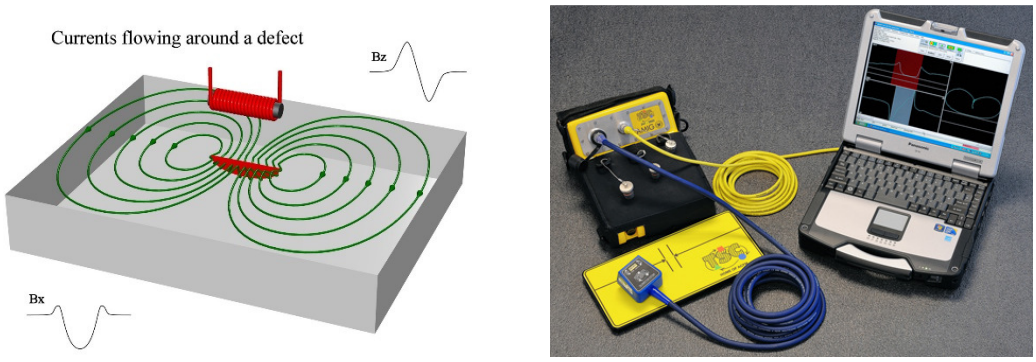

(a) (b)

Figure B.6 ACFM method principle (a); and equipment (b) from TCS corporation (Topp 2014).

B.1.6 Acoustic emission techniques (AE)

Acoustic emissions are transient elastic waves produced by the quick release of energy from localized sources (e.g. cracks) within a material or structure. AE is a NDT method that aims at characterizing those sources of emitting waves by "listening" to the elastic waves that are propagated across the structure. The cracks emitting elastic waves are active ones; therefore an advantage of AE method is that it only concerns with active cracks and neglects the inactive ones (Seyedianchoobi 2012).

To localize cracks, several piezoelectric sensors (minimum three sensors) are attached to the member or structure under study. The elastic waves (also called noise signals) emanated from the propagating crack are recorded by sensors. The crack location and/or its features can be deduced from the signal data including amplitude, energy, travel time, and duration of the signal.

Due to problem in identifying many noise sources in a large bridge, currently AE is not effective for monitoring the whole bridge to detect the cracks. Instead, its use is restricted to monitoring the activity (propagation) of known cracks in steel bridges. Such application is shown in Figure B.7b. A study in LTU (Boström 1999) was carried out for application of AE in crack detection across steel bridge structures in laboratory conditions.

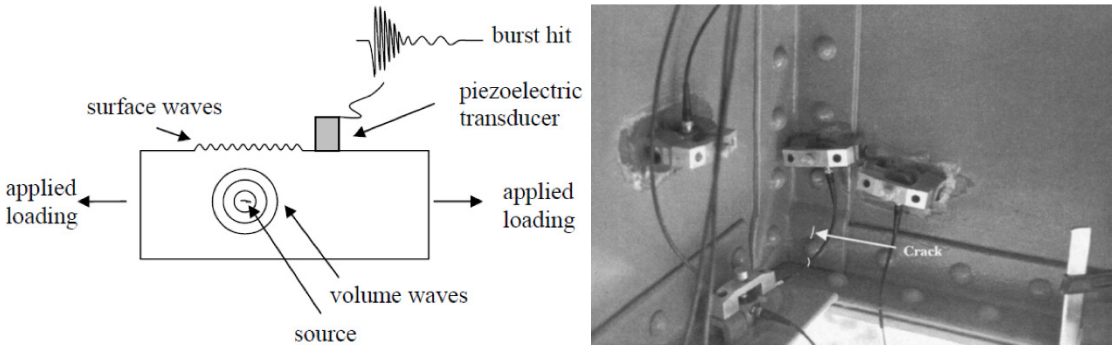

(a) (b)

Figure B.7 (a) Basic principle of Acoustic Emission (AE) method (Seyedianchoobi 2012); (b) Application example of AE method for propagation monitoring of a pre-existing crack in a riveted still bridge (Rosemarie Helmerich and Niederleithinger 2007).

B.1.7 Summary of the methods

A summary of reference values for the NDE tests discussed in this section is provided in Table B-2, coupled with some remarks on their applicability range. Nonetheless, the likelihood always exists that a crack larger than those reference values remains undetected by corresponding NDE method. See next section on a discussion on probability of detection of non-destructive tests.

Table B-2 Detectability of the cracks for various NDE methods, reproduced from FKM Guideline (Pyttel et al. 2007).

NDE method	Crack width w [mm]	Crack length $2c$ [mm]	Crack depth $a, 2a$ [mm]	Comments	Application limits
VT	0.1	2	-	For clean surface, using optical aids	Complex geometry, lack of contrast
PT	0.01	1	0.5	Material-independent use	Porous materials, filled cracks, opening to the surface necessary, rough surface
MT	0.001	1	0.1	For fine cracks at the surface or close to it	Only ferromagnetic materials, dependent on magnetization, surface roughness, and illumination
ET	0.01	1	0.1	Non-contact method	Limited penetration depth
UT	0.001	1	1	For internal and surface defects, arbitrary component thickness	Result dependent on acoustic properties of material, complexity of geometry, and defect geometry

B.2 Probability of detection (PoD)

The response of an NDT method can be in the form of a signal output or an image. Having the response, acceptable conditions should be recognized from unacceptable ones. For example, in the case of visual inspection this means seeing or not seeing a crack, while for an NDT based on an electric signal (e.g. ACFM), this should mean defining a "threshold discrimination" scheme. The definition of recording and acceptance criteria can be different for different parts and applications (Lüthi 2013).

A relationship between NDT result and a feature of studied structure needs to be defined. There are uncertainties inherent to this relationship. These uncertainties originate from the fact that non-destructive evaluation involves the measurement of complex parameters with natural variations in both the measurement itself as well as the studied structures. From this viewpoint, the outcome of an NDT measurement can

be treated as a conditional probability problem. Output can be classified into the following four categories:

- True positive (TP): a defect exists and is detected;
- False positive (FP): no defect exists but one is identified (also named false call);
- False negative (FN): a defect exists but is not detected;
- True negative (TN): no defect exists and none is detected

The number of outcomes which NDT gives the correct answer is TP+FN. The rest, i.e. FP+TN, are the outcomes where NDT gives false alarm. The probability of detection (POD) is defined as the probability of a crack being detected, given that a crack really exists:

$$PoD = \frac{TP}{TP + FN} \tag{B-1}$$

For the application of NDT in crack detection, often PoD is described as a function of crack length (or depth) in the form of PoD curves (see Figure B.8).

Various PoD curves are suggested by several authors, for example (Madsen et al. 1987; Moan and Song 2000; Moan et al. 2000). DNV GL's (2015) recommended practice for offshore structures, proposes the same parametric shape for all PoD curves and gives the parameters to account for individual inspection methods. All curves are described by the same equation:

$$PoD(a) = 1 - \frac{1}{1 + \left(\frac{a}{X_0}\right)^b} \tag{B-2}$$

Where a is the crack depth and X_0 and b are distribution parameters fitted to experimental results. Values stated in DNV GL are reproduced in Table B-3.

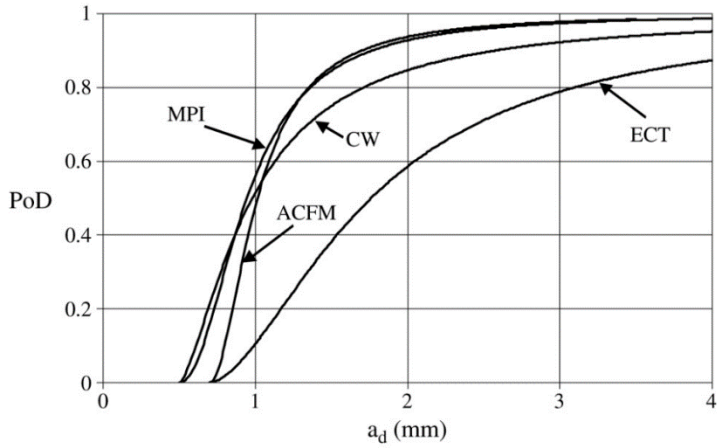

Figure B.8 Probability of Detection for some of the NDT methods for steel structures (Righiniotis 2006).

Table B-3 Parameters for PoD curves, Equation (B-2), for ET, MT, and ACFM inspection methods. Reproduced after DNV GL (2015).

Description	X_0	b

Good conditions above water	0.40	1.43
Normal working conditions above water	0.45	0.90
Below water and less good working conditions above water	1.16	0.90

The PoD curves can be effectively used in a probabilistic analysis using Bayesian analysis (conditional probability) to update the estimated reliability after an inspection is done. Also, they can give insight on comparison of various NDT methods and the size of the cracks that a NDT method can reliably detect. It should be highlighted that majority of past studies have been carried out on regard to inspection of modern structures and materials. Kühn et al. (2008) emphasize the need for research on evaluating acceptance criteria and probability of detection for old materials.

B.3 Choice of NDT scope

The non-destructive inspections should be aimed at the most critical details regarding fatigue and brittle fracture. For example, the details with high load cycles, or the details whose similar details have suffered fatigue damage in the past (Kühn et al. 2008). Due to time and economy considerations, a progressive sampling scheme is suitable for non-destructive inspections. This means a NDT campaign should be limited to most vulnerable details at the beginning (partial inspection). Afterwards, depending on the results of this first stage, planning for further non-destructive inspections will proceed. For example, if the inspection of a detail remains a defect, two additional similar details will be inspected using the same method. If those two are also defected, more intensive inspections should be considered. Guidelines of the Annex C of EN ISO 17635 are also helpful in deciding on further inspections if a flaw is detected. For partial inspection , the selection should make sure that the sampling covers as much the variety of the factors such as joint type, steel grade, welding equipment and personnel (if registered in the original construction documents) (Gerhard Sedlacek et al. 2007).

The extent of NDT includes both testing of surface or internal flaws. The NDT technique can be selected by requirements set out in EN ISO 17635 (2010). Depending on the type of flaws that are sought, Table B-1 can be used as a guideline. It is a common practice that ultrasonic testing (or to a lesser extent radiographic testing) is used for butt welds and liquid penetrant testing or magnetic particle inspection is used for fillet welds (Gerhard Sedlacek et al. 2007). All inspections should be carried out and documented according to EN 1090-2 (2008). If applicable, for the approval criteria Execution Class 4 (EXC 4) should be considered for fatigue-prone and fracture-prone details in steel and composite bridges.

Appendix C Material tests

In this appendix, the material tests concerning fatigue and fracture assessment of steel bridges are presented. Due to their high costs, these tests are generally intended for Phase III assessments, but as was mentioned in the main report, still the engineer may decide on undertaking some of the tests mentioned here in earlier phases. Also, information given here can be useful in understanding and interpreting existing experimental data available in the bridge documentation.

Kühn et al. (2008) warn about degraded steel qualities in some epochs during the 20th century, despite overall increase of steelmaking quality in the past century. These eras include the years of World War I (1914-1918), the great depression (1929-1939) and during and after World War II (1939-1950). The lower quality in these periods can be attributed to lack of some expensive alloying elements and the pressure for rapid production. They recommend conducting material tests for the structures built in those periods.

Majority of the material tests given here are destructive tests. Care should be taken to avoid jeopardizing the safety of the structure by taking samples from fracture-critical members. If necessary, appropriate repair and reinforcement measures should be taken. The exposed metal surfaces should be appropriately protected against corrosion.

C.1 General measurements

C.1.1 Dimensions

Table C-1 summarizes available measurement methods for actual dimensions of various geometric features of structure, based on Kühn et al. (2008) recommendations.

Table C-1 Recommended measurement methods for different structural dimensions. Adapted from (Kühn et al. 2008).

Feature	Available means of measurement
Geometry	manual measurement, surveying methods and geodesic instruments, GPS-based measuring systems, Laser scanners
Plate thickness Loss of section due to corrosion	manual measurement, destructive measurement by sample drilling, Ultrasonic measurement
Effective weld size	weld gauge
Effective weld penetration	NDT methods such as Ultrasonic Testing (UT), see B.1.4
Size, number and location of reinforcing bars in concrete deck	cover meter
Thickness of concrete slab and pavement (road surface)	Ultrasonic methods, Impact echo, sample drilling, see (Rosemarie Helmerich and Niederleithinger 2007)

C.1.2 Chemical analysis

Chemical analysis is especially important, because given the alloy composition, steel production method (see Section 3.2) can be identified. Chemical analysis should be performed in an accredited laboratory according to the guidelines of TDOK 2012:23 (Trafikverket 2014a) which is based on ASTM E415(ASTM E415 2017). The test method stipulated by standard is arc spark optical emission spectroscopy (spark OES). Weight percent of following elements in the alloy composition should be determined: C, Si, Mn, P, S, Cr, Ni, Cu, Mo, V and N.

The amount of material sample needed for the test varies depending in the equipment used, but generally a milling/swarf of size ⌀25 mm and 5mm thickness would be sufficient. The cleanliness of sample surface from paint residues and other impurities I important for ensuring the accuracy of test results. As pointed out in Section 3.2.1, for older steels (fabricated before 1966), the material composition could change through the thickness. Generally, material located at the mid-plane of the plate would be of lower quality and higher impurities. Therefore, it is recommended that the sample(s) for chemical composition being taken from the inner core of the plate.

C.1.3 Metallography analysis

If possible to take out parts of the welded joints in the structure, weld macrographs can be prepared. Size of the specimens for metallography depends on the weld size and plate thickness, but normally should not exceed 30×30 mm. Macrographs will be examined for following indications:

- Weld geometry: effective weld size, weld toe angle.
- Geometric flaws: porosity, undercut, slag inclusion, etc.
- Lack of penetration or lack of fusion
- Hardness of the heat affected zone: for steels up to grade S355 local hardness value HV10 should be below 380 (Gerhard Sedlacek et al. 2007). Higher hardness value indicates risk of brittleness in the weld zone.
- If necessary, identification of different microstructures in the HAZ, as schematically shown in Figure C.1. Properties of some of these microstructures are briefly discussed in Section C.3.2.

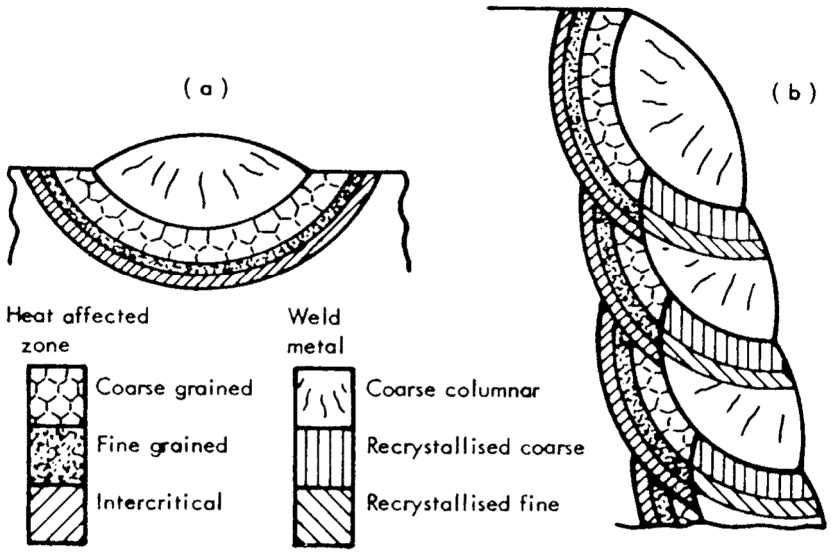

Figure C.1 Schematic microstructure types at (a) single-pass, and (b) multi-pass welds. After (Easterling 1992). Some authors distinguish a narrow "subcritical" microstructure zone adjacent to intercritical zone.

C.2 Material tests for fatigue

C.2.1 Fatigue C-classes

It should be noted that extensive results data exists from the past for old and new steel bridge details. Therefore, it is seldom required to carry out time-consuming, costly, and destructive fatigue tests. Before conducting the tests, a cost-benefit analysis should be performed to justify the testing expenses versus alternative solutions, such as stress measurements or intensified inspections. One case that fatigue tests could be useful is a vulnerable welded detail that has been replicated many times over the structure and cannot be assigned to one of the available fatigue detail categories (e.g. a non-standard shear stud in an old composite deck).

It is recommended to keep the stress ratio R constant for all the tested specimens. Three different approaches for fatigue tests exist, each of which would require a distinct statistical analysis method for interpretation of the results (Hobbacher 2008; Schneider and Maddox 2006):

1. All specimens tested to failure,
2. First specimen tested to failure,
3. p out of n specimens tested to failure (the non-broken specimens $m = n - p$ are called run-outs).

For the reliable regression analysis, IIW recommends that ideally 10 specimens should be tested. Although testing with a smaller number of test specimens is possible, experience from the past tests shows that when the number of specimens is smaller than 6, the scatter band in the results will be so high that the resulted S-N curve will be of little practical use. The details of statistical treatment of the results are given in IIW recommendations (Hobbacher 2008) and in the "best practice" guide (Schneider and Maddox 2006). To simplify the statistical analysis process and validation of the results, Yu (2007) has developed some ready to use spreadsheets.

Regarding the specimens for fatigue tests, a distinction between two types of specimens is necessary: (a) welded details taken out of the actual structure to be tested; and (b) replicas of the details that are fabricated in the shop for the sole purpose of testing. In the latter case, the design of replicas should follow, as close as possible, the geometry (including tolerances and eccentricities) and fabrication (welding position, welding procedure, parent and weld materials selection).

The testing stress ranges should be selected such that the number of cycles to failure is larger than 50,000 cycles. Preferably, stress ranges for some of the specimens should be selected such that they fail somewhere between 2×10^6 and 5×10^6 cycles, which is the range of loading cycles experienced by most bridge details during their lifetime.

C.2.2 SHSS measurement

As indicated in Chapter 3, structural hot spot stresses (SHSS) can be evaluated either from FE analysis of the welded details, or they can be evaluated from in-situ measurements. For the latter case, strain gauges should be attached to the detail in two or three reference points in predefined distances from weld toe. SHSS is calculated by extrapolating measured strains in reference points to the weld toe location.

For hotspots that do not reside on the plate edges (Type 'a' hot spots), first reference point should be located at a distance of $0.4t$ from the weld toe, and the second reference point at $1.0t$ from the weld toe (Hobbacher 2008), see Figure C.2. The structural hot spot strain can be calculated by extrapolation using following relation:

$$\epsilon_{hs} = 1.67\epsilon_{0.4t} - 0.57\epsilon_{1.0t} \tag{C-1}$$

Where ϵ_{hs} is the structural strain at the weld toe and $\epsilon_{0.4t}$ and $\epsilon_{1.0t}$ are the measured strains in the reference points located at the distances $0.4t$ and $1.0t$ from the weld toe, respectively. In some cases where the plate is resting on a stiff elastic support (like a beam flange supported by the web) the linear extrapolation may underestimate the hot spot stress. In those cases, quadratic extrapolation should be used, according to IIW recommendations (Hobbacher 2008).

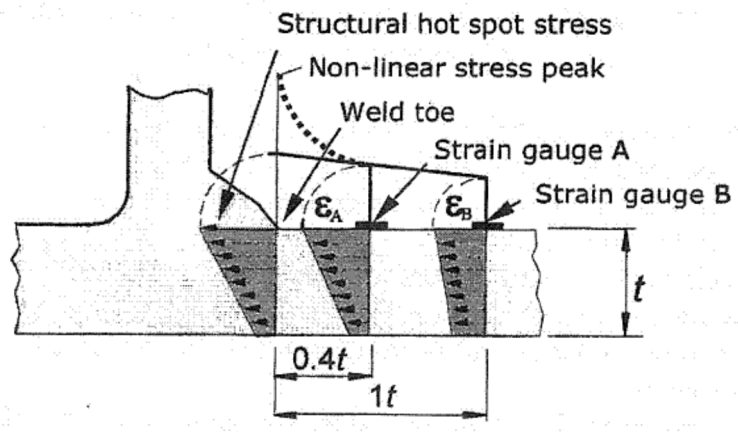

Figure C.2 Linear extrapolation of strains into the weld toe to evaluate SHSS stress in type 'a' hotspots, after Niemi et al. (2006).

For conversion of strains to stresses and if the stress state is uniaxial, Hooke's law in simplest form can be used:

$$\sigma_{hs} = E \cdot \epsilon_{hs} \tag{C-2}$$

Where σ_{hs} is the structural hot spot stress and E is the modulus of elasticity for the steel. If the stresses in the plate are biaxial, the hotspot stress can be up to 10% larger than value calculated from the above relation. In this case, the ratio of the longitudinal and transverse strains ($\epsilon_{yy}/\epsilon_{xx}$) should be evaluated either from rosette strain gauges, or from FEA calculations. σ_{hs} then can be calculated from following relation:

$$\sigma_{hs} = E \cdot \epsilon_x \cdot \frac{1 + \nu \frac{\epsilon_{yy}}{\epsilon_{xx}}}{1 - \nu^2} \tag{C-3}$$

Where $\nu = 0.29$ is the Poisson's ratio of the steel. In the derivation of the above relation, it is assumed that the principal stress is approximately perpendicular to the weld toe.

For the joints made of tube sections, the same principles for extrapolation of surface stresses apply, but in a slightly different manner. For further details refer to CIDECT design guide 8 (Zhao et al. 2000).

C.2.3 Experimental evaluation of crack growth parameters

Fatigue crack growth (FCG) experiments to evaluate parameters in Paris' relation, namely C, m, and ΔK_{th}, should be done according to ASTM E647 (2015). ΔK_{th} is the asymptotic value at which da/dN approaches zero, see Figure A.7. According to ASTM standard, for most materials including steel, ΔK_{th} is given an operational definition by attributing it to fatigue crack growth rates of $\frac{da}{dN} = 10^{-10}$ m/cycle. This value is solely chosen for practical reasons.

For statistical treatment of the results, the same principles discussed for Fatigue tests (Section C.2.1) applies here also. Guidelines for interpretation of the results are given in ASTM E647 and in IIW recommendation (Hobbacher 2008). The mostly used specimen geometry for the tests is Compact Tension, C(T), specimen, see Figure C.6. ASTM E647 requires that the thickness and length of the specimen satisfy the following condition:

$$\frac{W}{20} \leq t \leq \frac{W}{4} \tag{C-4}$$

Where t is the thickness and W is the length of the specimen, as shown in Figure C.6.

Figure C.3 depicts an example of FCG test results conducted on old steel material from an existing bridge carried out by (Bucak and Mang 1998).

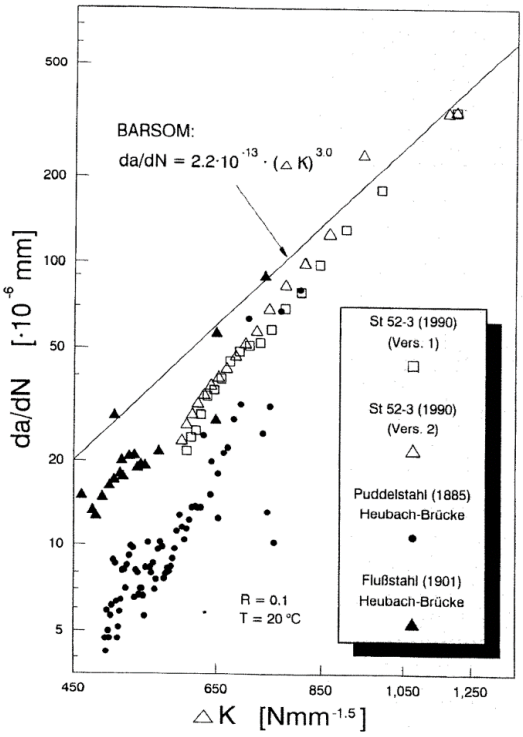

Figure C.3 Fatigue crack growth measurement for modern steel, puddle steel, and old mild steel from Heubach bridge in Germany; The straight line depicts the crack growth parameters proposed by Barsom (1999); the graph is reproduced from (Bucak and Mang 1998).

C.3 Material tests for brittle fracture

Charpy test has been one of the earliest test methods to evaluate resistance of steel against brittle fracture. The test is basically impact (dynamic) loading of specimen (size $10 \times 10 \times 55$ mm) with a V-notch at the middle at a prescribed temperature and measuring the absorbed energy during its fracture. Schematic setup of the test is shown in Figure C.4. For ferritic steels, including construction steels, the fracture resistance is temperature-dependent. If the Charpy test is conducted in a range of temperatures, the Charpy energy values versus test temperatures make up the temperature transition curve. The curve consists of two distinct asymptotes: "lower shelf" which represents the brittle (cleavage) fracture at lower temperatures, and "upper shelf" which represents ductile fracture in higher temperatures. The third region, that is the transition part between the two behaviours, is called transition region. Usually, the temperature corresponding to $A_v = 27\,J$ absorbed Charpy energy has been called ductile-to-brittle-transition temperature (DBTT) and is shown by T_{27J} , as can be seen in Figure C.5. All design rules for steel structures in Eurocode 3 are based on upper shelf behaviour.

To plot the transition curve for Charpy energy, the data from tests in various temperatures (belonging to all three regions: upper shelf, lower shelf, and transition region) are plotted and a curve with the following form is fitted to the data:

$$A_v = A + B \cdot \tanh\frac{T + C}{D} \tag{C-5}$$

Where A_v is the absorbed energy in [Joules], T is the test temperature in [°C], and A, B, C, D are parameters for the tanh curve that are calculated from a least squares

fitting. See Figure 6.6 for an example of this curve-fitting process. Charpy test method and specifications are laid out in (EN ISO 148-1 2016).

Charpy impact test has the advantage of being relatively quick and easy to perform and requiring just a small amount of material. However, as was discussed in Section 2.1.1, the test parameters represent neither the notch conditions, nor the loading rate for many real-life components. Therefore, it cannot be applied directly for fracture assessment studies and it is preferred to resort to more accurate fracture toughness tests when planning tests for phase III assessments. When the testing is not possible, K_c may be approximated from empirical relations which correlate Charpy V-notch (CVN) energy to fracture toughness. One lower-bound relation is given for steels on the lower shelf and transition region by BS 7910 (2013):

$$K_{mat} = \left[(12\sqrt{A_v - 20} \cdot \left(\frac{25}{B}\right)^{0.25}\right] + 20 \tag{C-6}$$

Where:

K_{mat} : the estimated fracture toughness of the material (in $MPa\sqrt{m}$),

A_v : the lower bound absorbed Charpy energy at the service temperature (in Joules),

B : the thickness of material for which K_{mat} is being estimated (in mm).

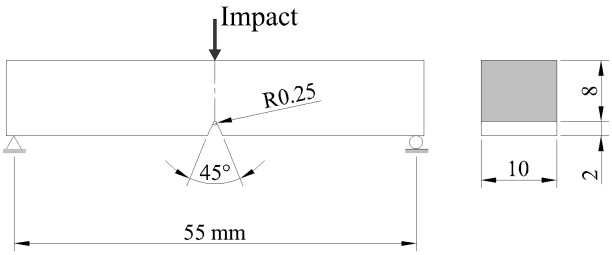

Figure C.4 Schematic view of the Charpy specimen and test. All dimensions are in [mm]; the impact loading is provided by strike of a falling hammer.

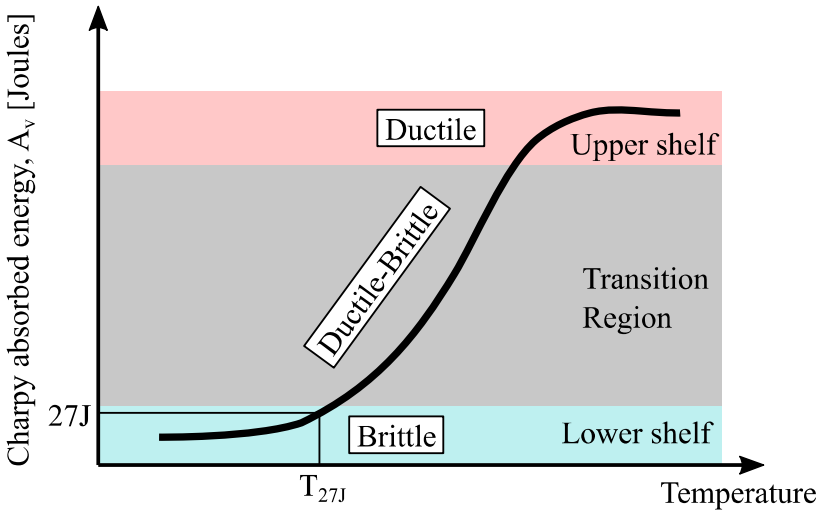

Figure C.5 Charpy impact energy transition curve.

It should be noted that in some older reports, CVN impact energy has been reported either in $[kg \cdot m] = [J]$ or in $\left[\frac{kg \cdot m}{cm^2}\right] = \left[\frac{J}{cm^2}\right]$ units. To convert $\left[\frac{J}{cm^2}\right]$ (so-called specific energy) to $[J]$ (energy), multiply the specific energy by the surface area of the ligament (dark area in the cross section shown in Figure C.4) in $[cm^2]$.

C.3.1 Fracture toughness test

Since plane strain fracture toughness is a property of material, theoretically it can be measured by testing any kind of cracked specimen, provided that the plastic zone in the crack front is small. But in order to simplify the procedure, some simple specimen geometries are standardized by various standards (David Broek 1989).

Trafikverket's TDOK 2013:0267 (2017) document stipulates that for bridges built in 1970 and earlier, if the engineer decides, the steel composition and its toughness properties will be tested according to TDOK 2012:23 (Trafikverket 2014a). this document requires these tests to be done in accordance with (ASTM E1820 2015). Fracture toughness tests are done in following manner (TWI 2015):

1. Milling a standard specimen in the form of Compact Tension C(T), or Single-Edge Notched Bend SE(B), or Disk-shaped Compact DC(T) specimen. See Figure C.6.
2. Careful application of a cyclic load to grow a fatigue pre-crack, typically in room temperature.
3. Attaching a clip-in displacement gauge to the two sides of the notch to measure the crack opening displacement during the test.
4. Changing the specimen's temperature to the desired temperature, which is usually minimum service temperature, and maintaining the temperature steady before and during the test. TDOK 2012:23 requires this temperature to be $-30℃$ or lower.
5. Applying a monotonically increasing load with prescribed speed until failure and monitoring the load and crack opening displacement during loading. The loading speed should correspond to the speeds of service loads experienced by actual component. See Section C.4.1 for details on selection of loading rate for bridges.
6. If the specimen is not completely broken during the test, breaking open the specimen for close investigation and measurement of crack front.
7. Calculation of the toughness parameter J or K_{Ic}.
8. Verification of the result. Note that after test some results might deem unacceptable (e.g. in case a fatigue pre-crack is too large or too small).

For more details on sampling and number of required samples, refer to Section C.4.1.

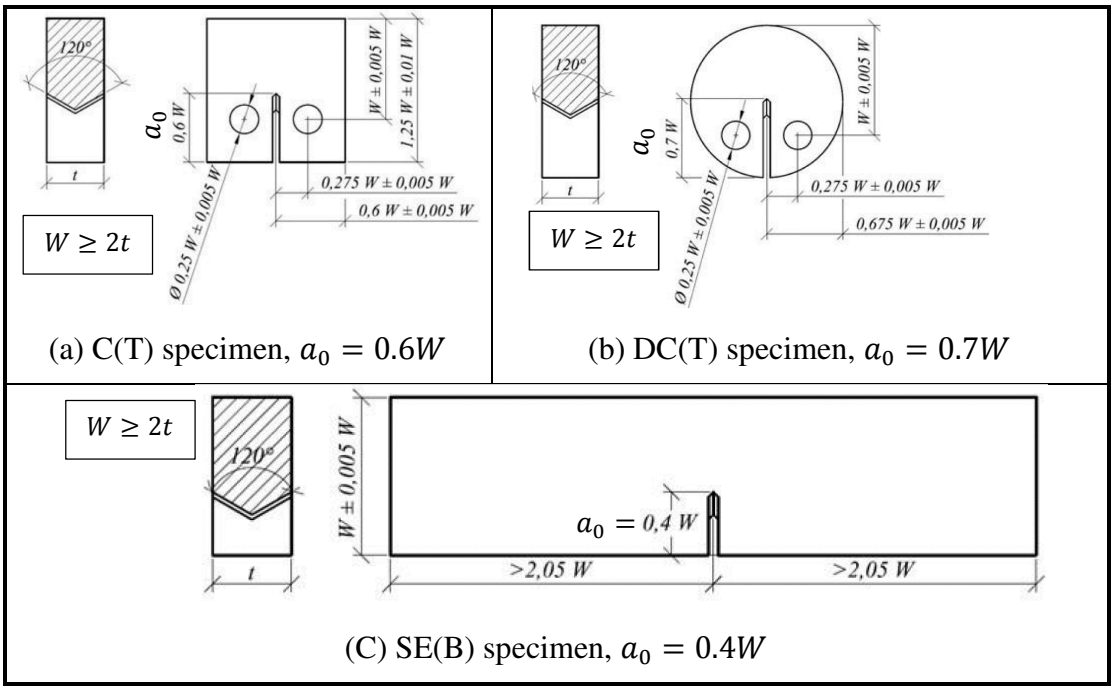

Figure C.6 Most popular specimen shapes for fracture mechanics tests; The values of a_0 (the distance from physical crack front to the specimen's edge) are given for each specimen type; reproduced form (Trafikverket 2014a).

C.3.1.1 Master curve approach

The fracture toughness data for ferritic steels in lower shelf and in brittle region of transition curve show a large scatter. Numerous specimens need to be tested to get a reasonable statistical distribution. This can be both time-consuming and costly. To overcome this limitation, Wallin (2002) has proposed master curve concept as a statistical method for treatment of the scatter in the brittle behaviour region using weakest-link theory. The technique has now been widely adopted and standardized as ASTM E192 (2015). The safety concept for avoiding brittle fracture in Eurocode 3 is also based on the Master curve concept (G. Sedlacek, Feldmann, et al. 2008).

Another advantage of the method is that small-scale specimens (e.g. Charpy-sized specimens $10 \times 10 \times 55$ mm) can be used for fracture toughness assessment. According to Wallin (2002) the fracture toughness is calculated from following relation:

$$K_{Jc,Pf\%} = 20 + [77 \exp(0.019(T - T_{K100})) + 11] \left(\frac{25}{b_{eff}}\right)^{0.25} \cdot \left[\ln\left(\frac{1}{1 - P_f}\right)\right]^{0.25} \quad \text{(C-7)}$$

where:

$K_{Jc,Pf\%}$: also shown by K_{mat}, fracture toughness at temperature T in $MPa\sqrt{m}$ with the probability of failure equal to $Pf\%$ (see below); equivalent to K_{Ic} if plain strain conditions are met (Nussbaumer, Borges, and Davaine 2012),

T : the temperature in ℃,

T_{K100} : the temperature at which median toughness will not be less than $100\ MPa\sqrt{m}$; also called "reference temperature" in ASTM E1921,

$25/b_{eff}$: the term to consider effect of thickness and constrain at the crack front. As a simple conservative assumption, $b_{eff} = 2 \cdot t$, where t is the plate thickness in [mm],

P_f : failure probability; in other words, required probability for reaching a specific value of K_{mat}; For the characteristic values of K_{mat}, $P_f = 5\%$.

Master curve is defined as the median curve in the above equation, for which the probability of failure is $P_f = 50\%$:

$$K_{Jc,med} = 20 + [70\exp(0.019(T - T_{K100})) + 10]\left(\frac{25}{b_{eff}}\right)^{0.25} \quad \text{(C-8)}$$

Where $K_{Jc,med}$ is the median fracture toughness as a function of thickness (constraint) and temperature. As can be seen from above equations, only one parameter, T_{K100}, is needed for determining the fracture toughness curve of a ferritic steel in the lower shelf and transition regions.

The number of valid test results for evaluation of reference temperature and master curve varies, but normally a minimum of 7 valid results are required. See Section C.4.1.1 for guidelines on determining the minimum number of required specimens. The fracture tests can be done according to ASTM E1820 (see previous section). Test specimens can be taken as fracture toughness specimens, i.e. C(T), DC(T), or SE(B) specimens. SE(B) specimens as small as $W = t = 10$ mm (see Figure C.6 for definitions) can be used, which corresponds to the size of standard Charpy specimens. ASTM E1921 (2015) identifies these as pre-cracked Charpy (PCC) specimens.

The test temperatures should be selected close to T_{K100}; thus, an approximate evaluation of T_{K100} is required prior to testing. Equations (C-16) and (C-17) can be used for this. Other test temperatures can be used as long as they belong to the brittle behaviour region. For the validity range of the fracture toughness values using master curve, see Equation (C-9) in next section. Although performing all the tests at a single test temperature is possible, it is recommended that the tests being conducted in various temperatures to minimise the error in estimation of master curve (Sattari-Far and Wallin 2005).

C.3.1.1.1 Determining reference temperature from existing fracture toughness test results

If the fracture toughness data for the steel material exists from previous tests, the reference temperature T_{K100} (and subsequently the master curve) can be estimated through the procedure described here. In this section, only the evaluation method for existing test data for a single test temperature is given. This is generally the case for available test data for steel bridges. For example, Trafikverket's TDOK 2012:23 has prescribed temperature of $-30℃$ for fracture toughness tests. Details of evaluation procedure are given in ASTM E1921 for the case that the fracture toughness data are available over a range of test temperatures.

The test temperature at which the fracture tests have been performed (T_{test}) should be at the transition region or at the onset of lower shelf. The validity window is:

$$T_{K100} - 50℃ \leq T_{test} \leq T_{K100} + 50℃ \quad \text{(C-9)}$$

Therefore, after the determination of T_{K100}, the validity of the test temperature should 7difference between median curve and $K_{Jc,5\%}$ or $K_{Jc,95\%}$) it is preferable that the test temperature to be close to reference temperature.

To convert elastic-plastic fracture (J_c) test data to elastic fractur test data, Equation (A-5) (plane strain conditions) can be used. Therefore:

$$K_{Jc}^{x} = \sqrt{\frac{J_c \cdot E}{(1-\nu)^2}} \tag{C-10}$$

where K_{Jc}^{x} is the elastic fracture toughness of the specimen with the thickness of x. To ensure that the plane-strain conditions have been held at the specimen's crack front, the calculated values from Equation (C-9) should be less than the maximum elastic fracture toughness of specimen, $K_{Jc,limit}$, from to the following equation:

$$K_{Jc,limit} = \sqrt{\frac{\mathrm{E} \cdot (\mathrm{W} - \mathrm{a_0}) \cdot \sigma_{\mathrm{YS}}}{30(1-\nu^2)}} \tag{C-11}$$

where:

$K_{Jc,limit}$: limit value of elastic fracture toughness [$MPa\sqrt{m}$],

σ_{YS} : material's yield stress at test temperature [MPa],

W : specimen's width according to Figure C.6,

a_0 : The distance between crack tip to the specimen's edge (see Figure C.6).

If some of the fracture toughness test results are larger than the limit value ($K_{JC}^{x} > K_{Jc,limit}$) a data censoring scheme needs to be implemented. This normally does not happen for standard-sized old steel specimens tested in low temperatures. For detailed methodology of data censoring scheme, see Appendix L of BS 7910:2013 or ASTM E1921.

The values given by Equation (C-10) should be adjusted for a full-size specimen (Thickness: 1T=25 mm) according to the following expression:

$$K_{Jc}^{1T} = \left[K_{Jc}^{x} - 20\right]\left(\frac{x}{25}\right)^{0.25} + 20 \tag{C-12}$$

where x is the specimen thickness in [mm]. When dealing with brittle fracture, the $\mathrm{K_{Jc,1T}}$ is a desirable factor for assessment of fracture, since it is independent of the shape of the crack and the geometry of the detail. The thickness-adjusted fracture toughness values, $\mathrm{K_{Jc,i}^{1T}}$, will then be used to evaluate the K_0 parameter[7]:

$$K_0 = \left[\sum_{i=1}^{N} \frac{\left(K_{Jc,i}^{1T} - 20\right)^4}{N}\right]^{0.25} + 20 \tag{C-13}$$

where N is the number of specimens. The median value (50% probability) of fracture toughness is then obtained from:

[7] K_0 is the scale parameter for underlying Weibull distribution of fracture data. It corresponds to 63% cumulative probability in the assumed Weibull-distribution.

$$K_{Jc,med} = 0.9124 \cdot (K_0 - 20) + 20 \quad \text{(C-14)}$$

Finally, the reference temperature T_{K100} is calculated from the following relation:

$$T_{K100} = T_{test} - \frac{1}{0.019} \cdot \ln\left(\frac{K_{Jc,med} - 30}{70}\right) \quad \text{(C-15)}$$

for $P_f = 50\%$, Equations (C-7) and (C-15) are equivalent. Having the value of reference temperature, T_{K100}, fracture toughness value can be calculated for various temperatures and thicknesses using Equations (C-7)or (C-8).

As a demonstration of application of this procedure, the master curve for the steel used in Götaälvbron is shown in Figure 6.14. The value of $T_{K100} = -0.4℃$ was evaluated from 9 fracture toughness test results conducted at $T_{test} = -30℃$.

C.3.1.1.2 Determining reference temperature from Charpy test results

Despite its inherent shortcomings for evaluating fracture toughness, Charpy test data can still be used for a rough estimation of fracture toughness using empirical equations such as Equation (C-6). Instead of directly correlating the CVN energy to fracture toughness, another category of the empirical formulas exist that correlates the transition temperature for CVN energy to the reference temperature T_{K100}. Two of such relations for ferritic steels in the lower shelf and transition region are given in ASTM E1921 (2015) and BS7910 standards:

$$T_{K100} = T_{27J} - 18℃, \quad \text{(standard deviation:13℃)} \quad \text{(C-16)}$$

$$T_{K100} = T_{40J} - 24℃, \quad \text{(standard deviation:15℃)} \quad \text{(C-17)}$$

where:

T_{K100} : the temperature corresponding to a median toughness of $100\ MPa\sqrt{m}$ in 25 mm thick specimens (also called reference temperature). T_{K100} is used for the characterization of transition curve in Master curve method (see C.3.1.1),

T_{27J} : the temperature corresponding to 27 J Charpy energy for a standard Charpy specimen,

T_{40J} : the temperature corresponding to 40 J Charpy energy for a standard Charpy specimen.

Note the relatively large error margin in the above equations. The equations are mainly aimed at acquiring a preliminary value of reference temperature, so that the test temperature for more accurate tests can be determined.

C.3.2 Note on fracture toughness at weld region

The fracture toughness tests discussed before were targeted on the relatively homogenous un-welded steel material. For the welds, there is another source of the scatter in fracture toughness data due to the inhomogeneity of microstructure in the heat affected zone. In Figure C.1 various types of microstructure are identified, based on the temperature cycles that has been experienced by different parts in the HAZ. The temperatures as low as 450℃ can alter the microstructure. As a rule, the regions that reach temperatures above 800℃ undergo considerable microstructural change. The longer the cooling times (typically the time for cooling from 800℃ to 500℃), the

coarser the grains [8] become. Coarse-grain microstructures exhibit lower fracture resistance.

Fracture behaviour of the various microstructures in the weld region is the subject of ongoing research. An ISO standard (ISO 15653 2010) has been released recently for fracture toughness evaluation of welds. Basically, the test methods are similar to the methods discussed earlier. Special care should be taken for the tip of the fatigue pre-crack in the specimens is located in the chosen microstructure within the HAZ. Figure shows such a "notch placement" procedure. The master curve analysis method can be applied to the weld and HAZ metals as well (Gerhard Sedlacek et al. 2005).

Zerbst et al. (2014) provide a comprehensive review of the progress on the topic. NCHRP 10-95 is an ongoing research project in United States with the aim of evaluating required fracture toughness in the HAZ of welded structural steels for highway bridges (Roy, Park, and Valeti 2015). Following statements can be given for fracture toughness of weld microstructure (Zerbst et al. 2014):

- Weld metal: Case dependent; For modern steels, the superior chemical composition of the weld usually makes the weld metal more tough compared to the base metal. But for old steel structures this may not hold.
- Coarse-grain HAZ (CGHAZ): Much lower toughness than the base metal.
- Fine-grain HAZ (FGHAZ): Equal to, or better fracture toughness than base metal.
- Intercritical reheated HAZ: Fracture toughness varies with grain size and microstructure constituents.
- Subcritical reheated HAZ: More brittle than the base metal (for the types of steel discussed in this report).

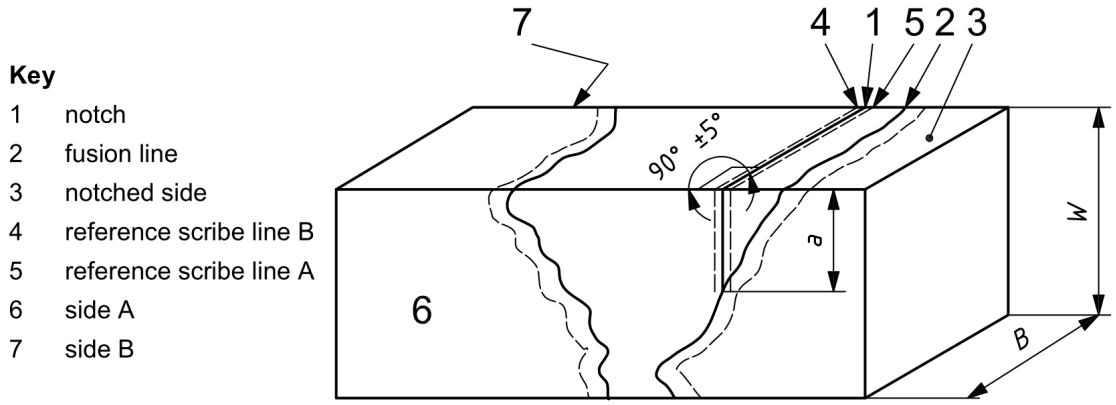

Figure C.7 Notched placement procedure, i.e. growing the pre-crack tip to the desired location in the HAZ before fracture toughness testing of HAZ, after ISO 15653 (2010).

C.4 Sampling guidelines

For the recommended types of material tests and number of tests for steel and composite bridges proposed by Kühn et al. (2008) can be consulted. The number of tests depends on the pre-existing information available in the documentation and/or acquired during

[8] A grain is the region within which the metal's crystal lattice is continuous.

site inspection. The idea is basically to avoid costly and extensive tests whenever possible and instead refer to the extensive data existing that is available for most of the steels used in old steel bridges. A structure that is well-documented, well maintained, and is not highly overstressed beyond its intended service loads seldom needs extensive material tests for the assessments.

Regarding the size of samples for destructive tests, the general guideline is **"As large as necessary but also as small as possible!"** (Kühn et al. 2008). This means that special care should be taken for design of specimen geometry to maximize the utilisation of extracted material. It often happens that enough sample material cannot be extracted from structural members in old bridges. Based on past experience, Kühn et al. (2008) recommend in these cases circular samples (e.g. Figure C.8) to be used. See also following subsections for guidance on sample geometries.

Destructive sampling should not impair the load-bearing capacity of the components. In principle, the specimens should be taken from more vulnerable members and details, but of course not from their critical sections! So, finding the suitable locations for sampling is a rather difficult question with no general answer. The location should be chosen based on the structural configuration, the loading, and the accessibility of the detail (Kühn et al. 2008). Due to the involved complexities, the sampling region need to be selected by experienced experts.

As for the method of sample extraction, sawing and drilling should be used. Flame-cutting should be strictly avoided, as overheating the steel members causes temporary decrease in yield strength, permanent microstructural changes, and probably increased brittleness. After the extraction, exposed surfaces of the members should be properly protected against corrosion after the sampling.

A summary of material sampling should be prepared, containing following information:

- Exact locations that samples were extracted, coupled with justification on why those locations were chosen,
- Individuals and experts who were involved in choosing sampling locations and carrying out sample extraction,
- Loading direction on the sample according to loading direction on original structural component,
- Naming of the samples and sampling data.

Table C-2 Recommended number of samples. Reproduced from (Kühn et al. 2008).

Situation before test	Recommended number of …				Notes
	$N_{samples}$	$N_{tensile\ test}$	$N_{chem.analy}$	$N_{fracture\ m}$	
Steel grade, quality, and producer are known. This information is validated in site visits and inspections.	0	0	0	0	Use statistically verified data (characteristic values)
All structural members are made of the same steel grade from only one manufacturer. The obtained information cannot be verified by the observations from Site visits.	3	6	1	3	-Locations for random sampling can be chosen freely - Tests being done to identify material. Afterwards, characteristic values can be used
Structural members are built from various steel grades or by various steel manufacturers. The obtained information cannot be verified by the observations from Site visits.	1 of each type of detail	2 per sample	1 per sample	1 per sample	-Locations for random sampling can be chosen freely - Tests being done to identify material. Afterwards, characteristic values can be used
Information from bridge documentation is insufficient, or probably wrong (when compared to on-site inspections)	≥3 of each type of detail	2 per sample	1 per sample	1 per sample	-Locations for random sampling can be chosen freely, but as close as possible to highly stressed details - After material identification by testing, either measured values or characteristic values can be used

All-in-one specimens

In order to optimize material usage for tests on extracted samples, a special small scale specimen was developed in RWTH Aachen (G. Sedlacek, Feldmann, et al. 2008), as shown in Figure C.8. Several test specimens can be milled from the extracted ⌀60 mm

bored metal piece, including ½CT fracture specimen, CVN sample, cylindrical tension specimen, and the residue material for metallographic tests.

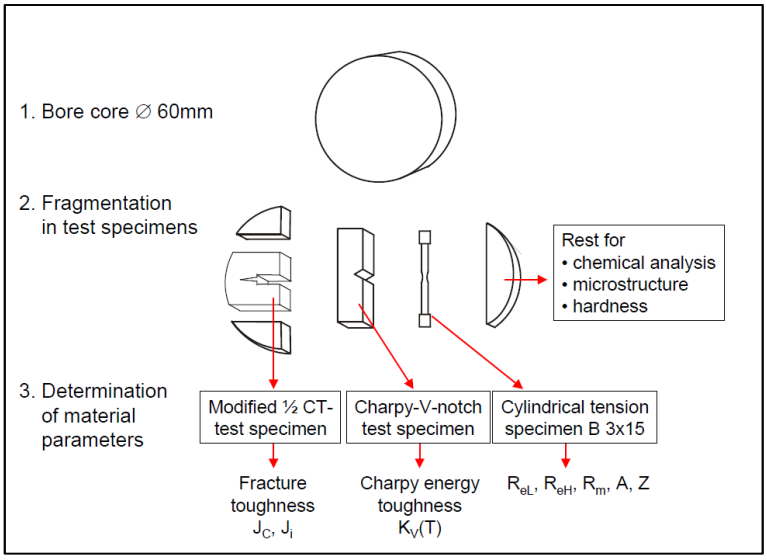

Figure C.8 Special small scale test specimen (G. Sedlacek, Feldmann, et al. 2008). CVN samples can also be used for evaluating transition temperature using Master Curve approach (see C.3.1.1).

C.4.1 Fracture mechanics test specimens (TDOK 2012:23)

TDOK 2012:23 (Trafikverket 2014a) gives regulations for fracture testing (and also chemical analysis) of steel bridge members. The fracture mechanics test method is according to ASTM 1820 (ASTM E1820 2015). Various test specimen geometries are approved:

a. Three-point bending single edge notched bend, SEN(B), specimen with rectangular cross section,
b. SEN(B) specimen with non-rectangular cross section (in Swedish: Trepunkts böjprovstav med brutna sidor),
c. Compact tension, C(T), rectangular specimen,
d. C(T) round specimen.

In terms of optimized use of material, SEN(B) specimens use less material than C(T) specimens with the same thickness. For items a, c, and d above, the original surfaces of the specimens should be kept intact regardless of the surface condition. Item b concerns SEN(B) specimens with non-rectangular sections such as specimens extracted from flanges of INP profiles. In this case guidelines are given for milling the specimen surface, see Figure C.9.

The loading direction should be marked on the extracted samples so that crack orientation and direction of tests load can be aligned to the actual loading conditions.

As for the number of specimens Boverket guidelines (Boverket 1994) can be used. At least three specimens should be tested; although a larger number of tests is preferable because it gives a better understanding of the scatter and significance of outliers. If the results of a test series is not conclusive, additional test series (each series comprising of

three samples) should be carried out (Tobias Larsson 2009). The evaluation of the results will be based on the minimum of three equivalent (MOTE) concept:

- If there are 3 to 5 results, the lowest fracture toughness value is used,
- If there are 6 to 8 results, the second lowest value is chosen,
- If there are 9 or more results, the third lowest value is chosen.

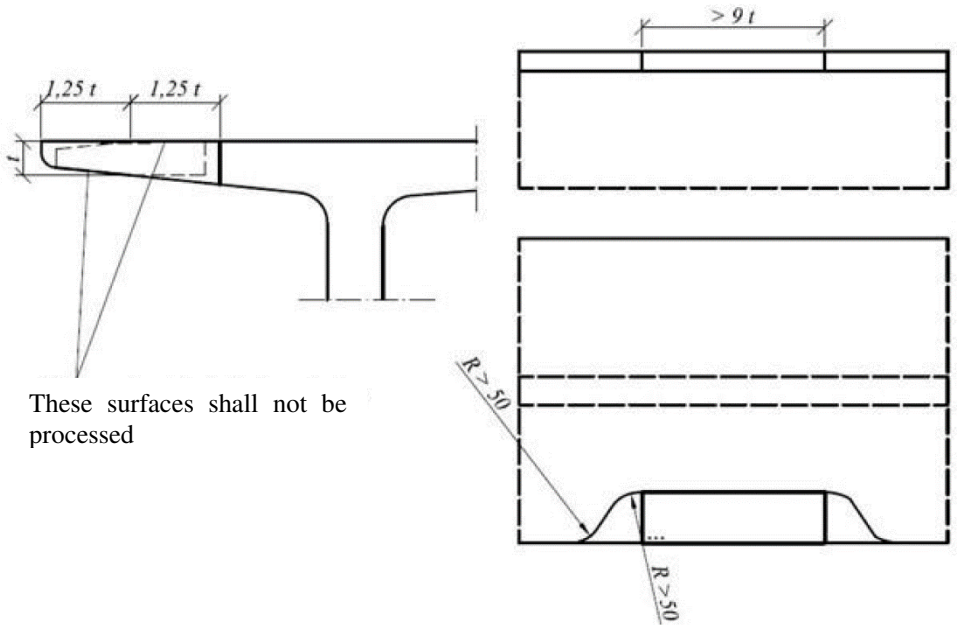

Figure C.9 Sample extraction for SEN(B) test specimens in rolled members with unparallel faces according to TDOK 2012:23 (Trafikverket 2014a).

Loading rate: The loading speed of the test shall be chosen according to the reference speed of the traffic and the length of the influence line of the original component. The loading speed expressed in MPa/s can be calculated as the maximum effect form traffic load divided by time to achieve this maximum in the design element. The traffic load is design traffic load according to calculations or, if possible, measured traffic load.

For a practical evaluation of loading rate, a fictional crack with a nominal length of at least 50 mm can be assumed, which is in the mostly stressed part of the actual component. The fictional crack should be oriented so that its plane is perpendicular to the largest principal stress of the actual structure. The load speed at the crack tip in the test specimen should be at least equal to the load speed at the tip of that fictional crack. For the case of railway bridges, the test loading rate according to old Banverket regulations (Banverket 2003) can be selected as:

$$\dot{K} = \frac{dK}{dt} = 255v\frac{\sqrt{a}}{L} \tag{C-18}$$

Where v is the train speed, a is a fictitious crack with the length of 50 mm, and L is the length of influence line of the girder under study.

Immediately after the test, the fracture surfaces must be preserved, e.g. by spraying with rust-proof lacquer. Test results should be documented including following information:

- Origin of the specimens and specimen naming,

- Date,
- Test temperature,
- Loading rate,
- Specimen dimensions,
- Pre-crack size.

C.4.1.1 Number of samples for master curve method

According to ASTM E1921, if the calculated median fracture toughness for 1T specimens, $K_{Jc,med}^{1T}$, at test temperature is greater than 83 $MPa\sqrt{m}$, the minimum number of 6 specimens are required for evaluating the master curve. However, when testing small-sized specimens, such as pre-cracked Charpy (PCC) specimens, some test values may turn out to be invalid in the subsequent analysis, see Equation (C-11). Therefore, it is recommended to carry out the tests in temperatures below the reference temperature T_{K100} and also account for probable invalid test results. Table C-3 gives the number of needed valid results and estimated number of invalid results in relation to the selected test temperature for the case that all tests are performed at the same temperature. It is evident that choosing a test temperature well below the reference temperature ensures less invalid results. The only drawback is that the uncertainty in evaluation of T_{K100} will increase. To reduce this uncertainty, increasing the number of specimens can be recommended.

Table C-3 Number of valid K_{Jc}^{x} test results needed for evaluation of reference temperature T_{K100}, according to ASTM E1921 (2015). The table is given for the case that all the tests are performed at the same temperature. The possible number of invalid results for pre-cracked Charpy (PCC) specimens is given only as an aid to determine the number of test specimens.

$T_{test} - T_{K100}$ range [°C]	Estimated value of $K_{Jc,med}^{1T}$ $[MPa\sqrt{m}]$	Required number of valid K_{Jc}^{x} values	Possible number of invalid results (PCC specimens)
50 to -14	212 to 84	6	3
-15 to -35	83 to 66	7	1
-36 to -50	65 to 58	8	0